COMBUSTION & FLAME

Quarterly Journal of The Combustion Institute

Contents

VOLUME 1 NO. 2 JUNE 1957

	Page
Smouldering Combustion in Dusts and Fibrous Materials. *K. N. Palmer*	129
Some Limiting Oxygen Concentrations for Diffusion Flames in Air Diluted with Nitrogen. *R. F. Simmons and H. G. Wolfhard*	155
Some Factors Influencing Stability Limits of Bunsen Flames. *P. F. Kurz*	162
Mixing and Combustion in Free and Enclosed Turbulent Jet Diffusion Flames. *P. D. Sunavala, C. Hulse and M. W. Thring*	179
A Law of Similarity for Temperatures in Enclosed Turbulent Flames. *C. Codegone*	194
On the Positive and Negative Ions in Diffusion Flames. *Tosirô Kinbara and Hideô Ikegami*	199
Influence of Diborane on Blow-off Limits of Hydrocarbon Flames. *P. F. Kurz*	212
Flame Zone Studies IV—Microstructure and Material Transport in a Laminar Propane–Air Flame Front. *R. M. Fristrom and A. A. Westenberg*	217
On Generalized Scaling Procedures for Liquid-fuel Rocket Engines. *S. S. Penner and A. E. Fuhs*	229
Experimental Techniques for the Study of Flat Flames by Infra-red Spectroscopy. *D. J. Cole and G. J. Minkoff*	241
Recent Developments and Notes. *W. A. Kirby*	250
Overseas Correspondents' Notes	254

Published quarterly. Annual subscription including postage—U.K. £5 5s. 0d.; U.S.A. $16.00. Combined subscription with Fuel*—U.K. £8 8s. 0d.; U.S.A. $25.00. Editorial Offices, Showroom, Binding and Trade Departments:* 4-5 Bell Yard, Temple Bar, London, W.C.2. *Telephone:* Chancery 6681. *Publishing and Advertising Offices:* 88 Kingsway, London, W.C.2. *Telephone:* Holborn 6900. *Distributors: U.S.A., Interscience Publishers Inc., 250 Fifth Avenue, New York 1, N.Y. All other countries except U.K., Canada, Australia, New Zealand and South Africa: I. R. Maxwell & Co. Ltd. 4-5 Fitzroy Square, London, W.1.*

BUTTERWORTHS SCIENTIFIC PUBLICATIONS

Smouldering Combustion in Dusts and Fibrous Materials

K. N. PALMER

The smouldering rates of several types of dust and of a rigid combustible board were measured under various conditions, and the temperatures of the smouldering zone and the minimum depth of dust deposit required for sustained smouldering were also determined. The propagation of smouldering inside dust deposits, following ignition at or near the base of the deposits, was studied with several dusts in layers up to 85 cm in depth.

SMOULDERING is a form of flameless combustion of solids that is of common occurrence, and is of importance in relation to the development of fires, especially industrial and storage fires. Smouldering combustion has, however, received little experimental investigation and there is little available information on the necessary conditions for the establishment of smouldering and on the rates of propagation. Descriptions of various types of combustion which dust layers may undergo were given by L. COHEN and N. W. LUFT[1], who studied a variety of materials including powdered metals and wood sawdust. When some dusts are ignited by a flame they may continue to burn with a stable flame after the removal of the igniting source, the flame propagating over the surface of the dust layer; in other cases the flame disappears and then smouldering combustion may occur. Cohen and Luft listed the rates of propagation of smouldering in still air of a range of dusts, together with measurements of the temperatures of combustion. Approximate expressions were derived for the variation of the smouldering rate with the depth of the dust layer and for the dependence of the minimum depth of the dust layer for sustained smouldering upon the particle size of the dust. Experiments on the smouldering of coal dust were reported by H. E. NEWALL and F. S. SINNATT[2] and later by W. C. F. SHEPHERD and S. JONES[3].

Although only limited information was available on the smouldering of dust layers, the combustion of carbon and coal in fuel beds and in dust clouds has been extensively investigated and there are summaries of available knowledge by H. H. LOWRY[4], H. R. HOY and G. WHITTINGHAM[5] and M. W. THRING[6]. Combustion in fuel beds has been treated theoretically by M. W. THRING[7] and R. S. SILVER[8]. C. M. TU, H. DAVIS and H. C. HOTTEL[9] made a detailed study of the combustion of single carbon particles heated in an air stream and concluded that at elevated temperatures the rate of combustion was governed by the rate of transfer of oxygen to the carbon surface. Similar results were obtained more recently by J. M. KUCHTA, A. KANT and G. H. DAMON[10], who measured the combustion rate of carbon rods in an air stream. Discussions upon the combustion of single carbon particles have been published by G. A. E. GODSAVE[11] and by D. B. SPALDING[12, 13].

In view of the importance of smouldering as a fire hazard, a detailed investigation of the smouldering of a range of common industrial granular

and fibrous materials of vegetable origin has been undertaken, some results of which have already been reported in brief[14, 15]. The experiments may be divided into three groups, which differed according to the type of combustible used or in the conditions under which the combustion took place; the three groups were:

(*1*) The smouldering of small trains of dust, either in still air or under an applied air flow, and the measurement of smouldering rates and temperatures together with observations on the transition from smouldering to combustion with flame. In all these experiments the smouldering was initiated by an igniting source applied to the surface of the dust train.

(*2*) The smouldering of a rigid porous combustible board, with which it was possible to measure smouldering rates over a wide range of air flows and also to determine whether smouldering could be extinguished with high rates of flow.

(*3*) Smouldering initiated below the surface of a heap of dust by a buried source of ignition. Combustion under these conditions is known in waste heaps, for example, and also occurs at an early stage in some fires in solid materials stored or transported in bulk. Quantitative information on the burning rates of waste heaps and stored materials was scanty and would be difficult to obtain directly owing to the variable composition and packing of the combustible.

EXPERIMENTAL

Materials—The dusts used in the experiments with small trains were cork dust, beech and deal sawdusts, and grass dust; they were selected primarily because they were representative of common industrial hazards. In addition cork dust was obtainable in quantity over a wide range of particle sizes, including very coarse material, and beech wood could be reduced to a series of dust fractions having little variation in composition. Some characteristics of the cork, deal, and grass dusts are shown in *Table 1*; those for beech sawdust are included in *Table 5*.

Table 1. Characteristics of dusts used for trains

Dust		*Cork**		*Deal*		*Grass†*	
Sieve fraction	*Mean particle diam., cm*	*Moisture content* %	*Packing density g/ml*	*Moisture content* %	*Packing density g/ml*	*Moisture content* %	*Packing density g/ml*
−240 *B.S.*	<0·0065	8·8	0·18	—	—	7·5	0·28
−120+240 *B.S.*	0·0095	8·6	0·13	—	—	—	—
− 72+120 *B.S.*	0·017	8·3	0·11	9·8	0·20	—	—
− 60+ 72 *B.S.*	0·023	8·3	0·11	9·0	0·20	—	—
− 25+ 60 *B.S.*	0·043	6·7 3·4	0·09 0·06	11·6	0·20	—	—
− 12+ 25 *B.S.*	0·10	2·2	0·07	11·9	0·20	—	—
− 7+ 12 *B.S.*	0·19	2·4	0·07	—	—	—	—
−0·5 *cm*+7 *B.S.*	0·36	4·2	0·07	—	—	—	—
+0·5 *cm*	>0·48	4·2	0·07	—	—	—	—

*The fine and the coarse cork dusts were obtained from separate sources but both samples yielded a (−25+60 B.S.) fraction.
†99 per cent passed a 0·0063 cm mesh.

In the experiments on the smouldering of a rigid combustible board, four samples of fibre insulating board were used; all the boards were obtained in sheets 1·3 cm thick and were then sawn into strips whose widths ranged from 1·3 to 117 cm. Some characteristics of the boards are given in *Table 2*.

Table 2. Characteristics of the fibre insulating board samples

Board sample	*Moisture content* %	*Density of dry board* g/ml	*Mineral ash content* %
1	10·0	0·27	4·3
2	9·3	0·29	3·0
3	6·6	0·22	0·5
4	10·8	0·23	0·9

Fresh supplies of dust were required for the experiments on smouldering combustion inside dust heaps, and some of the characteristics of the cork dust, elm sawdust, and a commercial mixed wood sawdust obtained for these investigations are included in *Table 3*. All the cork dust was from a single batch, but its moisture content varied slightly; the mixed wood sawdust was used mainly in large-scale experiments, and some variation in moisture content was not eliminated owing to the difficulty of mixing and storing the quantity of dust involved.

Table 3. Experimental details for smouldering initiated at base of dust deposit

Dust	*Particle size B.S.*	*Moisture content* %	*Dry wt packing density* g/ml	*Experimental arrangement of dust*	*Depth of initiating heap* cm	*p* (equation 5)	*K* (equation 5)
Cork	−25	8·0 *to* 8·6	0·14	***Heaps***	—	1·90	$3·6 \times 10^{-2}$
				30 cm box	2·5	2·05	2·5
Elm sawdust	−12	11·3	0·18	*Heaps*	—	1·95	3·5
Mixed wood sawdust	−12	10·7 *to* 18·0	0·20	*30 cm box*	2·5	2·05	6·5
				30 cm box	5·2	2·15	3·2
				60 cm box	5·2	2·15	2·5
				90 cm box	5·2	2·15	2·1

Apparatus—In the determinations of the smouldering rates of dust trains the moulds used for the formation of the trains were 15 to 20 cm long and their cross sections were segments of circles. The nominal dimensions of the trains formed from the moulds are shown in *Table 4*; in some

Table 4. Nominal dimensions of the dust trains

Train	*A*	*B*	*C*	*D*	*E*	*G*	*H*	*J*
Base width cm	1·35	2·35	3·55	5·10	7·25	11·3	17·6	26·1
Vertical depth along centre cm	0·30	0·80	1·00	1·65	2·40	2·40	3·70	5·70

experiments the actual size of train differed slightly from the nominal owing to its expansion on removing the mould. Further details are given later.

The same series of moulds was used for forming the dust trains when the temperatures of the smouldering zones under air flow conditions were measured, using an optical pyrometer. For measurement of the temperatures of smouldering in still air the trains were formed from a mould which was similar to that giving trains of size *D*, *Table 4*, but with three slits cut at 3 cm intervals to allow the passage of thermocouple wires (chromel–alumel, 36 s.w.g. unless stated otherwise). The thermocouples were strung across a movable horizontal frame, mounted apart from the train support, and this arrangement enabled the vertical distributions of temperature in the smouldering trains to be determined. The apparatus is shown in *Figure 1*, with a dust train in position.

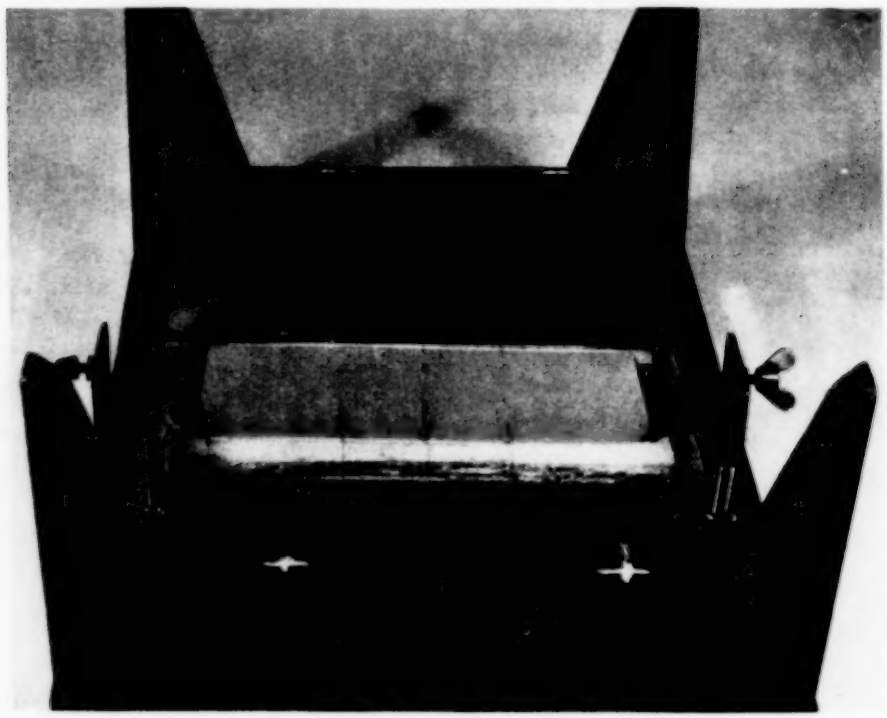

Figure 1. (*Development of a smouldering fire in a heap of cork dust.*) *Dust train with thermocouples in position*

A further set of moulds was made for the determinations of the minimum depth of dust layer necessary for smouldering to be sustained. These moulds gave trains which were wedge-shaped with a slope of 6·3°, and of uniform width (5·70 cm).

In the experiments on smouldering inside dust heaps a series of flat-topped conical moulds was used in forming the heaps (*Figure 2*); all the moulds except one were geometrically similar, the top and base diameters being respectively 7 *L*/2 and 3 *L*/2 where *L* is the depth of the mould

($L = 2{\cdot}5$ to $14{\cdot}9$ cm). The corresponding diameters of the remaining mould were 13 $L/2$ and 9 $L/2$ ($L = 5{\cdot}6$ cm).

In other experiments the dusts were contained in boxes; this method allowed both easier manipulation and greater economy in dust than with conical heaps exceeding 15 cm in depth. Each box was approximately cubic with an internal linear dimension of 30, 60 or 90 cm; the 30 cm box had base and walls of asbestos wood 0·5 in. thick, the other two boxes had bases of this material screwed to metal walls. The boxes were without lids.

Two wind tunnels were constructed for the study of smouldering in an air stream; both tunnels were straight, of square cross section and were mounted horizontally. The smaller tunnel (12·7 cm × 12·7 cm) gave air flows up to 1000 cm/s and the larger tunnel (33 cm × 33 cm) gave air flows up to 420 cm/s. An extension of reduced cross section could be fixed to the smaller tunnel; by this means air flows faster than the maximum of the original tunnel were obtained. All air velocities were measured with rotating vane anemometers.

Procedure—The dust trains were formed by packing a known weight of dust evenly into a mould until the dust surface was level with the top of the mould. The contents of the mould were then turned out on to a strip of dried asbestos board (unless stated otherwise), any change in the height of the train was measured, and the smouldering was usually initiated by a small flame applied to one end of the train. In determinations of the smouldering rates of strips of fibre board each strip was marked on one face by lines drawn across the width at centimetre intervals. The strip was then supported by clamping at one end so that in most experiments the strip projected horizontally from the clamp and the marked face of the strip was either horizontal or vertical. In experiments in which smouldering propagated in directions other than horizontal the strip was tilted, but the marked face was kept in a vertical plane. Smouldering was initiated across the whole width of the unsupported end of the strip by a small flame. The smouldering dust or board was then placed either in a wind tunnel with known air flow or in a draught-free fume cupboard; the combustion zone was allowed to advance 2 or 3 cm along the train or strip and then the time of travel was measured at centimetre intervals over a total distance of 10 cm. The mean linear smouldering rate was then calculated; if combustion ceased before 10 cm were completed the train was classified as 'not smouldering'.

The temperatures in the smouldering zones of dust trains in still air were measured by adjusting thermocouple wires to the required height (*Figure 1*), forming the train, and connecting the thermocouples to galvanometers. Smouldering was then initiated and galvanometer readings taken at 30 second intervals as the smouldering zone approached and passed each junction. Care was taken to record the peak value, which usually persisted for several of the routine readings. The temperatures of smouldering of dust trains and board strips in an air flow were measured with an optical pyrometer through transparent plastic windows in the sides of the wind tunnels. Estimations of the temperatures near the centre of the smouldering zone were made, with and without a red filter, by two observers.

The minimum depths of dust layer necessary for sustained smouldering were determined by forming the wedge-shaped trains already described and initiating smouldering at the thicker end of the wedge. The depth of the dust at the point where smouldering ceased was then measured. The values for the minimum depth obtained by this method were found to be generally consistent with estimations made from observations on trains of uniform depth (*Table 4*) which were just able to sustain smouldering.

The procedure used in experiments on smouldering inside heaps of dust differed from those given above. A conical heap was formed by packing a weighed amount of dust evenly into a mould, applying a small flame centrally for 1 min, allowing a further 5 min of open smouldering (as in *Figure 2*), and then turning out the dust on to an asbestos board (*Figure 3*).

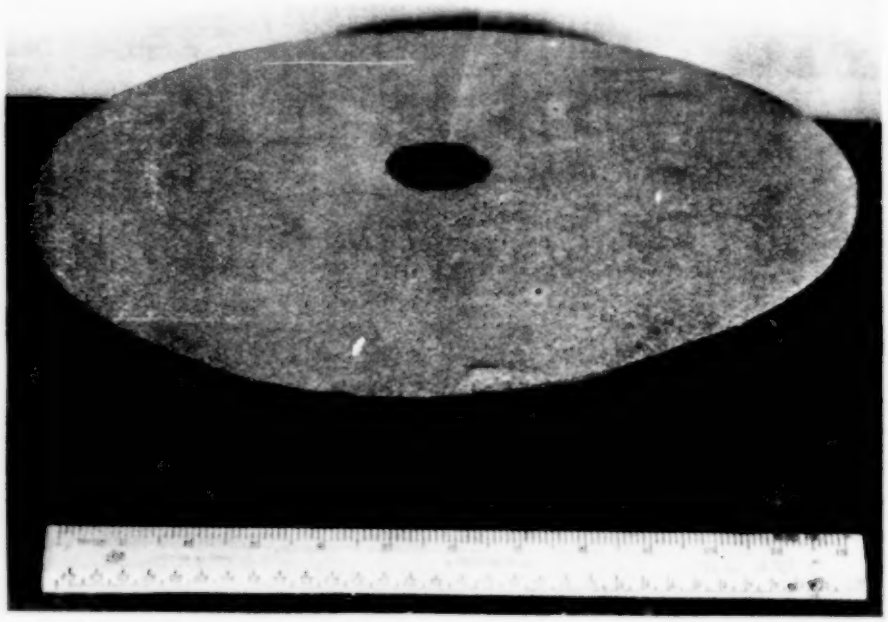

Figure 2. Development of a smouldering fire in a heap of cork dust: 0 to 1 min flame application, 1 to 6 min preburn.

The time was measured from the removal of the mould to the appearance of a charred spot 1 or 2 cm in diameter on the top surface of the heap (as in *Figure 4*). In the experiments with the dust in boxes smouldering was usually initiated at the base of the dust deposit with an igniting source consisting of a small conical heap of dust either 2·5 or 5·2 cm high (*Table 3*). The heap was formed and ignited, as described above, and then left on the bottom of the box until the smouldering had almost penetrated the heap; the remainder of the dust was then rapidly put into the box. The time was measured from the filling of the box until the appearance of smouldering on the top surface of the dust; the distance of propagation was taken as that between the dust surface and the base of the igniting heap. A similar

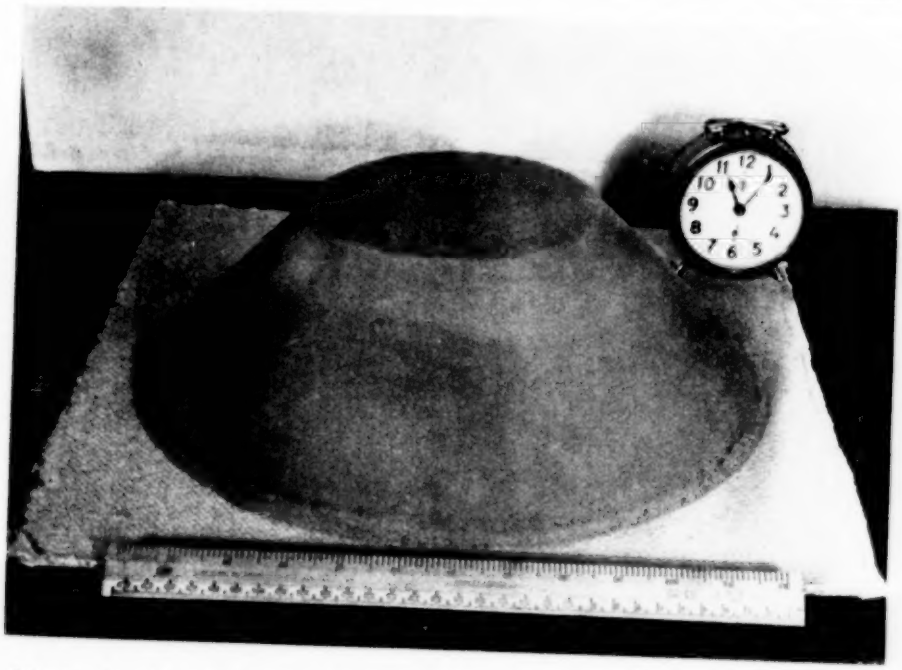

Figure 3. Development of a smouldering fire in a heap of cork dust: 6 min formation of dust heap

procedure was used in experiments in which smouldering was initiated at a point within the dust deposit, instead of at the base. A conical heap 5·2 cm high was used as an igniting source and was placed on top of a layer of dust in the box; finally more dust was added until the total depth was three times that of the original layer. The time and distance of propagation were then measured as before.

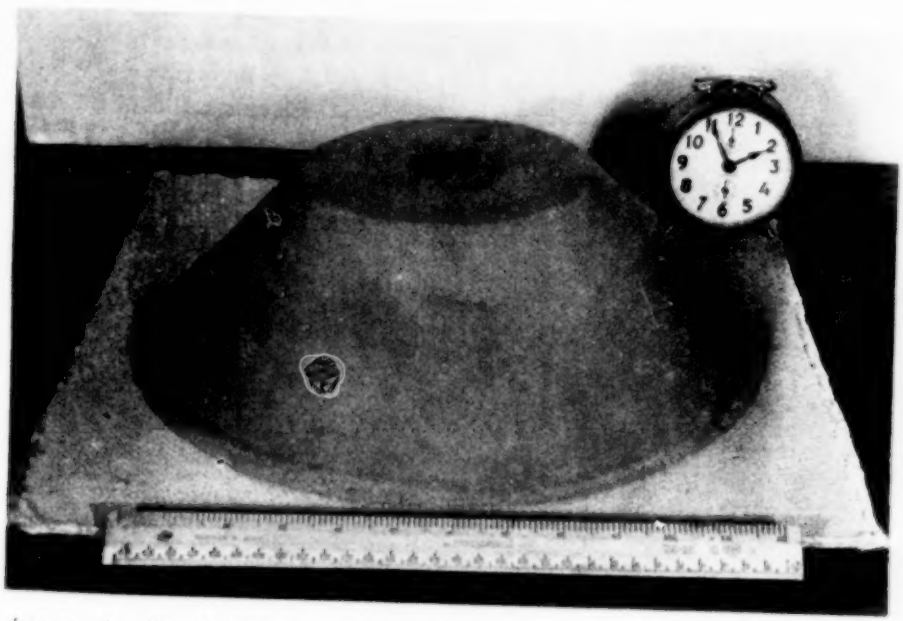

Figure 4. Development of a smouldering fire in a heap of cork dust: 2 h 55 min penetration of the smouldering

RESULTS

The smouldering of dust trains

Appearance of the smouldering

The rates of propagation of smouldering along the dust trains were not difficult to measure since the surface of the trains usually darkened and the division between the burnt and unburnt portions was thus easily visible. In still air the sides of the trains did not burn right down to the base board although in the centre of the trains the entire depth of dust was affected. Glowing was not usually visible in still air, except with very coarse dusts, and the smouldering zones were covered by a grey-black residue which was frequently of lesser volume than the original dust and remained after the trains had burnt out. Smouldering in an air stream was frequently accompanied by visible glowing of the dusts; the brightness and extent of the glowing increased with the air velocity until the division between burnt and unburnt portions of the trains became very marked. Experiments were discontinued when the air velocity was sufficiently great for serious mechanical disturbance of the dust trains to interfere with the smouldering.

Smouldering rates of dust trains

Variation with particle size—The smouldering rate of beech sawdust in still air increased as the particle size was diminished, as shown in *Table 5*, and a similar tendency was observed with the deal sawdust. Detailed

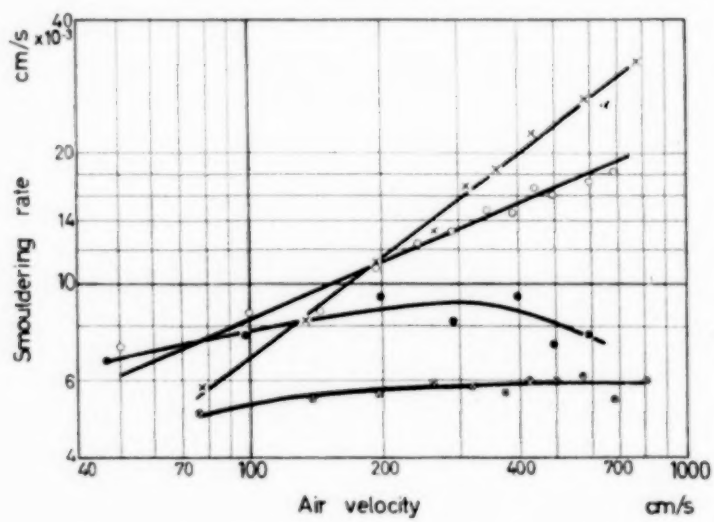

Figure 5. Variation of smouldering rate of fine cork and grass dusts with air flow :

× *grass dust* } *smouldering and air flow in same direction*
○ *cork dust – 240 B.S. fraction* }
⊗ *grass dust* } *smouldering and air flow in opposing directions*
● *cork dust – 240 B.S. fraction* }

investigations with deal and cork dusts were not carried out owing to the possibility of small variations in the composition of the different fractions of these materials.

When the dusts were smouldering in an air stream there was a marked dependence of the smouldering rates upon the magnitude and the direction of the air flow; usually the propagation of smouldering and the air flow were in the same direction, but in some cases they were opposed. The variation of the smouldering rate of very fine dusts (−240 B.S. fraction) with the air flow is shown in *Figure 5*, and *Figure 6* shows the results for

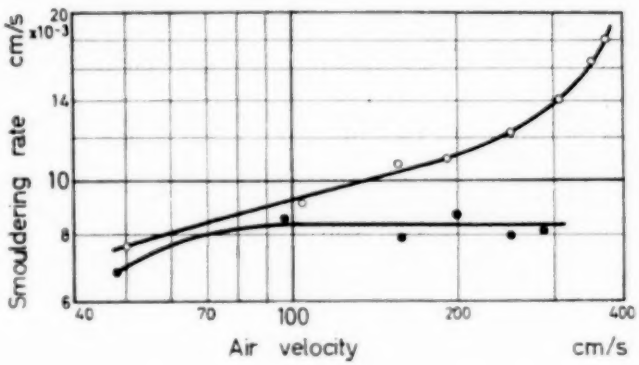

Figure 6. Variation of smouldering rate of cork dust (−72+120 B.S. fraction) with air flow: ○ smouldering and air flow in same direction; ● smouldering and air flow in opposing directions

a coarser fraction of cork dust (−72+120 B.S.). The effect of an air flow on the smouldering rates of a range of beech sawdusts is represented in *Figure 7*. Most of the trains were of the same size (*D*) but size *B* was used in experiments with beech sawdust in which the smouldering and the

Table 5. Smouldering rates of beech sawdusts in still air, cm/s (packing density 0·26 to 0·33 g/ml calculated on a dry weight basis)

Sieve fraction I.M.M.	*Mean particle diameter cm*	*Moisture content %*	*Nominal train size*				
			A	*B*	*C*	*D*	*E*
− 20+ 40	0·048	9·4	*ns**	*ns*	*ns*	$10^{-3}\times$ 1·51	$10^{-3}\times$ 1·41
− 40+ 60	0·027	9·8	*ns*	*ns*	*ns*	1·54	—
− 60+ 80	0·019	9·4	*ns*	*ns*	$10^{-3}\times$ 1·38	1·61	—
− 80+100	0·014	9·8	*ns*	$10^{-3}\times$ 1·74	1·58	1·68	—
−100+120	0·012	9·7	*ns*	1·87	—	1·70	—

**ns* indicates 'smouldering not sustained'

air flow were in the same direction. The original powdered cork from which the sieve fractions were prepared was obtained from two sources and, as shown in *Table 1*, two (−25+60 B.S.) cork fractions were thus extracted. The results for these two fractions were not identical (*Figure 8*), the fraction corresponding to the finer dusts smouldered more rapidly than the fraction from the coarser original material. The results for the latter fraction were obtained with size *G* trains but all other results given in *Figure 8*, including those for deal sawdust, were obtained with train size *D*.

The variation of the smouldering rates of coarse dusts with an incident air flow is shown in *Figure 9* which is plotted on log/linear axes; in all experiments the air stream and the smouldering moved in the same direction. The behaviour of the coarse cork dust fractions differed considerably from

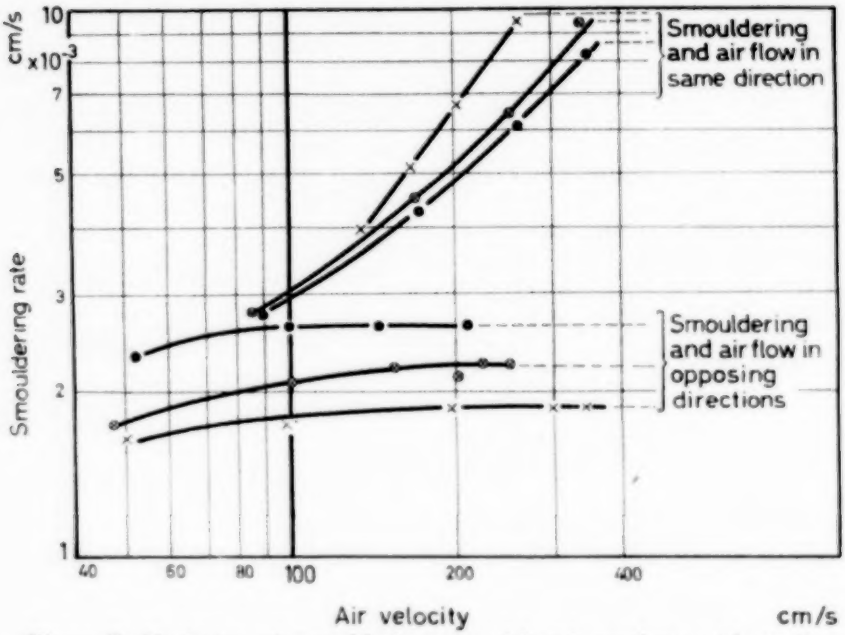

Figure 7. Variation of smouldering rate of beech sawdusts with air flow :
× – 20 + 40 I.M.M. fraction; ⊗ – 60 + 80 I.M.M. fraction;
● – 100 + 120 I.M.M. fraction

that of the finer fractions, given above; thus the (– 12 + 25 B.S.) cork dust smouldered very slowly in still air, and under air flows of less than 130 cm/s, with comparatively little carbonization of the surface of the dust train. Under an air flow of about 150 cm/s the smouldering was much more rapid and was accompanied by visible glowing; under these conditions the dust burnt away almost completely. With intermediate air flows long periods of slow carbonization were interrupted by short spurts of combustion with visible glowing. Smouldering accompanied by glowing was noted with the (– 7 + 12 B.S.) cork fraction at air flows of 53 cm/s and greater, and still coarser fractions glowed visibly even in still air. The change from slow to rapid smouldering was not found with the (– 12 + 25 B.S.) deal sawdust, the smouldering rate of which increased regularly with air velocity (*Figure 9*).

The smouldering of trains of coarse dust in an air stream was frequently accompanied by the sudden appearance of flame on the surface of the trains; the flaming usually appeared either in the smoke above the smouldering zone or above partly burnt material at the sides of the trains. In some cases flaming did not develop until sufficient of the train had burnt for the smouldering rate to be estimated, although observations were not always made over the full distance of 10 cm, and these results are marked *f* in *Figure 9*. Flaming did not develop from smouldering in any trains of a dust with a mean particle diameter less than 0·1 cm (– 12 + 25 B.S.).

Variation of smouldering rate with train size—The smouldering rates in still air of a range of beech sawdust fractions were little affected by variation in the train size (*Table 5*), and similar results were obtained with deal

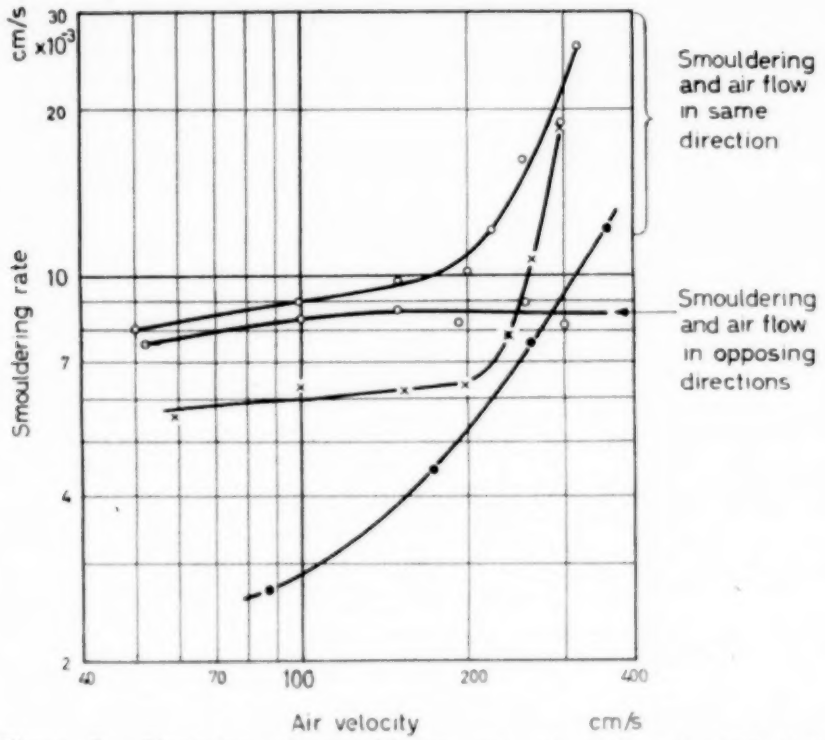

Figure 8. Variation of smouldering rate of cork and deal dusts (−25+60 B.S. fraction) with air flow: ○ cork dust from same stock as finer fractions; × cork dust from same stock as coarser fractions; ● deal sawdust

sawdusts. A more marked effect was shown by considerably finer dusts and their smouldering rates are given in *Table 6* together with the depths of the dust trains for comparison with the results of earlier workers.

Table 6. Variation of smouldering rate in still air with dust depth, cm/s

Dust	*Depth of dust train, cm*				
	0·30	0·80	1·00	1·65	2·40
Cork (−240 *B.S.*) $10^{-3}\times$	5·71	5·50	4·93	4·51	4·29
Grass $10^{-3}\times$	4·76	4·12	4·12	3·37	3·13

Under air flow conditions the smouldering rates of beech sawdusts were affected by variation of the train size. The results for the (−20+40 I.M.M.) fraction are shown in *Figure 10*, which is plotted on log/linear axes; the broken lines indicate that some trains were too shallow to sustain smouldering in still air or under gentle air flows.

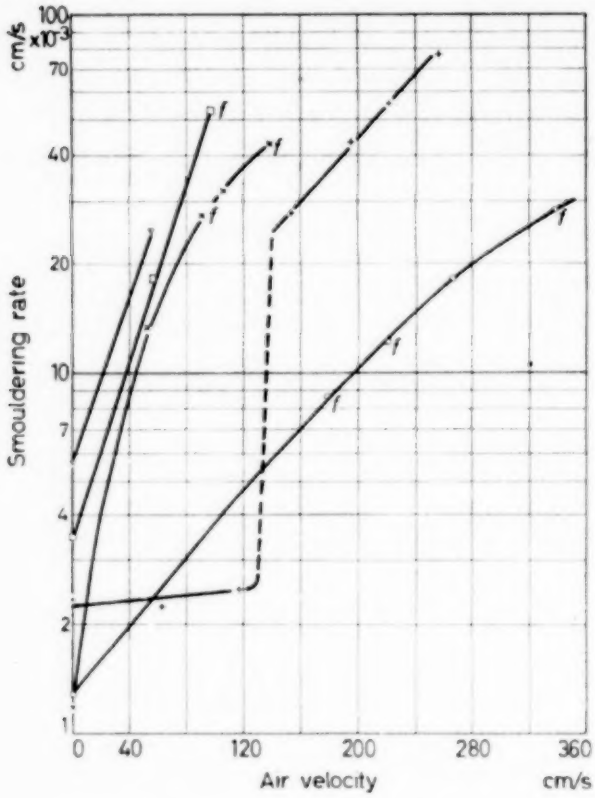

Figure 9. Variation of smouldering rate of coarse cork and deal dusts with air flow: + −12+25 B.S. cork dust, train size H; ○ −12+25 B.S. deal sawdust, train size E; × −7+12 B.S. cork dust, train size J; □ −0·5 cm +7 B.S. cork dust, train size J; ▽ +0·5 cm cork dust, train size J; f indicates flaming developed

Variation of smouldering rate with packing density—Investigations with beech sawdusts in still air indicated that any alteration of the smouldering rate caused by change in the packing density was small compared with that produced by variation in air flow. In addition, although it was only possible to vary the density of packing over the range 0·25 to 0·32 g/ml some

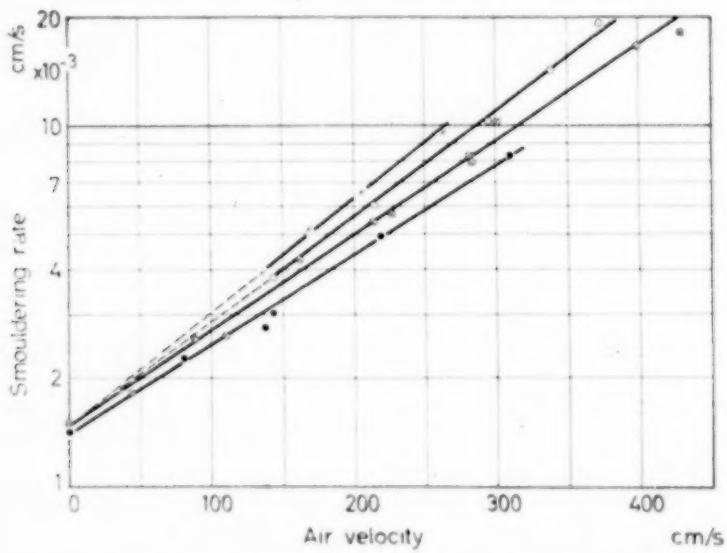

Figure 10. Effect of train size and air flow on smouldering rate of beech sawdust; train size: × B; ⊙ C ⊗ D; ● E

expansion of the trains ahead of the smouldering zone always occurred with the higher packings. Detailed further investigations were accordingly not undertaken.

Variation of smouldering rate with moisture content—Samples of beech sawdust (− 20 + 40 I.M.M.) with moisture contents ranging between 0 and 19 per cent were prepared by either oven drying or humidifying the normal dust. As would be expected the smouldering rate in still air was reduced by increasing the moisture content (*Table 7*). By contrast, under air flow conditions the effect was reduced and became comparable with normal experimental error.

Table 7. Variation of the smouldering rate of beech sawdust in still air with moisture content

Moisture content per cent*	0·5	9·4	18·8
Smouldering rate, cm/s	$10^{-3} \times 1{\cdot}78$	$10^{-3} \times 1{\cdot}51$	$10^{-3} \times 1{\cdot}40$

*Calculated as a percentage of the original dust

Variation of smouldering rate with thermal conductivity of dust support—Comparison of the smouldering rates of cork dust trains was made with fractions finer than 25 B.S. resting on asbestos and on metal. The metal base was an aluminium sheet in contact with a large mass of iron. No significant difference was found in the smouldering rates in still air or in the minimum depth of dust layer to sustain smouldering.

Temperatures of smouldering of dust trains

The temperatures attained within dust trains smouldering in still air were determined for beech and cork dusts by means of thermocouples. The cork dusts (all finer than 25 B.S.) were from the same source as those used in experiments on smouldering rates described above, but differed slightly in moisture content; some characteristics of the beech sawdust have already been given (*Table 5*). The peak temperatures obtained for beech (− 20 + 40 I.M.M. fraction) and cork (− 25 + 60 B.S. fraction) are shown in *Figure 11* but the curves do not represent the instantaneous vertical distribution of temperature in the dusts since the peak temperatures were not attained simultaneously at all points in the same vertical plane. The effect on the peak temperature of using finer thermocouple wires is also shown in *Figure 11*; interference by the wires was only noticeable in regions with steep temperature gradients. It was therefore concluded that in the centre of the smouldering zones the thermocouple wires did not exert a serious cooling effect. The horizontal distribution of temperature in the smouldering zone of a train of cork dust (− 25 + 60 B.S. fraction) is shown in *Figure 12* for an arbitrary height (1·0 cm) within the train. In visual determinations of smouldering rates the advance of the point on the train surface at which charring begins is measured and this point is slightly behind the foremost part of the smouldering zone in the interior of the train; the hottest part of the zone is well to the rear of the initial charring.

Since the smouldering rate of beech sawdust in still air varied with both the particle size and the moisture content of the dust, the effect of these

variables on the smouldering temperature was also studied. On comparing the peak temperatures at an arbitrary height (1·0 cm) near the centre of each train variation of the particle size of the dust was shown to have no significant effect on the peak temperature, within the range of particle sizes

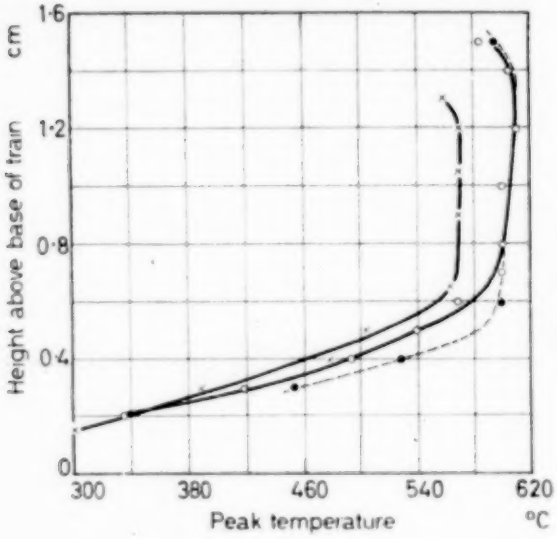

Figure 11. Variation of smouldering temperature with height in dust trains in still air: × beech sawdust, thermocouple 36 s.w.g.; ○ cork dust, thermocouple 36 s.w.g.; ● cork dust, thermocouple 40 s.w.g.

studied (0·012 to 0·048 cm). The variation of the peak temperatures with the moisture content of the dust was also slight and of doubtful significance, the temperature increasing from 565° to 575 °C as the moisture content was increased from 0·8 to 22·5 per cent.

When the dusts were smouldering in an air stream and glowing visibly, the temperature of the smouldering zones as measured by an optical pyrometer appeared to be uniform, except for some random flickering which did not seriously interfere with the measurement. The temperature estimated with a red filter in position tended to be less than with direct vision, but the difference was seldom greater than 20 °C and the mean of

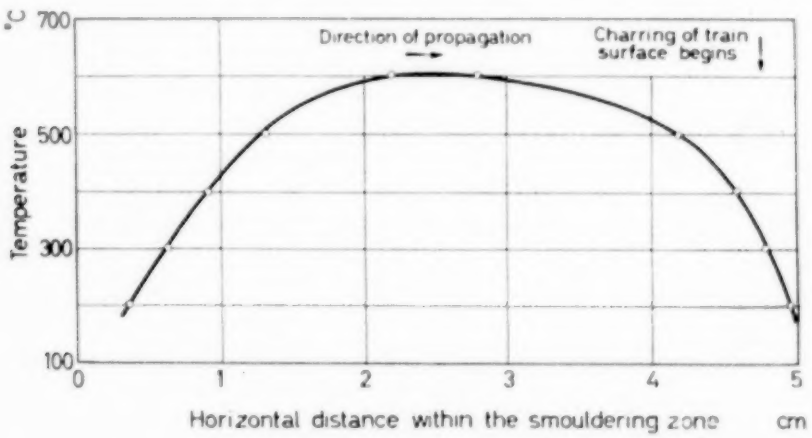

Figure 12. Horizontal distribution of temperature at a height of 1 cm within a smouldering cork dust train in still air

the four values obtained by two observers in each experiment is listed in *Table 8*. The air velocity is given to the nearest 10 cm/s for velocities below 500 cm/s, and to 20 cm/s for the remainder.

Table 8. Variation of smouldering temperature, T°C, with air velocity, V cm/s

Dust	Nominal train size	V cm/s						$\frac{\Delta T}{\Delta V}$
		0	100	200	300	400	600	
Beech (−100+120 *I.M.M.*)	*D*	—	—	790	790	—	—	0
Cork (−240 *B.S.*)	*D*	—	—	790	—	—	840	0·13
Grass	*D*	—	—	700	—	—	760	0·15
Cork (−72+120 *B.S.*)	*D*	—	—	770	790	—	—	0·20
Beech (−20+40 *I.M.M.*)	*D*	—	—	780	—	860	—	0·40
Deal (−12+25 *B.S.*)	*D*	—	—	780	—	900	—	0·60
Cork (−25+60 *B.S.*)	*D*	—	—	730	830	—	—	1·00
Cork (−0·5 *cm*+7 *B.S.*)	*J*	760	900	—	—	—	—	1·40
Cork (+0·5 *cm*)	*J*	780	930	—	—	—	—	1·50

The mean rate of increase in temperature with air velocity ($\Delta T/\Delta V$) increased with the particle size of the dust and became comparatively large for those materials in which the smouldering could lead to flaming.

Minimum depth of dust layer for sustained smouldering

With beech, deal and fine cork dusts an approximately linear relationship was found between the minimum depth for sustained smouldering in still air and the dust particle size (*Figure 13*). However, with cork dusts coarser

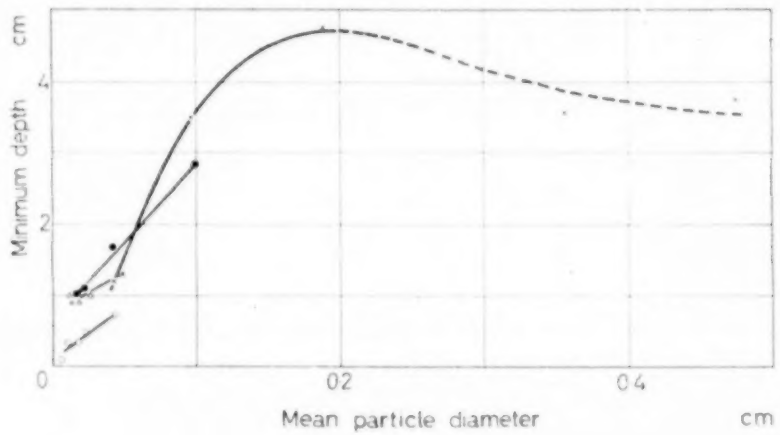

Figure 13. Minimum depth of dust for sustained smouldering in still air: × and ○ cork dust; ● deal sawdust; △ beech sawdust

than 0·3 cm the smouldering in still air was accompanied by glowing, as described above, and the minimum depth was reduced. These results are joined by a broken line in *Figure 13*. The minimum depth for the sustained smouldering of grass dust layers was less than 0·2 cm in still air and was too small to warrant the investigation of the effect of variation in air flow conditions. The results obtained for beech and deal sawdusts smouldering in an air stream are plotted on log/linear axes in *Figure 14* and show large

reductions in the minimum depth as the air velocity was increased. With cork dusts the reductions were less marked; thus with a (−12+25 B.S. fraction) the minimum depth only decreased from 3·5 cm in still air to 2·8 cm under an air flow of 150 cm/s.

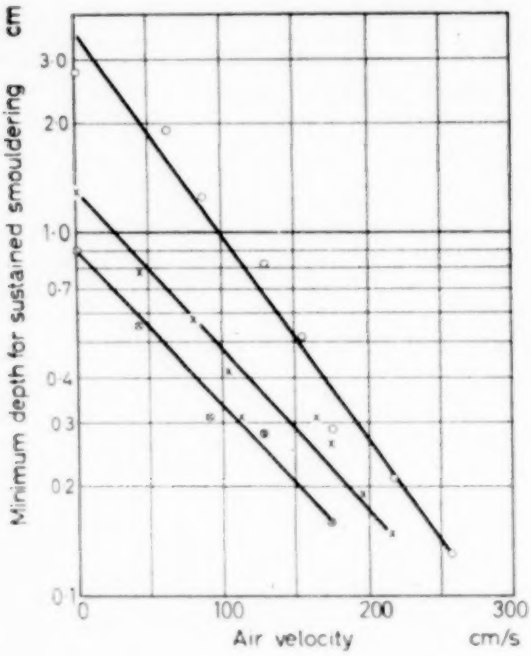

Figure 14. Variation with air flow of minimum depth for sustained smouldering: ○ deal sawdust −12+25 B.S.; × beech sawdust −20 +40 I.M.M. ⊗ beech sawdust −60+80 I.M.M.

The smouldering of board strips

Variation of smouldering rate with air flow—A series of experiments with air flow in the same direction as the smouldering was carried out with strips 1·3 cm in width from each of the board samples. The results are shown in *Figure 15*, where both the smouldering rate and the air velocity are on logarithmic axes. In further experiments, with board sample No. 2, the width of the strips was varied, but the results obtained were similar to those shown in *Figure 15* for the same board. Further experiments with each board sample were carried out using air velocities greater than 1000 cm/s in an attempt to extinguish smouldering with rapid air flows. The smouldering rates obtained under these conditions are included in *Figure 15* and are represented by broken lines; for these determinations the air velocities were measured to the nearest 25 cm/s. In addition to these results it was found that the strips of board samples Nos. 3 and 4 did not sustain smouldering under an air flow of 1450 cm/s. It was noticeable that under high rates of air flow the corners of the strips smouldered less readily than the central portions and this observation, together with the extinction of smouldering in two instances, indicates that the smouldering was cooled by the draught.

The variation of the smouldering rate of fibre insulating board with air velocity was also investigated when the propagation of smouldering and the air flow were in opposing directions. For these experiments strips of

board sample No. 2, 5·1 cm wide, were used and were held with the marked face of the board horizontal. The results are included in *Figure 15* and show that the smouldering rate was little affected by the air flow at air velocities below 600 cm/s; at higher velocities the smouldering zone did not extend across the entire width of the strip and at 900 cm/s smouldering was barely sustained.

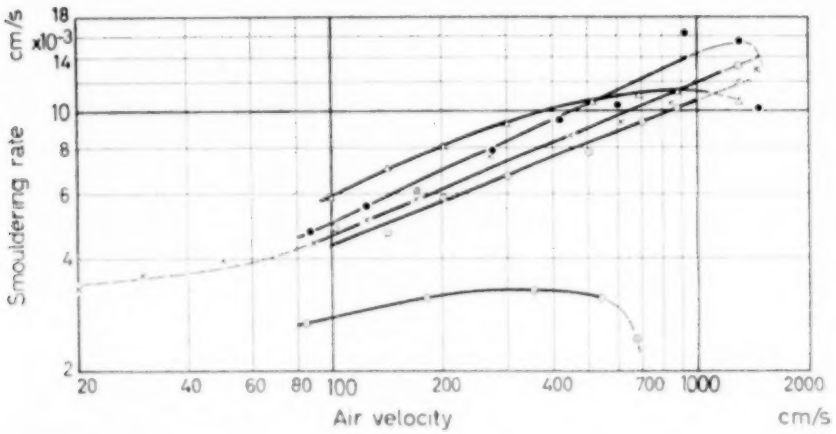

Figure 15. Variation of smouldering rate of fibreboard with air flow:

- × *board sample No. 1*
- ● *board sample No. 2*
- △ *board sample No. 3*
- ⊙ *board sample No. 4*

Smouldering and air flow in same direction

○ *board sample No. 2: smouldering and air flow in opposing directions*

The lack of development of flaming from the smouldering was a feature of all the experiments with fibre board, which were confined to the smouldering of single strips of board. Further, in no instance was there any development of vigorous smouldering in still air, accompanied by glowing and the copious evolution of smoke, similar to that obtained with trains of coarse dusts before the transition to flaming. The visual appearance of the smouldering in single board strips was thus similar to that in trains of fine dusts, although combustion with flame could be produced with board strips if the strips were allowed to smoulder in still air and accumulate a carbonized residue before the application of an air draught; smouldering in trains of fine dusts did not exhibit this behaviour.

Variation of smouldering rate in still air with strip size—The smouldering rates for horizontal propagation in still air were measured with the three board samples Nos. 1, 3 and 4, and the results are given in *Figure 16*, where the smouldering rate is plotted against the width of the strips and also against the ratio of the perimeter to the area of cross section of the strips. The ratio is given by $2(b+d)/bd$, where b is the width of the strip and d the thickness, and for wide strips the ratio may be reduced to $2/d$ ($=1{\cdot}54\,\text{cm}^{-1}$) so that estimations of the smouldering rates of wide strips may be made by extrapolation from measurements upon smaller specimens.

Variation of smouldering rate in still air with direction of propagation—Determinations were made of the rates of propagation of smouldering advancing upwards or downwards at various angles to the vertical, and the

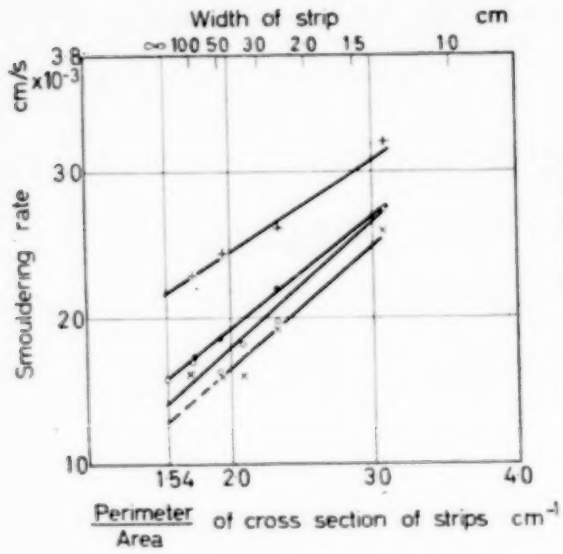

Figure 16. Relation between smouldering rate in still air and width of fibre insulating board strips: ○ board sample No. 1, strip face horizontal; × board sample No. 1, strip face vertical; + board sample No. 3, strip face vertical; ● board sample No. 4, strip face vertical

results are shown in *Figure 17*. The most rapid smouldering was with propagation vertically upwards, the least rapid was with horizontal propagation, and an intermediate rate was found for smouldering vertically downwards.

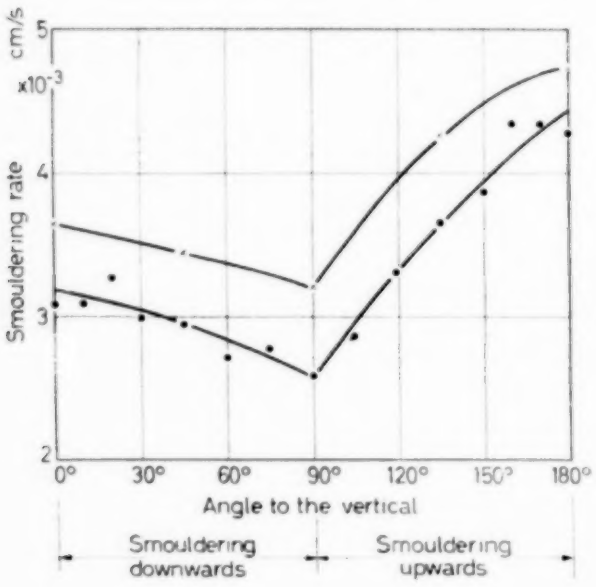

Figure 17. Smouldering rates in still air of boards at various angles to the vertical
● board sample No. 1
× board sample No. 3
strip width: 1·3 cm

Temperature of smouldering zone—Observations made on a strip of board sample No. 2, 1·3 cm wide, showed that the temperature of the smouldering zone was little affected by variations in air flow. Thus a temperature of 770°C was recorded for an air velocity of 200 cm/s and

this value increased by only 20°C when the air velocity was raised to 900 cm/s. The mean rate of rise in temperature was thus 0·03°C cm^{-1} s and was similar to that found for trains of fine dusts (*Table 8*).

Smouldering in interior of dust deposits

Sustained smouldering was obtained inside conical heaps of cork dust and elm sawdust throughout the range of depths tested (2·5 to 14·9 cm). The variation of the time of travel of the smouldering with the depth of the heap is shown for cork dust in *Figure 18*, which is plotted on logarithmic

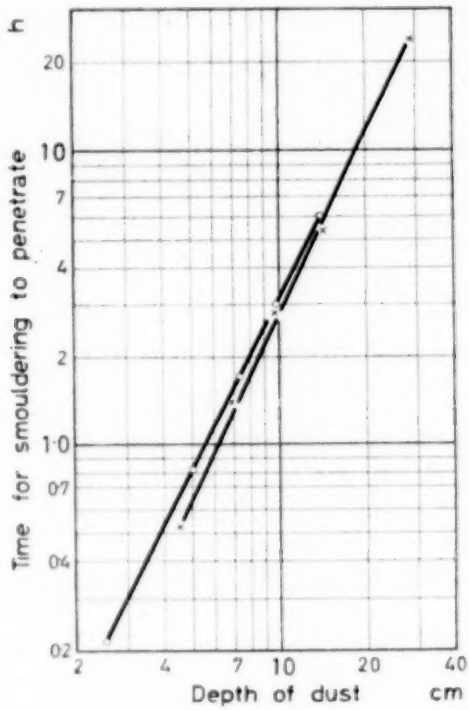

Figure 18. Smouldering within deposits of cork dust: ○ dust in heaps; × dust in 30 cm box

axes; similar results were found for elm sawdust. The time required for smouldering to propagate through the heap varied with the density of packing and the moisture content of the dust. Thus a heap of oven-dried cork dust 5·2 cm in depth required only 39 min (0·65 h) for smouldering to penetrate through the heap whereas the same depth of normal cork dust required 50 min (0·83 h). On increasing the packing density of the dust from 0·14 to 0·16 g/ml the time required by the smouldering increased from 50 to 60 min (1 h). By contrast, variation in the width of the heap had less effect; smouldering in a heap 5·6 cm deep whose top diameter was three times the usual, required 63 min (1·05 h) to burn through whereas the value interpolated from neighbouring results would be 58 min (0·96 h).

After the formation of the heaps there was no visible sign of the combustion until a few minutes before the smouldering reached the top surface of the heap; the surface then became damp near the centre, shortly afterwards the centre of the damp patch dried out to a lighter colour, and this was soon followed by charring. The various stages are shown in

Figure 4; the visible changes were accompanied by steaming and the evolution of acrid smoke. The buried smouldering was accompanied by a faint musty smell and the normal acrid burning smell only developed when signs of the combustion were visible. There was little change in volume of the dusts during the burning and the carbonized material formed in the cork heaps was sufficiently rigid to enable the heaps to be cut open for inspection, as in *Figure 19*. There was a sharp division between the carbonized area and the unburnt dust. On exposure to air the carbonized mass, originally uniformly black, commenced to glow over its entire depth.

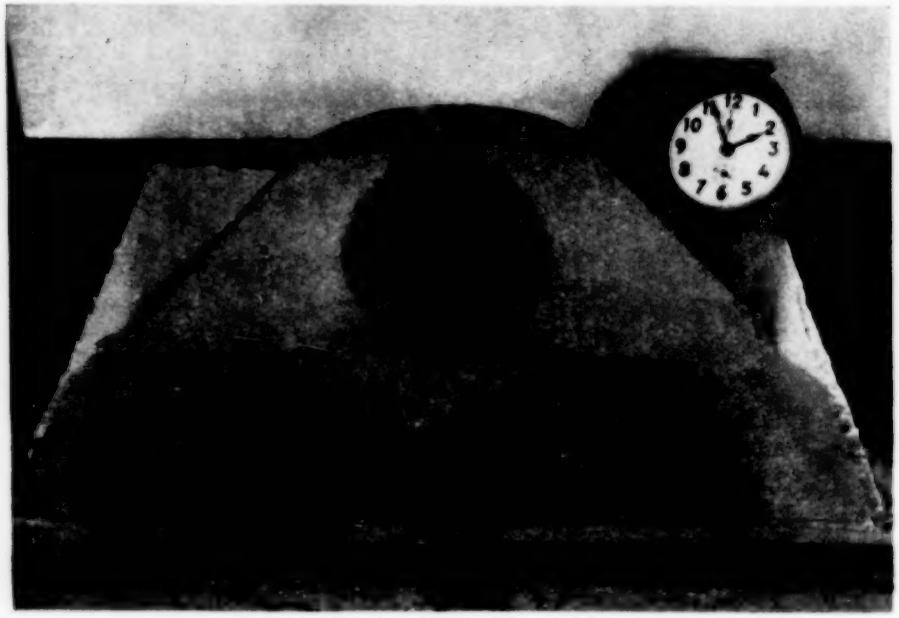

Figure 19. Development of smouldering in a heap of cork dust: section of heap showing carbonized core

The times required for smouldering to burn through various depths of cork dust contained in a 30 cm box, following ignition at the base of the dust layer, are included in *Figure 18* so that comparison may be made with the results for conical heaps. The results for larger-scale experiments, with mixed wood sawdust, are given in *Figure 20*. The appearance of the layers less than 60 cm deep during the burning was very similar to that of the dust heaps described above; a musty smell was again produced and little visible sign was given until the smouldering had almost emerged. Pronounced surface cracking occurred with the 85 cm layer after about 10 days. In every experiment a core of carbonized dust was produced which glowed soon after exposure to the air: the width of the core seldom exceeded about half that of the box.

When the igniting source was put within the dust layer, and completely surrounded by dust, sustained smouldering was obtained in mixed wood sawdust in the 30 cm box and propagated both upwards and downwards from the point of ignition. Although the results were scattered it could be seen that the time required for smouldering to propagate upwards through

a given distance was greater than in dust deposits ignited at the base, over the range of depths tested (up to 20 cm). The general appearance of the smouldering was identical with that for dust deposits ignited at the base.

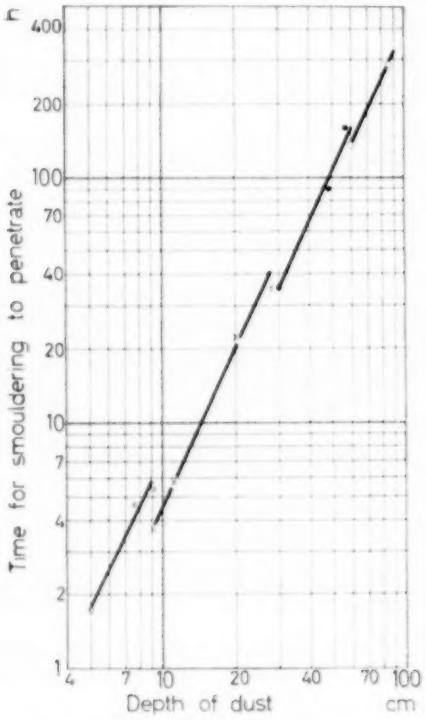

Figure 20. Smouldering within deposits of mixed wood sawdust:
⊙ *initiating heap 2·5 cm, 30 cm box;*
× *initiating heap 5·2 cm, 30 cm box;*
● *initiating heap 5·2 cm, 60 cm box;*
○ *initiating heap 5·2 cm, 90 cm box*

DISCUSSION

Effect of air flow on smouldering rate of dust trains and board strips— The relation between the air velocity and the smouldering rate of dust trains was dependent upon the particle size of the dust. The results given in *Figure 5* for fine cork and grass dusts, the air flow and the smouldering being in the same direction, may be represented approximately by the equation

$$R = cV^n \qquad \ldots [1]$$

where R is the smouldering rate (cm/s), V is the air velocity (cm/s), and c and n are constants. For cork dust $n = 0{\cdot}41$ and $c = 1{\cdot}3 \times 10^{-3}$; for grass dust $n = 0{\cdot}77$ and $c = 1{\cdot}9 \times 10^{-4}$. A similar relation was found to hold for three of the samples of fibre insulating board (*Figure 15*) and values for c and n are given in *Table 9*. The variations in the value of the exponent n given in *Table 9* may have little significance owing to the scatter of the results, noticeable in *Figure 15*; this scatter was greater than that expected from the accuracy of the measurement of the smouldering rate and air velocity. The cause of the scatter in the results was not traced but it could have arisen from irregularities in the board itself and in the residue behind the smouldering zone.

An equation of the same form as equation 1 was obtained experimentally by Tu, Davis and Hottel[9] for the combustion of carbon particles and by

Kuchta, Kant and Damon[10] for carbon rods. Both these groups of workers found values for the exponent n within the range 0·4 to 0·5, and such values would be expected on theoretical grounds if the rate of transport of oxygen to the surface of the carbon were the process determining the combustion rate. With smouldering combustion, the hypothesis that the

Table 9. Values of the constants in equation 1 for various fibre insulating board strips

Board Sample	*Width of strip cm*	*Plane in which marked face of strip was held*	n	c
1	1·3	*Vertical*	0·41	$7·0 \times 10^{-4}$
2	1·3	*Vertical*	0·46	6·0
	2·5	*Vertical*	0·44	4·3
	1·3	*Horizontal*	0·39	8·0
	2·5	*Horizontal*	0·47	4·3
	3·6	*Horizontal*	0·46	4·6
	5·1	*Horizontal*	0·49	3·5
	10·1	*Horizontal*	0·44	4·9
4	1·3	*Vertical*	0·39	7·4

rate of supply of oxygen to the smouldering surface is a factor controlling the smouldering rate is consistent with the observed marked effect of an air flow on the smouldering rates of fibre insulating board and dusts.

As dust trains and board strips are able to smoulder in still air, *i.e.* the smouldering rate is not zero with no applied air flow, some modification of equation 1 is necessary at low air velocities. The smouldering rate of one sample of board was measured for a range of low air velocities (*Figure 15*) and the results could be represented approximately by the following modification of equation 1

$$R = c(V + A)^n \quad \ldots . [2]$$

where c and A are constants. It was calculated from the results that $A = 30$ cm/s approximately and that the smouldering rate would be $2·63 \times 10^{-3}$ cm/s with zero applied air flow as compared with the value of $2·58 \times 10^{-3}$ cm/s found experimentally. The constant A was not evaluated for other boards or dusts since equation 1 appeared to be a sufficiently good approximation over the range of air flows used.

With coarser dusts the smouldering of the trains under rapid air flows was faster than would be expected from equation 1 and the results for beech sawdust (*Figure 10*) may be better represented by an equation of the type

$$\log(R/R_0) = mV \quad \ldots . [3]$$

where R_0 is the smouldering rate with zero applied air flow and m is a constant. Equation 3 also held approximately for deal sawdust (*Figures 8* and *9*) and for the (−72 + 120 B.S.) cork dust (*Figure 6*), but became less accurate at low air velocities. A transition from slow to more vigorous smouldering, often leading to the development of flaming, was observed with cork dusts having a mean particle diameter not less than 0·1 cm (−12 + 25 B.S.); the transition occurred at lower air velocities as the particle size was increased. With dusts coarser than those tested, flaming might

develop from the smouldering with no applied air draught; for such materials smouldering combustion would be unstable. In addition flaming might develop with finer dusts, or lesser air flows, under more favourable conditions than in small open trains in a steady draught. The reason for the abrupt change to a more vigorous smouldering is not clear, indeed the two modes of propagation have been observed in only the one material (powdered cork). It may be that a rate of access of oxygen sufficient for the vigorous smouldering to occur is only possible with the wider interstices in trains of coarse dusts; there is some evidence that a breakdown of the laminar flow of the interstitial air into turbulence can occur with particle sizes and air velocities of the same order as those required for the development of the vigorous smouldering[16]. Further experimental work is necessary on this point.

When the air flow and the smouldering were in opposing directions the relation between the air velocity and the smouldering rate of the dusts and boards could be represented approximately by

$$V^n/R = a + bV \qquad \ldots . [4]$$

where R is the smouldering rate, V is the velocity, a and b are constants, and $n = 0{\cdot}8$ for dust trains and $n = 0{\cdot}5$ for board strips. The smouldering rate of board strips calculated from equation 4 passes through a maximum of $3{\cdot}27 \times 10^{-3}$ cm/s at an air velocity of 314 cm/s, in fair agreement with the experimental results (*Figure 15*); with dust trains any maximum is masked by the scatter of the results (*Figures 5* to *8*).

Variation of smouldering rate with size of dust train—In still air the smouldering rate of fine dusts (cork and grass) decreased as the size of the train was increased, but with coarser dusts (beech) there was no evidence that the train size affected the smouldering rate (*Table 5*) provided that the trains were sufficiently deep for smouldering to be sustained. Values for the smouldering rate of beech sawdust in still air may also be obtained from the results of air flow experiments by extrapolation to zero applied air velocity (*Figure 10*), and these results also indicate that the size of the train has little effect on the smouldering rate in still air. The smouldering of beech, cork and grass dusts in still air thus differs considerably from that of magnesium, described by Cohen and Luft[1], for which the smouldering rate was reported to increase markedly with depth of dust layer.

Minimum depth of dust layer for sustained smouldering—The variation of the minimum depth of cork dust and sawdusts with particle size was approximately linear in still air and no evidence was found that any of the dusts could be too coarse to smoulder. By assuming that with dust layers of the critical minimum depth the rate of loss of heat by conduction is of the same order as that transferred ahead of the smouldering zone, Cohen and Luft[1] showed that the minimum depth should be directly proportional to the diameter of the dust particles, in approximate agreement with the results above. The lack of dependence of the minimum depth upon the thermal conductivity of the surface supporting the dust may result from the temperature at the base of the train being low compared with the peak temperature within the smouldering zone.

Smouldering in the interior of dust deposits—A feature of all the experiments was that the smouldering was initiated by a small source and continued to propagate in each of the dusts tested; deep deposits of dust are thus able to smoulder for many hours without visible sign of burning. There was no indication that a dust deposit could be made so deep that smouldering would be prevented, although all the dusts used were finely divided. Experiments with cork dust showed that increasing the width of the dust heap or changing the experimental arrangement from dust heaps to dust contained in boxes had little effect on the time of propagation of the smouldering. The time required for smouldering to burn through was thus markedly dependent on the depth of the dust but was less affected by variation of the conditions at points away from the path of the smouldering.

It may be seen from *Figures 18* and *20* that the relation between the depth of dust (L) and the time (t) for smouldering to travel from the bottom to the top surface of the dust deposit is of the form

$$t = KL^p \qquad \ldots . [5]$$

where K and p are constants. Values of these constants for cork dust, elm, and mixed wood sawdusts are included in *Table 3*; the values of p are given to the nearest 0·05. The time required for smouldering to travel from the base to the top of a deposit of dust, either in a heap or contained in a box, was therefore approximately proportional to the square of the depth of the dust.

The relation, given as equation 5 with $p = 2$, may also be derived from simple theoretical considerations by assuming that the smouldering rate is proportional to the rate of supply of oxygen to the smouldering front and also that the rate of supply is inversely proportional to the thickness of the dust layer traversed by the oxygen (or that the resistance to the flow of the oxygen is directly proportional to the thickness of the layer). Then

$$-\mathrm{d}y/\mathrm{d}t = f/y$$

where y is the vertical distance between the smouldering front and the top surface of the dust deposit, and f is a constant.

On integrating

$$-\tfrac{1}{2}y^2 = ft + \text{constant}$$

When $t = 0$, $y = L$ where L is the total depth of the deposit.

When smouldering has burnt through the deposit

$$t = t_L \text{ and } y = 0$$

$$i.e. \qquad t_L = \tfrac{1}{2}L^2/f \text{ as in equation 5, when } p = 2.$$

It follows directly from the above assumptions that the rate of propagation of smouldering at a given depth within a dust deposit is inversely proportional to that depth. In practice the rate is probably affected by other factors such as the presence of the hot carbonized material behind the smouldering front and by the extent of the lateral propagation within the deposit. The simple argument outlined above can therefore at best be only a rough approximation, but the theoretical value of the exponent p in equation 5 is close to those determined experimentally (*Table 3*).

CONCLUSION

Experiments with dusts formed into trains and with strips of a combustible board have shown that the smouldering rates were low in still air and were markedly increased by an applied air flow. The simple approximate relation between the air velocity and the smouldering rate of fine dusts and of board broke down with coarser dusts. If the dust was sufficiently coarse, flaming could develop from the smouldering; the transition occurred at lower air velocities as the particle diameter was increased. With combustible board the transition to flaming did not occur under a steady air flow, but could occur when board which had been smouldering in still air was exposed to a draught.

The smouldering rates of fine dusts in still air varied with the depth of dust, provided that the depth was not less than the critical minimum value for smouldering to be sustained; with some coarser dusts variation with depth was only apparent under air flow conditions. The minimum depth of dust layer necessary for sustained smouldering depended upon the particle size of the dust and the air flow but, like the smouldering rate, appeared to be independent of the thermal conductivity of the base upon which the dust rested.

Sustained smouldering could also be obtained inside deposits of dust up to 85 cm deep, and no indication was found that the depth could be so increased that smouldering would not be sustained. The dust deposit could be ignited at the base or at a point within the deposit. The time of propagation of the smouldering from the base to the top of the deposit was approximately proportional to the square of the depth of the dust, and for most of the period of burning there was no evolution of smoke or steam.

The work described in this paper forms part of the programme of the Joint Fire Research Organization of the Department of Scientific and Industrial Research and Fire Offices' Committee; the paper is published by permission of the Director of Fire Research.

The author is indebted to Dr F. E. T. Kingman for his guidance of the work and critical discussion of the results. Assistance in the experiments was received from Mr M. D. Perry and also from Mr G. Skeet, Mr P. S. Tonkin, Miss M. Ward, and Mr D. W. White.

Thanks are also due to the late Mr W. G. Campbell and to Dr R. H. Farmer of the Department of Scientific and Industrial Research Forest Products Research Laboratory, Princes Risborough, for supplying the beech and elm sawdusts, and to Mr K. C. Brown, H.M. Inspector of Factories, Safety-in-Mines Research Establishment, Buxton, who arranged for the supply of grass and cork dusts. Figures 1 to 4 and 19 are Crown Copyright reserved.

Fire Research Station,
Boreham Wood,
Herts

(Received November 1956)

REFERENCES

[1] COHEN, L. and LUFT, N. W. *Fuel, Lond.* 34 (1955) 154
[2] NEWALL, H. E. and SINNATT, F. S. *Saf.-i-Mines Res. Pap.* No. 63, 1930
[3] SHEPHERD, W. C. F. and JONES, S. *Saf.-i-Mines Res. Rep.* No. 43, 1952
[4] LOWRY, H. H. (Ed.) *Chemistry of Coal Utilization* Wiley: New York, 1945
[5] HOY, H. R. and WHITTINGHAM, G. *Mon. Bull. Brit. Coal Util. Res. Ass.* 15 (1951) 69
[6] THRING, M. W. *Science of Flames and Furnaces* Chapman and Hall: London, 1952
[7] — *Fuel, Lond.* 31 (1952) 355
[8] SILVER, R. S. *ibid* 32 (1953) 121
[9] TU, C. M., DAVIS, H. and HOTTEL, H. C. *Industr. Engng Chem. (Industr.)* 26 (1934) 749
[10] KUCHTA, J. M., KANT, A. and DAMON, G. H. *ibid* 44 (1952) 1559
[11] GODSAVE, G. A. E. *Nature, Lond.* 171 (1953) 86
[12] SPALDING, D. B. *Fuel, Lond.* 30 (1951) 121
[13] — *J. Inst. Fuel* 26 (1953) 289
[14] KINGMAN, F. E. T. and PALMER, K. N. *Chem. & Ind.* (1952) 739
[15] — *Proc. ann. Conf. Inst. Fire Engrs* (1953) 90
[16] MUSKAT, M. and WYCKOFF, R. D. *Flow of Homogeneous Fluids through Porous Media.* Edwards: Ann Arbor, Michigan, 1946

Some Limiting Oxygen Concentrations for Diffusion Flames in Air Diluted with Nitrogen

R. F. SIMMONS and H. G. WOLFHARD*

Fuels have been burned at the surface of a porous hemispherical burner of stainless steel, and the nitrogen concentration required to extinguish the flame has been determined. Results are given for a number of fuels in terms of the limiting oxygen index $[O_2/(O_2+N_2)]$, *and it has been found that the values are close to those obtained for pre-mixed flames involving the fuel and oxygen in stoichiometric proportions. Calculations of the adiabatic flame temperature for stoichiometric mixtures with limiting oxygen index indicate that the limit is primarily determined by the flame temperature.*

THE effect of an inert gas such as nitrogen on the limits of inflammability of a fuel in air has been studied for a wide variety of fuels[1]. As the amount of inert gas is increased the lean and rich limits approach and ultimately meet, and from a plot of the limits of inflammability the limiting safe mixtures of diluent and fuel and diluent and air can be obtained. The effect of inert gases on diffusion flames, however, has not been very extensively studied.

The amounts of inert gas which must be added to the fuel vapour or air to extinguish diffusion flames burning on cylindrical burners have been examined[2], but it was found that the amount required depended on the stability of the base of the flame, which was subject to cooling by the burner. In the present investigation diffusion flames have been burned at the surface of a porous stainless steel hemispherical burner, and the amounts of nitrogen which must be added to the air to extinguish the flame have been determined. This burner does not have the disadvantage of the cylindrical burner, since the flame has no unstable base, and hence more fundamental values can be obtained, not only for gaseous but also for liquid fuels.

EXPERIMENTAL METHOD

The limiting oxygen indices were initially determined using a Hefner candle in a jacket up which oxygen–nitrogen mixtures of the required composition could be passed. It was found that very reproducible results could be obtained but it became obvious that the values were affected by the flame size. As the nitrogen content of the 'air' was increased the flame became smaller and thus less heat was available to vaporize the fuel. In consequence, the oxygen indices obtained were not as low as might have been expected from data with pre-mixed flames and thus it was decided to burn the liquids on a burner of new design which overcame this difficulty of decreasing flame size.

*Present address: Bureau of Mines, U.S. Dept of the Interior, Pittsburgh, Pa., U.S.A.

The apparatus used is shown in *Figure 1*. It consists essentially of a hemispherical porous burner of sintered stainless steel surrounded by a glass jacket up which the 'air' was passed, and the fuel was burned at the surface of the hemisphere in a diffusion flame. The position of the flame depended on the fuel flow, but under the most favourable conditions for burning it was 3–4 mm away from the surface of the burner. The fuel

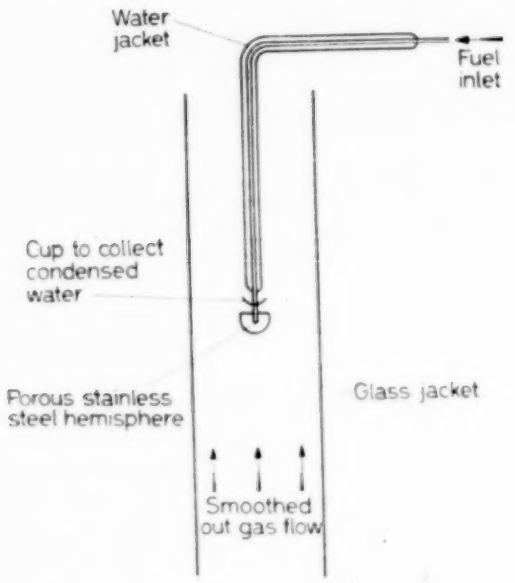

Figure 1

supply to the burner was cooled with water to prevent vaporization of the fuel in the fuel delivery pipe, since this was found to make the flame unstable.

The experimental procedure was to light the fuel in air and gradually increase the nitrogen flow (with a given air flow) until the flame was extinguished. Sufficient time was allowed after each change in composition to determine whether the flame would continue burning in that atmosphere. Initially the two-zone structure of fuel–air diffusion flames[3] could be clearly seen, but as the nitrogen content was increased the carbon zone became weaker and eventually disappeared leaving only the blue zone.

Before values of the limiting oxygen index (β) were determined for a number of fuels the effect of fuel and air flows and the size and shape of the burner were examined. Initially β was found to decrease with increasing fuel flow but reached a minimum value under the most favourable conditions for burning. With low fuel flows, i.e. insufficient fuel, the flame flickered badly and was very close to the burner. Under these conditions the burner became very hot and heat was lost by radiation. With high flows, on the other hand, dripping of the liquid fuel from the burner occurred and the flame was extinguished prematurely. Between these two extremes was a range of fuel flows over which quite constant values of β could be obtained.

Variation of 'air' flow had little effect on β, provided the flow was sufficient to clear the burnt gases from the jacket. With low flows (of the order of 4 cm/sec) it could be seen that recirculation of burnt gases took

place, but when the flow was increased to 6 cm/sec this effect was eliminated. A further increase in the flow rate to 10 cm/sec did not appreciably affect the values. Very high 'air' flows tended to increase the oxygen indices due to the increased mixing rate at the leading edge of the burner[4].

It will be seen, therefore, that to determine the limiting oxygen index under the most favourable conditions for burning necessitates values being obtained for a range of fuel flows. As an added precaution, these values were also determined for more than one air flow.

The effect of varying the size, shape and porosity of the burner has also been studied using acetone as the test liquid. With hemispherical burners the values of β were found to be the same for 0·625, 1·125 and 1·625 inch diameter burners. β was also found to be approximately independent of the radius of curvature of the burner, e.g. a disc 0·5 inch thick and 1·5 inch diameter with a very flat curved surface gave the same value as the hemispherical burners. The porosity of the burners had to be chosen with care, however, although this was mainly due to machining difficulties. Burners were made by machining down cylinders of the porous stainless steel, and it was found that material of too fine porosity 'smeared' badly, which resulted in an uneven distribution of fuel to the surface of the burner. A disc with a permeability coefficient of 3×10^{-5} in^2 (estimated pore size 34μ) was found to be a suitable material, and all results reported in the present paper have been obtained on burners made of this material.

It should be noted that this method can be used for both gases and liquids, and the limiting oxygen indices for a number of fuels are given in the following section. With liquids, however, the method cannot be used where the liquid decomposes on boiling, since the residues tend to block up the porous burners and thus prevent a free flow of fuel.

RESULTS

The physical constants of the liquids used are given in *Table 1*. In all cases the physical constants of the purest grade obtainable commercially were determined, and if these were sufficiently close to the constant for the pure compound the liquid was used without further purification. If purification was necessary the paraffins and long-chain alcohols ($> C_5$) were fractionally distilled, the head and tail fractions being rejected. The lower alcohols were fractionally distilled over anhydrous calcium oxide. The refractive index of liquids was determined using sodium light and an Abbe refractometer and densities were determined using a specific gravity balance. The accuracy of this latter method was probably of the order of 0·5 per cent.

The values of β for a number of fuels are given in *Table 2*. It will be seen that with six or more carbon atoms in the molecule β is the same (within 1 per cent) for both the paraffins and the alcohols, i.e. the introduction of an OH group into the chain does not affect the value of the limiting oxygen index.

With the paraffin series β decreased with decreasing chain length, from 0·135 for hexane to 0·118 for ethane, but then increased to 0·139 for

methane. With the primary alcohols, on the other hand, β decreased continuously from 0·131 for *n*-hexyl alcohol to 0·111 for methyl alcohol. With the secondary alcohols, however, β increased with decreasing chain length, showing that the position of the OH group affects β when the chain length is short, e.g. with propyl alcohol.

Table 1. Physical constants of the liquids used

Liquid	*Boiling point °C*		*Refractive index* $(n_D)^{20}$		*Density*$_{20}$	
	Sample	*Pure*	*Sample*	*Pure*	*Sample*	*Pure*
n-*Pentane*	35·9	36·1	1·3572	1·3577	0·624	0·6263
n-*Hexane*	68·7	68·7	1·3791	1·3750	0·657	0·6594
n-*Octane*	126	125·7	1·3978	1·3974	0·701	0·7028
n-*Decane*	174	174	1·4120	1·4120	0·728	0·7300
Methyl alcohol	64·6	64·6	1·3274	$1{\cdot}3306^{15\cdot0}$	0·793	0·7914
Ethyl alcohol	78·3	78·3	1·3617	1·3614	0·790	0·7895
n-*Propyl alcohol*	97·2	97·2	1·3861	$1{\cdot}3840^{23\cdot6}$	0·804	0·8036
n-*Butyl alcohol*	118	117·8	1·3998	1·3992	0·808	0·8096
n-*Hexyl alcohol*	157·5	157·5	1·4187	1·4179*	0·820	0·8183
n-*Octyl alcohol*	195	195	1·4291	1·4292*	0·825	0·8286
iso*Propyl alcohol*	82·3	82·3	1·3767	1·3775*	0·782	0·7851
sec*Butyl alcohol*	99·3	99·5	1·3968	1·3970	0·813	0·8069
sec*Octyl alcohol*	178·5	178·5	1·4254	1·4260*	0·821	0·8193*
n-*Amyl alcohol*	138	138	1·4109	1·4100	0·811	0·8145
sec*Amyl alcohol*	120	120	1·4064	1·4063	0·812	0·8092
tert*Amyl alcohol*	102·2	102·3	1·4046	1·4141	0·819	0·8090
Benzene	80·1	80·1	1·5012	1·5011	0·880	0·8790
cyclo*Hexane*	80·6	80·8	1·4270	1·4263	0·779	0·7785
Acetone	56·2	56·2	1·3597	1·3591	0·791	0·7905

All the data in *Table 1* for pure compounds have been taken from J. TIMMERMANS[3], except those marked *. The latter values have been obtained from *Handbook of Chemistry and Physics*, Chemical Rubber Publishing Co., Cleveland, Ohio, U.S.A.

This increase in oxygen index from normal to *iso*propyl alcohol suggests that a tertiary alcohol should have a higher oxygen index than the corresponding secondary alcohol, and it will be seen from *Table 2* that this has been confirmed for the amyl alcohols. It should be noted, however, that the remainder of the data given in *Table 2* suggests that this effect would become less pronounced as the chain length is increased.

Another conclusion which emerges when *Table 2* is examined is that unsaturated compounds have lower oxygen indices than saturated, i.e. the value for acetylene is lower than that for ethylene, and the value for ethylene is lower than that for ethane. The value of β for *cyclo*hexane is almost identical to the value for *n*-hexane, and it is interesting to note that the value for benzene is also approximately the same.

DISCUSSION

Before attempting to discuss in detail the results obtained in the present investigation it will be convenient to compare them with results obtained for pre-mixed flames. H. F. COWARD and G. W. JONES[1] have summarized

information on limits of inflammability for a number of fuel–air–nitrogen systems, and it has been found that, in general, the mixture which requires the most nitrogen to prevent flame propagation is slightly to the rich side

Table 2. Limiting oxygen indices for various organic liquids

Liquid	*Limiting oxygen index*	*Limit temp. °C*
Methane	0·139	1518
Ethane	0·118	1363
Propane	0·127	1422
n-*Pentane*	0·1325	1486
n-*Hexane*	0·1335	1498
n-*Octane*	0·134	1503
n-*Decane*	0·1345	1507
Methyl alcohol	0·111	1258
Ethyl alcohol	0·126	1405
n-*Propyl alcohol*	0·128	1439
n-*Butyl alcohol*	0·129	1442
n-*Hexyl alcohol*	0·1315	1469
n-*Octyl alcohol*	0·1315	1476
iso*Propyl alcohol*	0·138	1485
sec*Butyl alcohol*	0·135	—
sec*Octyl alcohol*	0·133	—
n-*Amyl alcohol*	0·130	1454
sec*Amyl alcohol*	0·133	—
tert*Amyl alcohol*	0·1375	1498
Ethylene	0·105	1335
Acetylene	0·085	1271
cyclo*Hexane*	0·134	1495
Benzene	0·133	1540
Acetone	0·1285	1462
Hydrogen	0·054	811
Carbon monoxide	0·076	1177

Where limit temperatures have not been calculated the necessary heats of formation data were not available.

of the stoichiometric proportion. From the limits of inflammability diagrams it is possible to calculate the limiting oxygen index for any limit mixture by considering only the air and nitrogen present, and *Table 3* gives the values for the nitrogen 'peak' and the stoichiometric mixture. *Table 3* also gives some of the limiting oxygen indices obtained in the present investigation for comparison.

It is very striking that the limiting oxygen indices obtained with the porous burner are very close to the values for a stoichiometric pre-mixed flame, although they are slightly higher than the values for the nitrogen 'peak'. The fact that a pre-mixed flame can be diluted with slightly more nitrogen than a diffusion flame is presumably due to the fundamental differences in the combustion processes in diffusion and in pre-mixed flames.

If it is assumed that under limiting conditions fuel and oxidant meet in stoichiometric proportions in the reaction zone of a diffusion flame, it is

possible to calculate the limiting flame temperature for a given fuel using its limiting oxygen index. This may be done by considering the combustion of one mole of fuel with the stoichiometric amount of oxygen diluted with

Table 3. Comparison of limiting oxygen indices obtained using the porous burner with those from limits of inflammability data

Fuel	*Limiting oxygen index using porous burner*	*Oxygen index from limits of inflammability data*	
		Stoichiometric mixture	*Nitrogen 'peak'*
Methane	0·139	0·133	0·133
Ethane	0·118	0·118	0·114
Propane	0·127	0·128	0·116
n-*Pentane*	0·132	0·136	0·118
n-*Hexane*	0·133	0·138	0·120
Ethylene	0·105	—	0·100
Benzene	0·133	0·135	0·115
Hydrogen	0·054	0·056	0·054
Carbon monoxide	0·076	0·078	0·069

an amount of nitrogen corresponding to the limiting oxygen index; for example, with ethane ($\beta = 0{\cdot}118$) the mixture is

$$C_2H_6 + 3{\cdot}5\,O_2 + (3{\cdot}5 \times 0{\cdot}882/0{\cdot}118)\,N_2$$

While the assumption on which these calculations are based may not be strictly justified the error introduced into the limit temperature will not be very great. This is confirmed by recent measurements of the temperature of methane plus oxygen and hydrogen plus oxygen diffusion flames[6]. These determinations show that the experimental values are close to the corresponding adiabatic flame temperature for a stoichiometric mixture.

The calculated limit temperatures together with the limiting oxygen indices are given in *Table 2* and it will be seen that as might be expected the trends in the limit temperatures are similar to those of the limiting oxygen index. For example, in the series of normal paraffins the limit temperature for ethane is lower than that of any other paraffin, and the limit temperature rises to an approximately constant value for the long chain compounds. Again, with the series of normal primary alcohols the limit temperature increases from 1258° C for methyl alcohol to an approximately constant value for the longer chain compounds.

It does not necessarily follow, however, that the change in the limit temperature with structure corresponds in every detail to the change in the limiting oxygen index. For example, consider the three C_6 compounds *n*-hexane, *cyclo*hexane and benzene. These three have almost identical limiting oxygen indices, but although *n*-hexane and *cyclo*hexane have approximately the same limit temperature that of benzene is 40° C higher. It is only to be expected that both the limiting oxygen index and limit temperature for *n*-hexane and *cyclo*hexane should be very similar since there is very little difference in structure and stability. On the other hand,

benzene is an endothermic compound and thus the limit temperature is higher. Again, consider the series ethane, ethylene and acetylene. It will have been noticed that the limiting oxygen index falls appreciably as the degree of unsaturation is increased, but although the limit temperature falls it does not fall to the extent which might be expected from an examination of the limiting oxygen indices. This can also be attributed to changes in the heats of formation; the value for ethane is $-20{\cdot}2$ kcal/mole whereas the heats of formation of ethylene and acetylene are $+12{\cdot}5$ and $+54{\cdot}2$ kcal/mole respectively.

These details suggest that the controlling factor with flames under limiting conditions is the limiting flame temperature, and that the limiting oxygen index is determined by this value, i.e. the amount of nitrogen which can be added before the flame is extinguished is that required to reduce the temperature of the flame to its limiting value.

When assessing the fire hazard associated with the use of a given liquid or gaseous fuel it is very useful to know the range of mixture compositions which are inflammable and the concentration of inhibitor or inert gas required to prevent flame propagation with any mixture. In general, the wider the limits of inflammability the greater is the concentration of inhibitor or inert gas required to prevent a flame propagating. With liquid fuels, however, these determinations become more difficult and less accurate as the boiling point of the liquid increases. The results given in the present paper show that the limiting oxygen indices determined on the porous burner with nitrogen dilution agree closely with the values for pre-mixed flames, and thus this method is particularly useful for assessing the ease with which a given liquid fuel will continue to burn, once ignited. It must be stressed, however, that the ease with which a fuel can be ignited must be also considered when assessing the fire hazard with a given fuel.

Royal Aircraft Establishment,
Westcott

(Received May 1956)

REFERENCES

[1] Coward, H. F. and Jones, G. W. *Bull. U.S. Bur. Min. No. 503* (1952)
[2] Wolfhard, H. G. Unpublished results
[3] Wolfhard, H. G. and Parker, W. G. *Proc. Phys. Soc. Lond.* A 65 (1952) 2
[4] Spalding, D. B. *Fuel, Lond.* 32 (1953) 169
[5] Timmermans, J. *Physico-Chemical Constants of Pure Organic Compounds* Elsevier, Amsterdam, 1950
[6] Diedrichsen, J and Wolfhard, H. G. *Proc. Roy. Soc.* A 236 (1956) 89

Some Factors Influencing Stability Limits of Bunsen Flames

P. F. KURZ

An investigation of the influence of burner diameter on the blow-off limits of shielded and unshielded laminar flames has shown that the limit of any given fuel–air mixture is independent of burner diameter when expressed as critical velocity gradient. The influence has been studied of annular streams of various gases flowing around laminar flames. Helium narrows both lean and rich blow-off limits, but neither helium nor nitrogen effect flash-back limits. Nitrogen and air widen the lean blow-off limit increasingly as the annular-jet velocity is increased. These effects are attributed to the relative ease with which the shielding gases are entrained into the fuel–air stream issuing from the burner port. At flash-back, entrainment is negligible because the flame is very close to the burner port, but at the blow-off limits entrainment appears to be substantial enough to cause significant changes in the limit.

THIS paper describes and discusses some of the factors which influence the stability limits of Bunsen flames, and includes a description of (*1*) the results of experiments to ascertain the influence of burner diameter on blow-off limits of shielded and unshielded laminar Bunsen flames and (*2*) the influence of various shielding gases, including nitrogen, helium and air, on the blow-off and flash-back limits of hydrocarbon–air flames on a modified Bunsen burner. The effect of changing the velocity of the annular shielding gas stream is also discussed.

Unshielded methane–air flames were studied on four different burners ranging from 3·05 mm to 17·5 mm internal diameter, and shielded methane–air flames were studied on burners of 7·8 mm, 11·1 mm and 17·5 mm internal diameter. It was found that the blow-off limits of shielded and unshielded flames of any given fuel–air mixture, when expressed as the critical velocity gradient at blow-off, are independent of burner diameter in the range studied. In studying shielded flames, the use of relatively small burners, i.e. those of 7·9 mm and 11·0 mm internal diameter, provided data for a continuous blow-off curve passing through a maximum. With the 17·5 mm burner, a continuous curve could not be obtained because the limits of laminar flow were reached before the maximum of the blow-off curves was attained.

In the studies on the influence of shielding gases on stability limits, rich blow-off could not be observed when air was used as the 'shielding' gas. Helium, on account of its high rate of diffusion, narrows both lean and rich blow-off limits, but both helium and nitrogen affect the flash-back limits in the same manner and to the same extent as do Smithells[1] tubes. The lean blow-off limit is extended as the flow rate of the nitrogen is increased. Similar results are obtained when air is used as the 'shielding' gas, and for unshielded flames in ambient air the lean blow-off limit is slightly narrower than for nitrogen-shielded flames.

The results of stability experiments with the modified burner are compared with the results of similar experiments on other burners identical in design except for the gas-shielding provisions.

DESCRIPTION OF APPARATUS

The burner auxiliaries for metering the air and fuel and for preparing a uniform fuel–air mixture before delivery to the burner tube have been described in detail earlier[2]. Briefly, these involved critical-flow orifices for measuring gas flow and a vortex chamber to insure good mixing. Each of the burners was fitted with a jacket through which water was circulated to maintain the burner rim at a uniform temperature.

Figure 1 shows a sketch of the 11·1 mm burner. The other burners used for studying the influence of burner diameter on blow-off were similar in construction, and the length of each burner tube was at least 50 times the burner diameter to insure laminar flow in the jet issuing from the burner

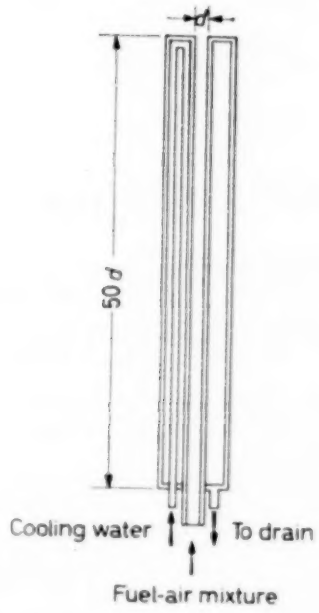

Figure 1. 11·1 mm Bunsen Burner

port. Provisions were made so that the Bunsen flame could burn unshielded in ambient air, could burn within a glass tube which permitted access of ambient air from the bottom, or could burn within a Smithells tube in the presence of its products of combustion only. When the flame was completely shielded from ambient air a copper plate with a $\frac{1}{2}$ in. hole in its centre was placed over the top of the Smithells tube to minimize back drafts of air which might influence the rich limits at low rates of flow through the burner.

Figure 2 shows a diagram of the gas-shielded burner. The burner tube is 17·5 mm in diameter, and has a water-jacket; surrounding and concentric with it is another tube which serves to confine and direct the flow of a

shielding gas around the Bunsen flame. The primary function of the shielding gas was to exclude the ambient atmosphere from the environs of the burner port so that rich blow-off limits could be observed.

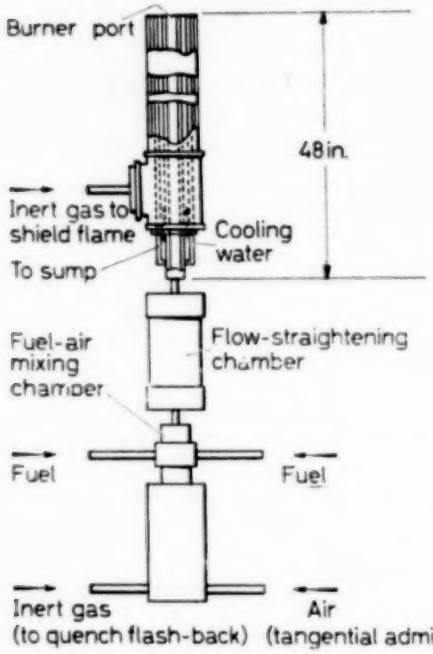

Figure 2. Schematic diagram of Bunsen burner shielded by inert gas, and mixing system

Air and fuel flows were metered by means of critical-flow orifices, and were mixed in a chamber at the bottom of the burner. The flow of shielding gas was controlled by means of a critical-flow orifice and was delivered into the annular space about 90 cm below the burner port. The annulus is about 0·45 cm wide and has an area of about 4·95 cm^2.

Flash-backs were controlled by admitting a sudden large flow of nitrogen to the fuel–air mixing chamber, the flame being then either quenched to extinction within the burner tube or driven from the tube and blown off.

EXPERIMENTAL PROCEDURE

To observe the blow-off of unshielded flames from Bunsen burners ranging in diameter from 7·9 mm to 17·5 mm, air was first admitted to the burner at a low rate of flow and then fuel was delivered to the burner at a rate sufficient to produce a stable flame. The rate of flow of fuel was then decreased by convenient amounts until the flame blew off. An increase of one unit in the flow of fuel again produced a stable flame. The rate of flow of air was then increased by about 5 to 10 per cent of the previous rate, depending on the burner used. The fuel flow was again increased to produce a stable flame, and the procedure repeated until a range of flow rates covering the region of laminar flow had been traversed. This procedure was also followed in several experiments in which the flames were burnt within glass tubes with free access of ambient air from the bottom of the glass tube.

With the 3·05 mm burner, the procedure was altered to speed up the rate of change of the fuel–air mixture. After a stable flame had been obtained, the rate of flow of air was increased by convenient units, ranging from about 4 per cent of the previous flow at low rates to about 2 per cent at higher rates, until blow-off resulted. A decrease of one unit in the air rate then produced a stable flame. The fuel flow rate was then increased by five units or about 8 per cent of the ultimate fuel rate and the air rate was increased step by step until blow-off resulted, and so on, until a range of jet velocities had been investigated.

With these procedures, lean-type blow-off was investigated, i.e. blow-off which results when the fuel–air mixture is made leaner, either by decreasing the fuel flow rate or by increasing the air flow rate. The first procedure described was used also to study shielded flames burning in the absence of ambient air but in the presence of their combustion products.

With completely shielded flames, two types of blow-off are possible at any given air rate which permits a stable flame. Lean-type blow-off has been discussed above; it is reached by making the fuel–air mixture leaner. Rich-type blow-off occurs when the mixture is too rich to permit the existence of a stable flame, and is brought about by increasing the fuel rate at a given air rate, or by decreasing the air rate at a given fuel rate, until blow-off results.

Rich-type blow-off is not possible with Bunsen flames to which ambient air has free access because the surplus fuel in the primary mixture burns with the ambient air in the form of a diffusion flame, which stabilizes the inner primary cone. With rich methane flames shielded by a Smithells tube, there is only one flame cone at the burner port; the second cone is 'split' from the primary cone because no ambient oxidizer is present to unite with the surplus fuel. Consequently, the 'split' cone burns as a diffusion flame at the top of the Smithells tube.

In the experiments with the burner shielded by flowing gas, flash-back limits as well as lean and rich blow-off limits were studied. When air was used as the 'shielding' gas, rich blow-off limits could not be observed for reasons given above. To determine the stability limits of a fuel the air flow was established at a low rate, and an increasing amount of fuel introduced until a stable, lean flame results. The flow of fuel was then decreased by convenient steps until blow-off occurred. This was the point of lean blow-off. The flow of fuel was then increased by steps until flash-back occurred. This is described as the 'lean' flash-back point. A decrease of one step in the flow again produced a stable flame.

By increasing the flow of fuel further, a region of flash-back was traversed and a stable flame again obtained. Decreasing the flow of fuel one step caused the flame to flash back, this being the point designated 'rich' flash-back.

Rich blow-off was then determined by increasing the flow of fuel until the flame lifted from the burner port. A decrease of one step in the fuel flow rate again produced a stable flame. The procedure was repeated over a range of air flow rates, the usual range of air rates through the burner

being from 5 to about 21·5 l./min. The rate of flow of shielding gas was held constant throughout an experiment.

All of the fuel and shielding gases used in these experiments (except the methane) were specified as being at least 99 vol. per cent pure. The methane was a technical grade specified as 96 vol. per cent pure. Compressed air in commercial cylinders was used to ensure close control over the air input in the burner at all times.

EXPERIMENTAL RESULTS

The experimental results are grouped into two main sections, namely those pertaining to the influence of (*1*) burner diameter on blow-off limits and (*2*) shielding gases on stability limits, and are presented in that order.

Blow-off limits of methane–air flames on a 17·5 mm burner

Figure 3 compares the blow-off limits obtained with shielded flames on the 17·5 mm burner with limits observed when the flame burns unshielded in ambient air and when the flame is surrounded by glass tubes of different sizes with free access of ambient air from the bottom of the glass tube. The abscissa describes the composition of the fuel–air mixtures in terms of the percentage of stoichiometric air in the mixture. The ordinate scale is given in units of the critical velocity gradient as defined by B. LEWIS and G. VON ELBE[3]. It is evident that the gradient, g, is a function of the velocity/diameter ratio, v/d.

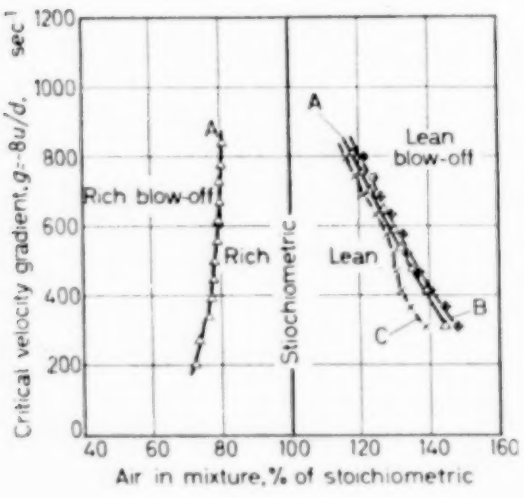

Figure 3. Blow-off limits of shielded and unshielded methane air flames on a 17·5 mm Bunsen burner: A 54·8 mm Smithells tube; B 54·8 mm and 75·4 mm chimney tubes unsealed at lower end; C unshielded flame

As *Figure 3* shows, the unshielded flames are less stable than completely shielded flames, and the enclosed flames to which ambient air has free access are the most stable ones. There are at least two possible explanations for these results: (*1*) flames burning in ambient air on this large-diameter burner lose considerably more heat than do either completely shielded flames or partially shielded flames and (*2*) entrainment of ambient air is enhanced in the absence of a shield or chimney (partial shield), which would tend to

narrow the lean blow-off limit. A chimney effect was produced when a glass tube left unsealed at the bottom was placed around the flame, so that there was free access of ambient air to the flame through the annulus at the bottom of the glass tube. With this arrangement, the entrainment of air by the flame was apparently decreased. The action of the jet issuing from the burner port imparts velocity to the air which it draws into the glass tube and thereby decreases entrainment. Accordingly, the lean limit is extended beyond the limits observed with an unshielded flame burning in quiescent ambient air or with a shielded flame burning in the presence of its own combustion products.

The rich blow-off curve is peculiar to the totally shielded flames. The reason why flames burning in ambient air are not susceptible to rich-type blow-off has been given in an earlier section.

Blow-off limits of methane–air flames on an 11·1 mm burner

Figure 4 shows the blow-off limits of methane–air flames on an 11·1 mm Bunsen burner with total shielding, with no shielding, and with a chimney arrangement. The shielded flames appear to be about as stable as the

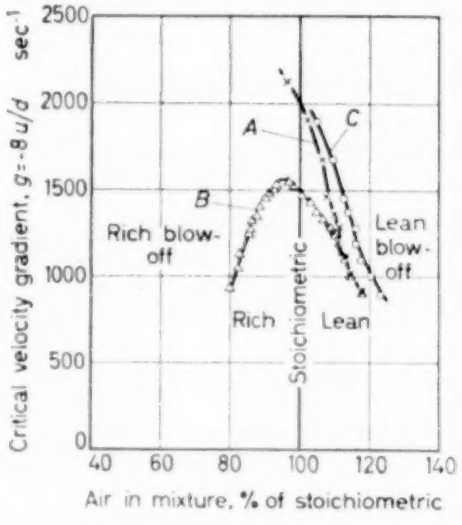

Figure 4. Blow-off limits of shielded and unshielded methane–air flames on an 11·1 mm Bunsen burner: A totally unshielded flame; B 41·3 mm Smithells tube; C 41·3 mm chimney tube unsealed at lower end

totally unshielded ones in the range of critical velocity gradients from 900 to 1200 sec^{-1}. At higher values of the gradient, the shielded flames tend toward the maximum shown at about 95 per cent of stoichiometric air which links the lean-type and rich-type blow-off curves. The flames burning in a 'chimney' are the most stable of the group for the same reasons as those given in the section describing the results obtained with the 17·5 mm burner.

Blow-off limits of methane–air flames on a 7·9 mm burner

Figure 5 shows blow-off limits of totally shielded and unshielded methane–air flames burning on a 7·9 mm Bunsen burner. At values of the critical velocity gradient ranging from 600 to about 1100 sec^{-1}, the shielded and unshielded flames are about equally stable.

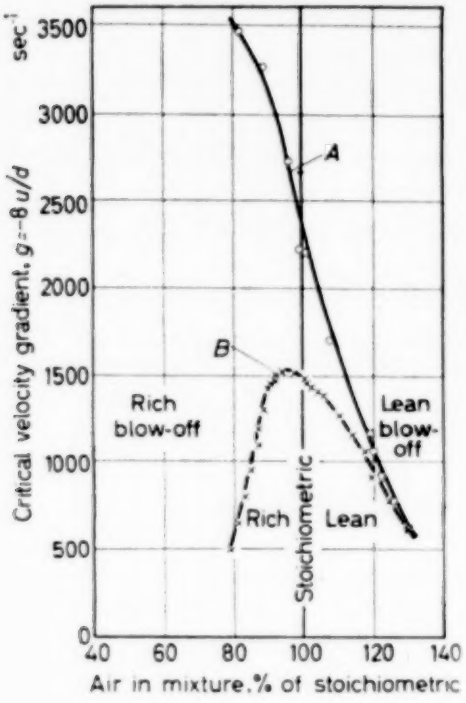

Figure 5. Blow-off limits of methane–air flame on a 7·9 mm Bunsen burner with and without a Smithells tube: A flame in ambient air; ambient air excluded from flame

Blow-off limits of methane–air flames on a 3·05 mm burner

Figure 6 shows the blow-off limits of methane–air flames on an unshielded 3·05 mm Bunsen burner. As orifice limitations did not permit studying flames on this burner at values of the critical velocity gradient less than 4000 sec^{-1}, it was not possible to stabilize flames when the burner was shielded to exclude ambient air from the burner port because totally shielded

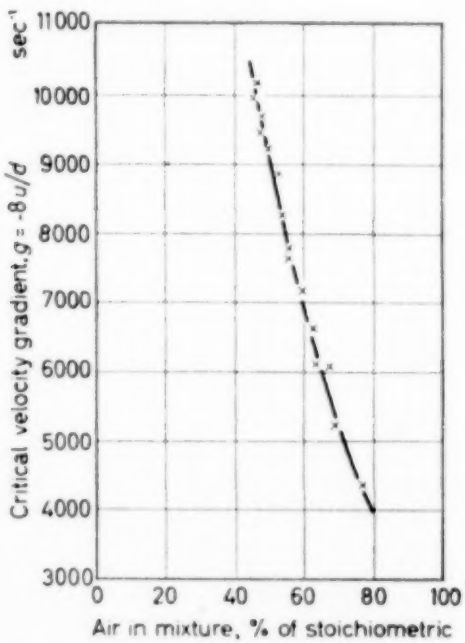

Figure 6. Blow-off limits of unshielded methane–air flames on a 3·05 mm Bunsen burner

methane–air flames will not stabilize when the critical velocity gradient exceeds about 1525 sec^{-1}.

Influence of burner diameter on blow-off limits of Bunsen flames

Figure 7 shows the blow-off limits of methane–air flames burning unshielded in ambient air on Bunsen burners of internal diameters ranging from 3·05 mm to 17·5 mm. Some of the data from each burner lie on a general curve which is reasonably smooth over the range of critical velocity gradients from about 300 to about 10 000 sec^{-1}. However, for each of the three large burners, the data depart from the general curve at the high jet velocities, i.e. as the Reynolds number increases and the flow is close to becoming turbulent.

It is presumed that the curve in *Figure 7* could be extended farther to the right by using smaller burners, and that the curve would not pass through a maximum value of critical velocity gradient for laminar Bunsen flames burning in ambient air.

In sharp contrast to the data shown in *Figure 7* are those given in *Figure 8* for shielded flames where ambient air is completely excluded. Here, the lean and rich blow-off limits of methane–air flames on 7·9, 11·1,

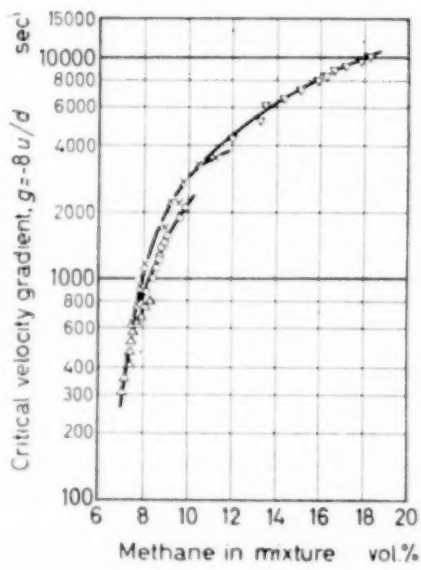

Figure 7. Blow-off limits of methane–air flames in ambient air on Bunsen burners 3·05 to 17·5 mm internal diameter: ▽ 3·05 mm; × 7·9 mm; ○ 11·1 mm; △ 17·5 mm

and 17·5 mm Bunsen burners are shown to produce a single continuous curve which passes through a maximum when the fuel–air mixture contains about 9·9 vol. per cent methane (the stoichiometric point is at 9·52 vol. per cent methane), and when the critical velocity gradient is about 1525 sec^{-1}. It is apparent, therefore, that when the critical velocity gradient exceeds 1525 sec^{-1} for a mixture containing about 10 vol. per cent methane, it will not be possible to stabilize a flame on a shielded burner.

Methane, burning alone with air, may be assumed to behave in a manner which is typical for gaseous hydrocarbons, and other hydrocarbons could

consequently be expected to give blow-off curves similar to those shown in *Figures 7* and *8* for methane–air mixtures. Indeed, the results of J. GRUMER, M. E. HARRIS and H. SCHULTZ[3] in blow-off studies with a variety of gases and gaseous mixtures corroborate this assumption for unshielded flames. Thus the nature of the particular hydrocarbon chosen for use in the present work was probably incidental and any other gaseous

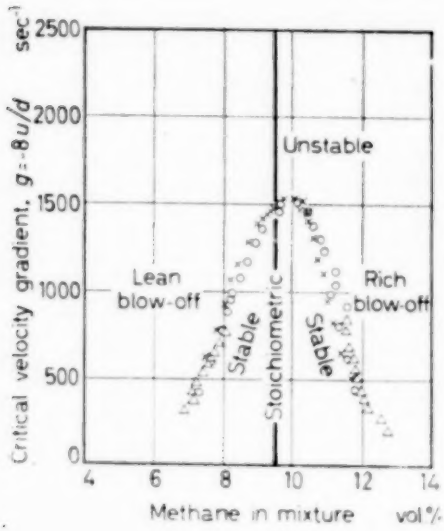

Figure 8. Blow-off limits of shielded methane–air flames on three Bunsen burners of different diameters: × 7·93 mm; ○ 11·1 mm; △ 17·5 mm

hydrocarbon would have served as well as methane for the purposes of the investigation. This reasoning applies also to the fuels used in the experiments described in the following sections which are concerned with the influence of shielding streams of flowing gas on the stability limits of laminar hydrocarbon flames.

Experiments with the gas-shielded burner

The flame-stability data obtained with the gas-shielded Bunsen burner shown in *Figure 2* are compared with similar data obtained earlier[2] with a Bunsen burner fitted with a Smithells tube. Both the annular gas stream and the Smithells tube are devices to exclude ambient air from the environs of the burner port. The influences on flame stability of various shielding gases are compared and discussed, and the effect of changes in the flow rates of the various shielding gases are described.

Comparison of stability data from shielded burners—*Figure 9* shows the stability limits of laminar, *iso*butane–air flames over a range of air rates on the 1·75 cm Bunsen burners shielded by a divergent conical Smithells tube of Pyrex glass, or by an annular stream of nitrogen flowing at an average velocity of 30·4 cm/sec. The abscissa gives the fuel flow rate and is a measure of the fuel requirements at the stability limits. The ordinate gives the air flow rate and is a close approximation to the relative velocities of the various mixtures because the fuel constitutes less than 6 vol. per cent of the total mixture in all instances. Burner jet velocities ranged from about 36 cm/sec to about 155 cm/sec. Within the limits of experimental

error, the results obtained with the two burners are practically identical. Similar agreement over the entire range of air rates used was obtained with ethylene–air and propane–air mixtures on the two burners.

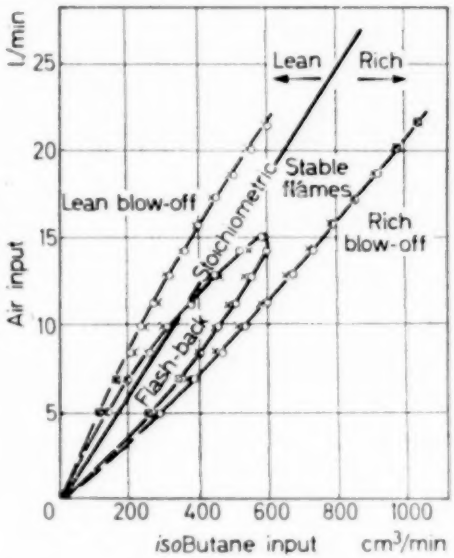

Figure 9. Stability limits of laminar isobutane–air flames over a range of air flows on 1·75 cm Bunsen burners shielded to exclude ambient air from the burner port by: × divergent Smithells tube; ○ annular stream of nitrogen

Figure 10 compares the stability limits of *iso*butane–air flames on the burner shielded by inert gas with similar data obtained when using a 7·6 cm cylindrical Pyrex Smithells tube. The results obtained with the two burners are in agreement within the limits of experimental error. The data shown in *Figures 9* and *10* indicate that, for studying the stability limits of laminar flames, a burner shielded by inert gas may be considered as satisfactory as a burner with Smithells tube.

Behaviour of helium as a shielding gas—Although nitrogen was used as the shielding gas in most of the experiments with the shielded Bunsen burner, the influence of other gases, including helium, on the stability limits

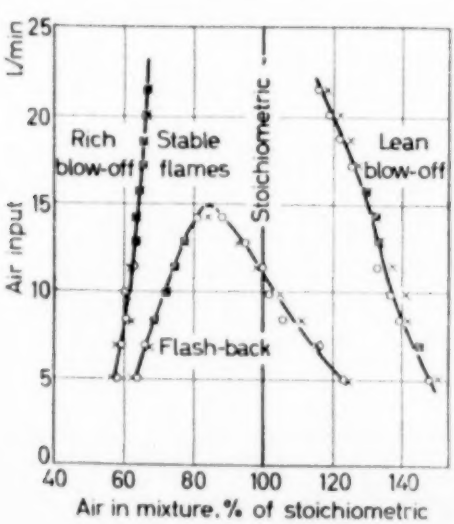

Figure 10. Stability limits of laminar isobutane–air flames over a range of air flows on a 1·75 cm Bunsen burner shielded to exclude ambient air from the burner port by: × cylindrical Smithells tube (7·6 cm diam); ○ annular stream of nitrogen

of laminar flames has been studied. *Figure 11* compares the stability limits of *iso*butane–air flames on the 1·75 cm Bunsen burner when two different shielding gases, namely nitrogen and helium, flowing at 30·4 and 31·1 cm/sec respectively, are used.

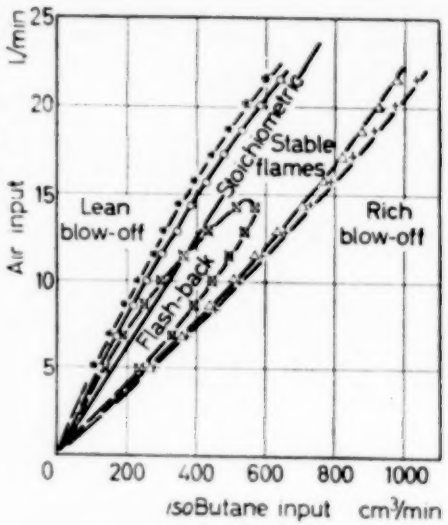

Figure 11. Stability of isobutane–air *flames over a range of air rates on a 1·75 cm Bunsen burner using nitrogen and helium as shielding gases to exclude ambient air from the burner port*

	Stability limit	*Shielding gas*
•	*lean blow-off*	*nitrogen*
○	*lean blow-off*	*helium*
×	*flash-back*	*nitrogen*
□	*flash-back*	*helium*
+	*rich blow-off*	*nitrogen*
△	*rich blow-off*	*helium*

It is evident that helium narrows the limits of both lean blow-off and rich blow-off, but has the same influence on flash-back as does nitrogen. The influence on the blow-off limits is understandable as helium diffuses much more rapidly than nitrogen, and so can diffuse readily below the burning cone and pass into the unburnt fuel–air mixture at the critical region at the base of the flame, thereby promoting blow-off. Near flash-back, the flame rests essentially on the burner port, thereby excluding helium or any other enveloping gas from the unburnt mixture, and so helium does not influence flash-back any more than nitrogen.

Several experiments with helium as the shielding gas at various annular

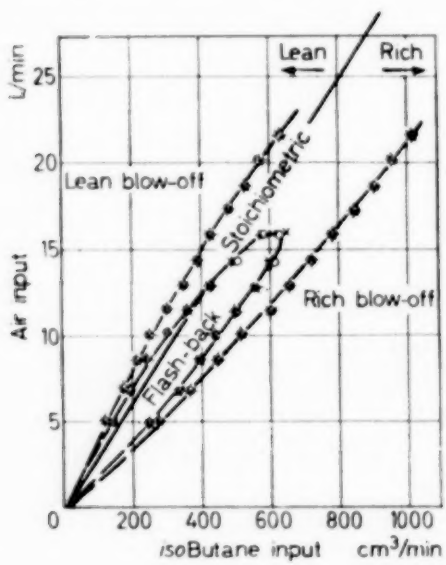

Figure 12. Stability limits of iso*-butane–air flames on a 1·75 cm Bunsen burner at three rates of flow of helium as the shielding gas: + 31·1 cm/sec; ○ 53·9 cm/sec; × 80·6 cm/sec*

velocities showed that, within the range studied, velocity had no influence on the blow-off limits. This is illustrated in *Figure 12* for helium velocities ranging from 31 cm/sec to about 81 cm/sec and having essentially the same influence on the blow-off and flash-back stability limits of *iso*butane–air flames on a 1·75 cm Bunsen burner. On the other hand, it will be shown in the next section that, when other gases denser than helium are used, changes in the flow rate of the shielding gas cause changes in the lean blow-off limit. The flash-back and the rich blow-off limits are not affected by nitrogen to a measurable extent by changes in the annular stream velocity in the range studied.

Influence of annular stream velocity—Figure 13 shows the influence of nitrogen at several annular velocities on the stability limits of laminar *iso*butane–air flames over a range of air rates on the 1·75 cm Bunsen burner.

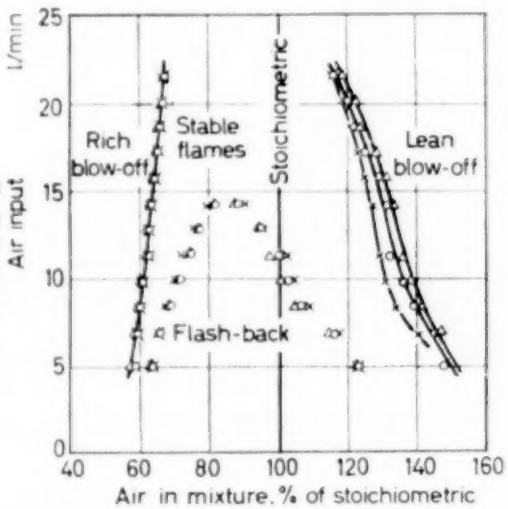

Figure 13. Stability limits of laminar iso*butane–air flames on a 1·75 cm Bunsen burner at three rates of flow of nitrogen as shielding gas: × 11·8 cm/sec; ○ 30·4 cm/sec; △ 50·6 cm/sec*

The rich limit is unaffected by the velocity of the nitrogen stream. The flash-back limit is influenced only slightly, and mostly so only on the lean side of the maximum point of the flash-back peninsula. It is concluded that, in general, the flash-back limit is not changed by changes in the stream velocity of the nitrogen. However, the lean blow-off limit is influenced by the nitrogen velocity, being widened as the nitrogen velocity is increased from about 12 cm/sec to about 30 cm/sec, and is widened slightly more as the annular velocity is increased further to about 51 cm/sec.

Figure 14 compares the stability limits of *iso*butane–air flames on the 1·75 cm Bunsen burner with and without a flow of shielding gas (nitrogen). With no shielding gas the flame burns in ambient, essentially quiescent, air which may be entrained by the jet issuing from the burner. The admixture of diluent air increases the volume of the gases entering the flame front and consequently lowers the flame temperature, and as a result the lean blow-off limit is narrowed in relation to the limit for the flame enveloped by flowing nitrogen.

When nitrogen is flowing around the flame, entrainment is decreased i comparison to ambient air inasmuch as the main velocity component of th inert gas stream is parallel to the main component of the jet issuing fro the burner. Accordingly, the lean blow-off limit of the nitrogen-shielde flame is wider than the lean blow-off limit of a flame entraining an ambie atmosphere which has no directed velocity.

It has been shown by the data presented in *Figue 11* that at flash-bac dilution of the unburnt mixture by entrainment is unlikely, and, i consequence, the cooling effect exerted on flames at flash-back by th enveloping gas or gases may be presumed to be external only. It seem reasonable to assume that ambient air does not carry away as much hea as does a flowing stream of gas surrounding the flame, and so the flash-back peninsula is slightly wider and higher when the flame is burning in ambien atmospheric air than when it is burning in a flowing envelope of nitrogen.

Conversely, a flowing stream may be assumed to carry away more hea from the flame cone by external cooling than will an ambient, quiescent

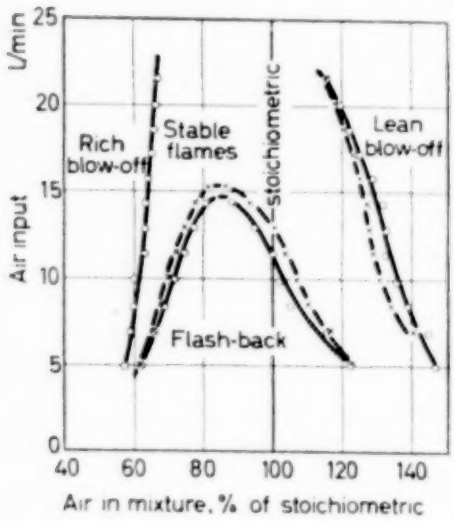

Figure 14. Stability of limits of laminar isobutane–air flames on a 1·75 cm Bunsen burner with and without a shield of inert gas

Shielding gas	*Velocity of shielding gas*
× *ambient air*	*random*
○ *nitrogen*	*30·4 cm/sec*

atmosphere, hence a narrower and lower flash-back peninsula is obtained for a flame burning in an envelope of flowing nitrogen than for a flame burning in ambient air, as shown in *Figure 14*.

Rich blow-off cannot be observed in a laminar flame burning in ambient air. The rich blow-off curve shown in *Figure 14* is for nitrogen-shielded flames.

Gas-shielded propane flames—Figure 15 shows the influence of the velocity of an annular stream of nitrogen on the lean blow-off limits of laminar propane–air flames at six burner-jet velocities on the 1·75 cm Bunsen burner. At any given jet velocity, the influence of increasing the annular velocity of nitrogen is to widen the lean blow-off limit.

Figure 16 shows similar data obtained when air was used as the 'shielding' gas. As was shown for nitrogen, the influence of increasing the velocity of the air stream in the annulus is to widen the lean blow-off limit at any given burner-jet velocity.

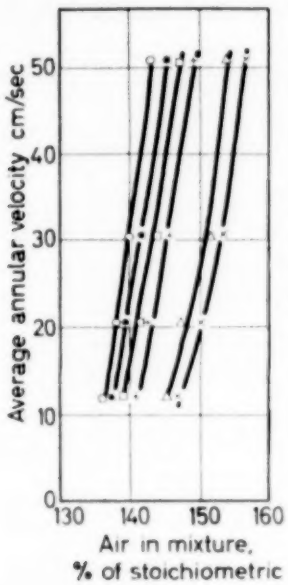

*Figure 15. Influence of velocity of annular nitrogen stream on lean blow-off limit of laminar propane–air flames at six burner-jet velocities on a 1·75 cm Bunsen burner. Average velocity at burner port, cm/sec: × 36·5; △ 49·5; + 61·0; □ 71·5; * 82·0; ○ 92·5*

Figure 17 compares the influence of the velocity of nitrogen and of air in the annular stream on the lean blow-off limits of propane–air flames on the 1·75 cm Bunsen burner. It is concluded that as the velocity of the annular stream is increased, the blow-off limit is widened because less of the gas surrounding the flame can be entrained by the gases issuing from the

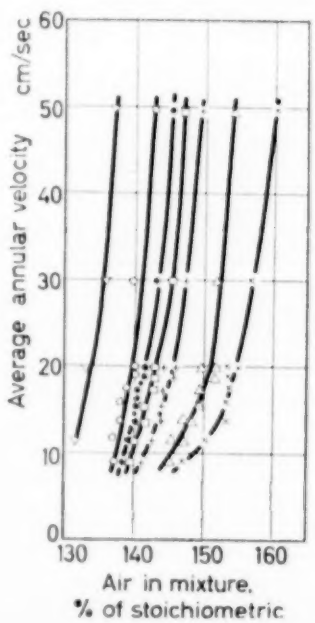

*Figure 16. Influence of velocity of annular air stream on lean blow-off limit of laminar propane–air flame at seven burner-jet velocities on a 1·75 cm Bunsen burner. Average velocity at burner port, cm/sec: × 36·5; △ 49·5; + 61·0; □ 71·5; * 82·0; ○ 92·5; ▽ 155·5*

burner jet. It appears that the effect is predominantly a thermal one as, at the higher annular velocities, less 'diluent' is entrained into the primary mixture issuing from the burner jet, and so the flame temperature is higher

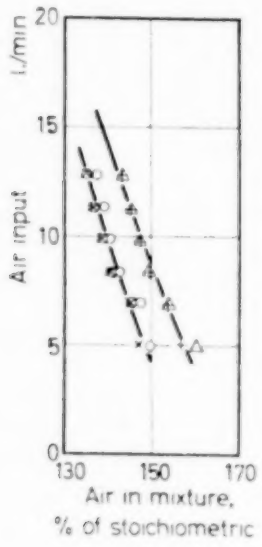

Figure 17. Influence of velocity of nitrogen and of air in the annular stream on the lean blow-off limits of propane–air flames on a 1·75 cm Bunsen burner

	Shielding gas	*Velocity of shielding gas, cm/sec*
×	*nitrogen*	*11·8*
+	*nitrogen*	*50·6*
○	*air*	*11·6*
△	*air*	*49·7*

than when the annular stream has a lower velocity, and the lean limit is thereby extended.

DISCUSSION

The results pertaining to the influence of burner diameter on blow-off show the capabilities and the limitations of burners of various diameters in stability studies with and without devices to exclude ambient air partially or totally. These results also show that the blow-off limits of shielded as well as unshielded flames are independent of burner diameter when they are related to the critical velocity gradient. This is similar to the findings of Lewis and von Elbe[3] with unshielded flames, upon which work they based the concept of using the critical velocity gradient to correlate stability data.

The blow-off limits of completely unshielded flames burning in ambient air on different burners show appreciable departures from the correlation curve only when flow conditions on the individual burners tend towards turbulence. Such deviations are to be expected as the flame configuration changes and the limit data are no longer directly comparable to data for essentially non-changing laminar flames.

A comparison of the blow-off curves for shielded and unshielded flames clearly shows the marked influence of the absence or presence of ambient air around the flame. With shielded flames, the blow-off curve reaches a maximum at $g = 1525$ sec^{-1}, so that any methane–air mixture flowing through a Bunsen tube of any diameter under conditions where g exceeds about 1525 cannot be stabilized on a shielded burner at room temperature. However, when the flame burns unshielded in ambient air, the 'pilot' action of the diffusion flame resulting from the combustion of the unburnt combustibles from the primary flame cone with entrained ambient air is capable

of stabilizing flames under conditions of flow and composition which cannot be obtained with shielded flames. Hence, the blow-off curve for unshielded flames approaches a maximum at a constantly decreasing rate but never achieves the maximum.

The stability limits observed with the burner shielded by flowing gas are essentially the same as those obtained on a burner fitted with a Smithells tube to exclude ambient air. This appears reasonable because the primary action of the shielding devices is to exclude ambient air from the environs of the flame.

A study of the influence of various gases as the shielding stream showed that helium narrows the lean and rich blow-off limits, but influences flash-back to the same extent as nitrogen. In the range from 31 to 81 cm/sec, the flame-stability limits are independent of the velocity of helium in the annulus. It appears that this increase of about two and a half times in annular velocity has no significant influence on the diffusion rate of the helium, so it is probable that an increase in annular velocity substantially larger than two and a half times would be required for helium to produce an effect similar to those achieved with air and nitrogen at different annular velocities.

At lean and rich blow-off, the behaviour of air and nitrogen, when used as shielding gases, differs from that of helium. An increase in the flow of nitrogen in the annulus widens the lean blow-off limit, but does not affect the flash-back and rich blow-off limits to a measurable extent. A stream of air in the annulus influences the lean blow-off limit in the same manner and to the same extent as does nitrogen. This seems reasonable because the molecular weights and diffusion coefficients of air and nitrogen are nearly the same.

It is concluded, therefore, that the shielding gases are entrained by the unburnt gases issuing from the burner jet. The extent of entrainment appears to be a function of (*1*) the burner-jet velocity—lean limit narrows as the jet velocity is increased because of increased entrainment, (*2*) the annular-jet velocity—at a given jet velocity the lean limit is widened as the annular velocity is increased because of decreased entrainment and (*3*) the density of the shielding gas—the lighter gases diffuse more rapidly and are more easily entrained, thus narrowing the blow-off limits. The influence of entrained, inert gases on the lean and rich blow-off limits can only be thermal in character because these gases do not change the stoichiometry. Accordingly, the inert gases behave solely as diluents, absorb heat and affect the limits according to their concentrations (which, at a given jet velocity, are a function of their diffusion rates) and to their heat capacities. At lean blow-off, it has been shown that air streams and nitrogen streams have the same influence on the blow-off limit. This indicates that the influence of flowing air on the lean blow-off limit, where the flame contains surplus oxidant delivered in the primary mixture, is essentially a thermal one and not a matter of changing the stoichiometry of the system. This is to be expected, provided the influence of diluting lean-limit mixtures with air is essentially a thermal effect, which it appears to be

as air and nitrogen have practically the same heat capacities and diffuse at almost identical rates.

Near the flash-back limit, the 'dead space', i.e. the space between the top of the burner and the base of the flame cone, becomes very small and approaches 'zero', and dilution of the primary mixture by entrainment is small. It is likely that the flowing gases surrounding the flame cause only a superficial external cooling of the flame. The essentially identical influence of helium and nitrogen envelopes on the flash-back limits of *iso*butane flames shows that the small cooling effect is independent of the diffusion properties of the enveloping gas.

At rich blow-off, increasing the annular velocity of helium about two and a half times does not appear to influence the blow-off limit. Likewise, when nitrogen is the shielding gas, an approximately fourfold increase in annular velocity does not change the rich blow-off limit observed with this enveloping gas. However, when helium is used in place of nitrogen as the shielding gas, the rich blow-off limit is narrowed significantly, and this is attributed to the ease with which helium diffuses as compared with nitrogen. It is concluded that the rich blow-off limit is not as sensitive to the velocity of the enveloping gas as is the lean blow-off limit, but that nevertheless the rich limit can be displaced toward the stoichiometric point if a shielding gas with a low molecular weight is used.

This work was carried out under the sponsorship of the Chemistry Research Branch, Aeronautical Research Laboratory, Wright Air Development Center, Wright-Patterson Air Force Base, Ohio.

The author wishes to express his thanks to Mr W. B. Thompson and Mr R. E. Poling for ably and faithfully assisting in the experimental work, and to Dr J. F. Foster, Division Chief at the Battelle Memorial Institute, for his helpful interest.

Battelle Memorial Institute,
Columbus, Ohio

(Received July 1956)

REFERENCES

[1] SMITHELLS, A. and INGLE, H. *J. chem. Soc. (Trans)* 61 (1892) 204

[2] KURZ, P. F. *Industr. Engng Chem.* 46 (1954) 746

[3] LEWIS, B. and VON ELBE, G. *J. chem. Phys.* 11 (1943) 75

[4] GRUMER, J., HARRIS, M. E. and SCHULTZ, H. *Industr. Engng Chem.* 47 (1955) 176

Mixing and Combustion in Free and Enclosed Turbulent Jet Diffusion Flames

P. D. SUNAVALA, C. HULSE and M. W. THRING

Experimental results of the concentration of nozzle fluid along the axis of the free jet can be expressed by the formula $1/C_m = 0{\cdot}22(x/d_0) - 1{\cdot}5$. *When the nozzle fluid is at a different temperature to the surrounding fluid the curves can be made to coincide with isothermal ones provided the jet diameter is replaced by an equivalent diameter* $d_0(T_a/T_0)^{\frac{1}{2}}$ *and experimentally this theory is found to be correct. Apart from a pressure effect which is not yet fully elucidated the half-jet angle is found to be independent of temperature and pressure of the jet nozzle at 6·45 degrees. When the free jet is actually burning, the concept of the equivalent nozzle diameter still gives a reasonable account of the effect of combustion. When the jet is enclosed by a comparatively large chamber, the dimensions of this chamber (l) and the proportion of air available become significant parameters, but if the mixing results are plotted in the form of* $(1/c_m)(d'_0/l) = \S(x/l)$ *then they become a set of curves with the single parameter* $(1/C_\infty)(d'_0/l)$ *where* C_∞ *is the concentration of burner fluid after it is completely mixed. The present experimental work shows that for high values of this parameter mixing can actually be faster over a certain portion of the distance than it is with a free jet.*

TURBULENT jet diffusion flames are used in both liquid and gaseous fuel fired open hearth furnaces, in cement kilns and in boilers. The rate of heat liberation along the flame depends on the entrainment of combustion air which arises from the energy of the jet.

Industrial flames are of the enclosed jet type: a high velocity jet, consisting either of fuel or of a mixture of fuel and atomizing agent, is projected into a surrounding stream of relatively slow-moving air contained in a suitable combustion chamber. The flow pattern is usually complicated by the effects of recirculation of combustion products. Recirculation takes place when the jet fails to fill completely the chamber by the time all the combustion air is entrained. Nevertheless, the behaviour of the early stages of the jet is closely similar to that of a free jet, and a knowledge of the properties of the latter is useful in predicting the effects of changes in the design variables of the nozzle. Moreover, the relatively easily studied free jet forms a useful standard with which to compare the performance of jets of the enclosed type.

This paper is accordingly concerned with a number of theoretical aspects of both free and enclosed jets, as well as an account of experimental work in which both isothermal and hot jets, with respect to the surrounding air, were used.

EXPERIMENTAL TECHNIQUES

As will be seen in a later section, the radial spread of both nozzle fluid concentration and temperature in a jet are identical and hence the axial

decay of these properties becomes identical if appropriate corrections are applied for temperature and density effects. Accordingly, it is possible to investigate mixing in a model, either by determining the variation of concentration of a suitable trace material mixed with the nozzle fluid, or, alternatively, by heating the nozzle fluid and determining the spatial variation of temperature. Both techniques were used in the present work.

Four nozzle sizes, of diameter $\frac{3}{16}$ in., $\frac{1}{4}$ in., $\frac{5}{16}$ in. and $\frac{3}{8}$ in., were used. In the concentration experiments, the technique was similar to that used by R. D. COLLINS and J. D. TYLER[1], except that the tracer gas added to the air supply representing the burner fluid was nitrous oxide. Analysis of samples drawn continuously through a probe of 1 mm bore was carried out by means of an infra-red gas analyser. The air supply to the burner and, in the enclosed jet experiments, the combustion air supply were measured by means of calibrated orifice plates; a rotameter was used to measure the nitrous oxide.

In the experiments involving the use of heated air, the air temperature measurements were made with chromel–alumel thermocouples with a linear e.m.f./temperature characteristic in the range involved. The thermocouple outputs were measured with a precision potentiometer. Differential thermocouples were used, thereby enabling the ratio of the differences $T_m - T_a$ and $T_o - T_a$ to be determined as a ratio of two potentiometer readings, where T_o and T_a are absolute temperatures of nozzle fluid and surrounding fluid, °K, and T_m is the temperature at point P_o. Values of $T_o - T_a$ up to 320° C were employed.

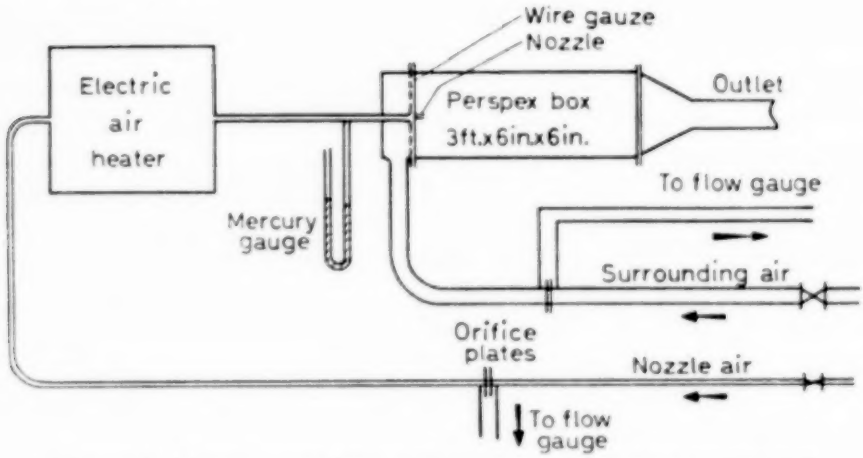

Figure 1. Diagrammatic layout of apparatus for hot jet experiments

In the enclosed jet work, the chamber consisted of a 3 ft long × 6 in. square Perspex box. Fine wire mesh was provided at the inlet end in order to ensure uniform distribution of the combustion air, and the jet tube protruded along the axis of the box for a distance of 1 in. beyond the wire mesh. Sets of small holes, transverse to the box axis, were provided at 2 in. intervals along the length of the box for probing. The outlet end of the box was connected to a 2 in. diameter exhaust pipe. A line diagram of the apparatus is shown in *Figure 1*.

Nomenclature

The following nomenclature is used:

- x distance along the axis of the jet from jet mouth O to points P and P_0. P_0 is on the axis
- x_{00} distance along the jet where its boundary strikes the walls
- y perpendicular distance to axis of the jet from point P
- η $=r/x$
- η_0 value of η at the boundary of the jet where $u=0$
- θ angle between OP and OP_0 ($\tan\theta=\eta$)
- u, u_m velocity parallel to the axis at P and P_0 at the same value of x respectively
- C, C_m mol. concentration of nozzle fluid in the mixture at P and P_0 respectively
- C', C'_m mass concentration of nozzle fluid in the mixture at P and P_0 respectively
- C'_T stoichiometric mass concentration of nozzle fluid
- $f_1(\eta)$ radial distribution function of jet fluid concentration $=C/C_m$
- $f_2(\eta)$ radial distribution function of velocity $=u/u_m$
- l characteristic length of system, for a cylindrical chamber $l=$ radius, for a square chamber $l=$ half the length of the side
- M_0 mass flow rate of nozzle fluid
- M_a mass flow rate of surrounding fluid
- M_E mass of surrounding fluid entrained by jet between nozzle and x_{00}
- ρ_0, ρ_a n.t.p. densities of nozzle fluid and surrounding fluid
- ρ'_f density of flame gases at their actual temperature—in models ρ'_f taken as equal to ρ'_a
- ρ'_0 density of nozzle gases at their actual temperature—rate of velocities v_a/v_0.

Free jets

With a free jet, unlimited fluid is available for entrainment. Using the method of H. C. HOTTEL[2] whereby the reciprocal of the jet fluid concentration along the axis of the jet is plotted against the distance along the axis in nozzle diameters, a curve is obtained which approximates after a short distance to a straight line. As discussed in a previous paper[3] the slope of this line is directly related to the angle of spread of the jet by the laws of conservation of momentum and of jet fluid.

Isothermal free jets—When the jet fluid and surrounding medium have the same density and temperature the relationship is given by

$$1/C_m = 1/C'_m = 2(K_{12}/K_{22}^{\frac{1}{2}})(x/d_0) \qquad \ldots.[1]$$

where d_0 is the true nozzle diameter and in which K_{12} and K_{22} depend on the radial distribution within the jet of jet fluid concentration and velocity

respectively, and are given by

$$K_{12} = \int_0^\infty 2\eta f_1(\eta) f_2(\eta)\, d\eta$$

$$K_{22} = \int_0^\infty 2\eta f_2^2(\eta)\, d\eta$$

Empirically it is found that beyond about 6 to 8 diameters downstream from the nozzle an approximately linear relationship is obtained between $1/C_m$ and x/d_0, showing that for these conditions the jet angle and K_{12} and K_{22} of equation 1 are constant.

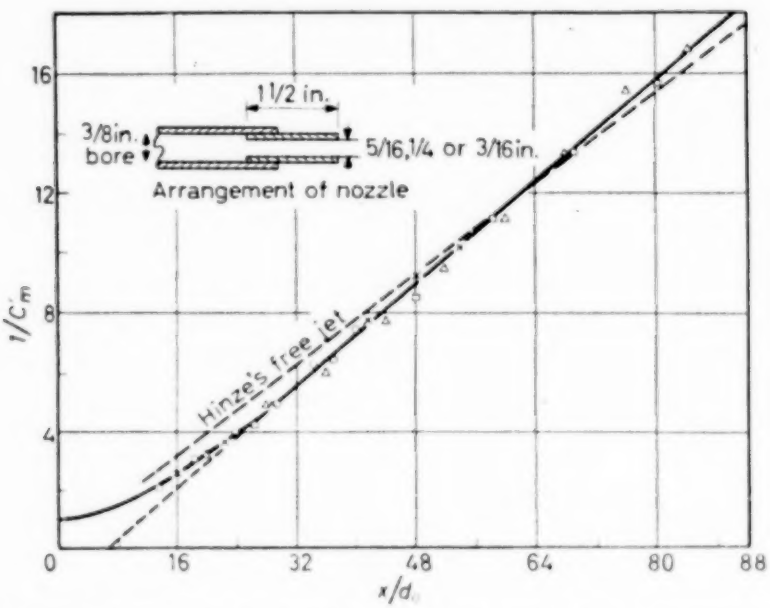

Figure 2. Concentration results, isothermal conditions, low pressure jets

Axial decay concentration results obtained by P. D. SUNAVALA are shown in *Figure 2* in comparison with the results of J. O. HINZE and B. G. v.D. H. ZIJNEN[1]. The jets were operated at low pressure, operational data being given in *Table 1*.

Table 1. Experimental conditions—isothermal free jets

Jet diameter	$\frac{3}{16}$ *in.*	$\frac{1}{4}$ *in.*	$\frac{5}{16}$ *in.*	$\frac{3}{8}$ *in.*
Velocity ft/s	520	294	187	131
Reynolds number	56900	42900	34200	28700

It will be seen that the present data differ slightly from Hinze and Zijnen's results. In the region where the relationship is linear the results of the latter may be represented by

$$1/C_m = 0{\cdot}19\,(x/d_0) + 0{\cdot}15 \qquad \ldots\ldots [2]$$

and the data of Sunavala by

$$1/C_m = 0{\cdot}22\,(x/d_0) - 1{\cdot}5 \qquad \ldots . [3]$$

Except for points near the origin, equation 3 represents the experimental data to an accuracy of ± 5 per cent. Non-linearity near the origin is to be expected since (*i*), as discussed by W. R. HAWTHORNE, D. S. WEDDELL and H. C. HOTTEL[5], the concentration on the axis remains at the value unity for a short distance downstream from the nozzle and (*ii*) a further distance downstream will be required before the constancy of the radial spread functions of concentration and velocity have been established.

It is possible that the differences in equations 2 and 3 may be due to differences in the Reynolds number or to the fact that Hinze and Zijnen's results were obtained with an orifice of tube ratio 3: 1, whereas the jet tubes employed in the present work were of uniform bore. The slope of 0·22 is in good agreement with the reported data[3].

Effect of jet pressure—The results discussed above were obtained for conditions in which the nozzle pressure, as measured 8 in. behind the outlet, was only slightly above atmospheric pressure. If the nozzle pressure is high so that the jet approaches or exceeds a Mach number of unity then the true nozzle diameter, d_0, must be replaced by an equivalent nozzle diameter d_0', as discussed by M. W. THRING and M. P. NEWBY[3], where d_0' is the diameter of the nozzle through which nozzle fluid would flow at mass rate M_0 and with momentum G_0 but with density ρ_f' instead of ρ_0'.

Non-isothermal free jets—Results obtained with low pressure jets of hot air, in which axial mixing was assessed by means of temperature measurements, are shown in *Figure 3*. The conditions for the experiments were as given in *Table 2*.

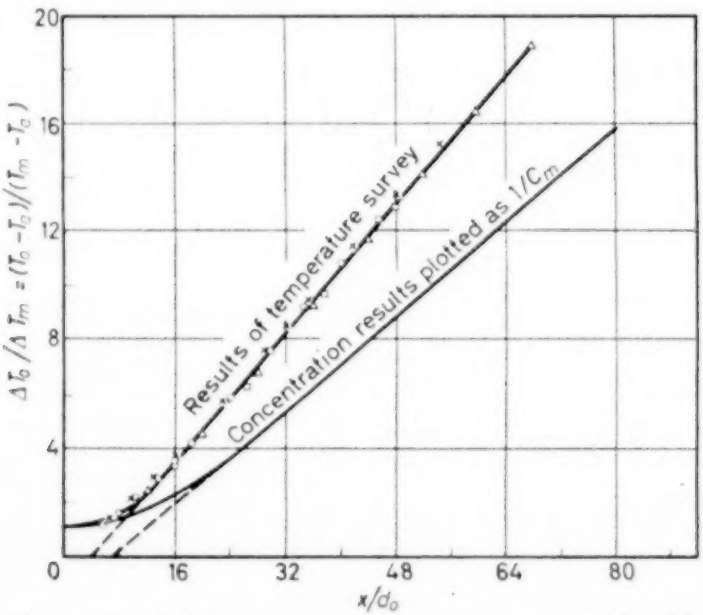

Figure 3. Axial decay of temperature compared with concentration results

A line corresponding to the concentration results of *Figure 2* is also given in *Figure 3*. It will be seen that, as predicted[3] by Thring and Newby, the slope of the hot jet line is greater than that for concentration. Moreover, if the hot jet results are corrected on the basis of the ratio $(T_a/T_0)^{\frac{1}{2}}$, for low jet pressures, they become identical with those for concentration. This is shown in *Figure 4*, in which experimental points for $\Delta T_0/\Delta T_m$ are compared with axial concentration decay.

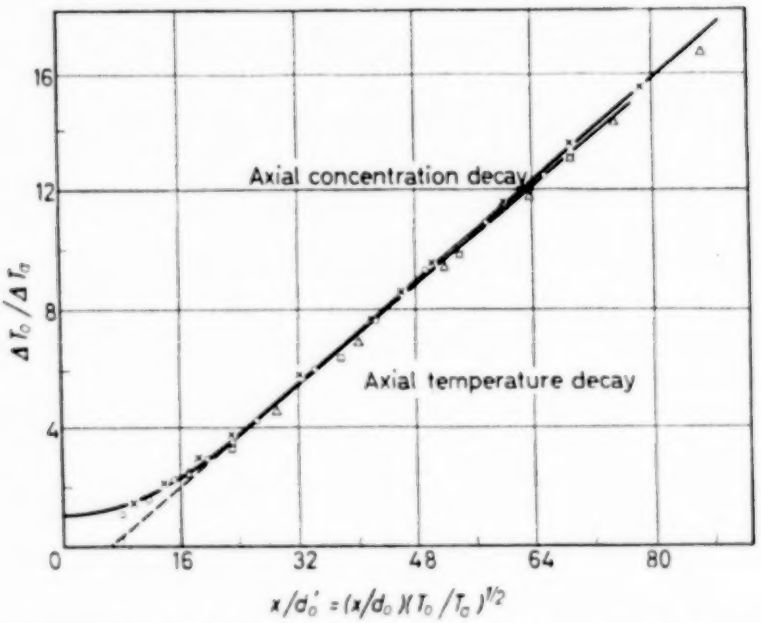

Figure 4. Axial decay of temperature plotted in terms of equivalent nozzle diameter [$=d_0(T_a/T_0)^{\frac{1}{2}}$ in this instance] for low nozzle pressures

The best line drawn through the temperature data has the equation

$$\Delta T_0/\Delta T_m = 0{\cdot}215\,(x/d_0') - 1{\cdot}5 \qquad \ldots . [4]$$

in which

$$d_0' = d_0(T_a/T_0)^{\frac{1}{2}}$$

Equation 4 is not significantly different from equation 3 for the concentration results.

The points for the $\frac{5}{16}$ in. and $\frac{3}{8}$ in. diameter nozzles are almost exactly correlated by the concentration decay line, but the results for the smaller nozzles are up to 6 per cent low. Further, *Table 2* shows that the nozzle

Table 2. Experimental conditions—non-isothermal free jets, low pressure

Jet diameter	$\frac{3}{16}$ *in.*	$\frac{1}{4}$ *in.*	$\frac{5}{16}$ *in.*	$\frac{3}{8}$ *in.*
Jet fluid temperature	320°C *above ambient* (25°C) *throughout*			
Velocity ft/s	750	490	480	450
Reynolds number	20500	17900	21900	24600
Jet pressure in. Hg gauge	5·2	2·55	1·85	0·25

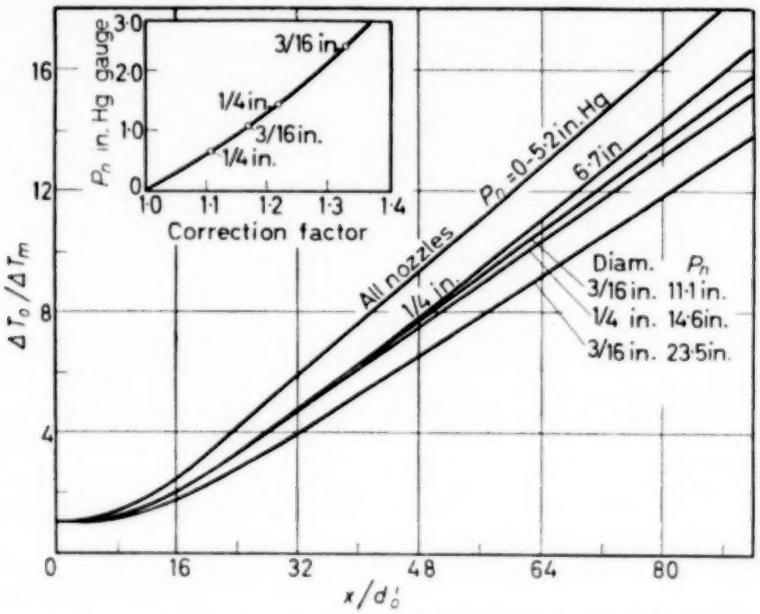

Figure 5. Axial decay of temperature at various nozzle pressures

pressures were somewhat greater for the smaller nozzles, particularly for the smallest. Experimental data for a series of nozzle pressures, P_n, up to 23·5 in. Hg gauge are shown in *Figure 5*. To avoid confusion experimental points are not shown; the curves represent the data to an accuracy of better than ±5 per cent. The experimental conditions and resultant slopes as obtained from *Figure 5* were as shown in *Table 3*.

Table 3. Non-isothermal free jets, various pressures

Nozzle size in.	*Mass flow rate lb./h*	*Velocity at jet outlet ft/s*	*Pressure behind jet in. Hg gauge*	*Slope as in Figure 5*
	18·9	750	5·2	0·213
3/16	23·9	950	11·1	0·186
	39	1550	23·5	0·167
	21·9	490	2·5	0·213
1/4	35·8	800	6·7	0·196
	55·5	1250	14·6	0·174
5/16	33·6	480	1·8	0·213
3/8	45·5	450	1·0	0·213

It would seem that the nozzle pressure, or some factor dependent thereon, has an effect on the axial decay of temperature, the rate of decay diminishing as the pressure is increased. The reason for this has not as yet been elucidated; if it were due to pressure/density effects at the point where the nozzle fluid emerges from the jet tube this would require the density of the nozzle fluid at this point to be greater than that calculated on the basis of the ambient pressure; that is, the static pressure in the region of the nozzle outlet would be greater than atmospheric. It is thought that further work in which the thrust on the nozzle is measured experimentally, so that a check may be obtained on the actual momentum flux developed by the jet

fluid, may enable this problem to be solved. An empirical correction factor for the slopes of the axial decay lines at the various pressures, correct to 4 per cent, is shown in *Figure 5*. It will be seen that the correction factor is shown to vary nearly linearly with P_n; equal accuracy would be obtained if it was made proportional to P_n^2.

The main conclusion of this section is that for low nozzle pressures the axial decay relationships for both temperature and concentration are the same, provided that the former are corrected on the basis of the use of d_n' instead of d_n. The result is of importance in the use of models. It is frequently found to be easier to study temperature distributions rather than concentration, using a tracer. The use of equation 4 enables mixing to be predicted on the basis of measurements, in the model, of axial temperature decay; at the same time it provides a means of ensuring similarity between model and original.

Constancy of the jet angle—Formula 1 can result in a linear relationship between $1/C_m$ and x/d_n only when K_{12} and K_{22}, and hence the jet angle, are constant. Where the nozzle fluid has a temperature or n.t.p. density different from the surroundings a linear relationship should still be expected provided that (*i*) the right hand side is multiplied by the factor $(\rho_f'/\rho_a')^{\frac{1}{2}} = [(\rho_n/\rho_a)(T_a/T_n)]^{\frac{1}{2}}$, and (*ii*) the jet angle remains unaltered. The experimental data illustrated by equation 4 accordingly serve as practical verification of these theorems. Actual assessment of the jet angle in the present work was in terms of the half-jet angle, defined as the angle between the jet axis and a straight line joining points at which the jet fluid concentration has fallen to 50 per cent of the corresponding axial value. The values obtained over a wide range of jet temperature (ambient, isothermal to 320° C) and for a wide range of flow rates and nozzle sizes was constant at 6·45°. The scatter in the concentration measurements amounted to ± 10 per cent; in the experiments based on temperature measurement it was negligible.

The effect of the density of the jet has been investigated by a colleague[6], using a horizontal jet of magnetite slurry injected into a large, slowly moving mass of water in a Perspex box. The main purpose of the work was to investigate the effect of buoyancy in combustion chambers, but although density ratios, between nozzle and surrounding fluids, of up to 2·0 were used, the earlier part of the trajectory was unaffected. The half-jet angle, as defined above, was determined photographically as illustrated in *Figure 6*, and was invariably found to be 4·25°. This agrees with the value reported by A. M. BINNIE[7], but is less than the results quoted for gaseous systems by the present authors and others. The main conclusion emerging from this work was that no variation in angle was found over the range of density ratio employed.

A comparison of the half-jet angle values obtained by a large number of workers together with their values of the slope $2(K_{12}/K_{22}^{\frac{1}{2}})$, in the form of equation 1 employing d_n' instead of d_n, is given in *Table 4*.

It will be seen that the slopes and angles reported on the basis of velocity determinations are less than those for concentration and temperature,

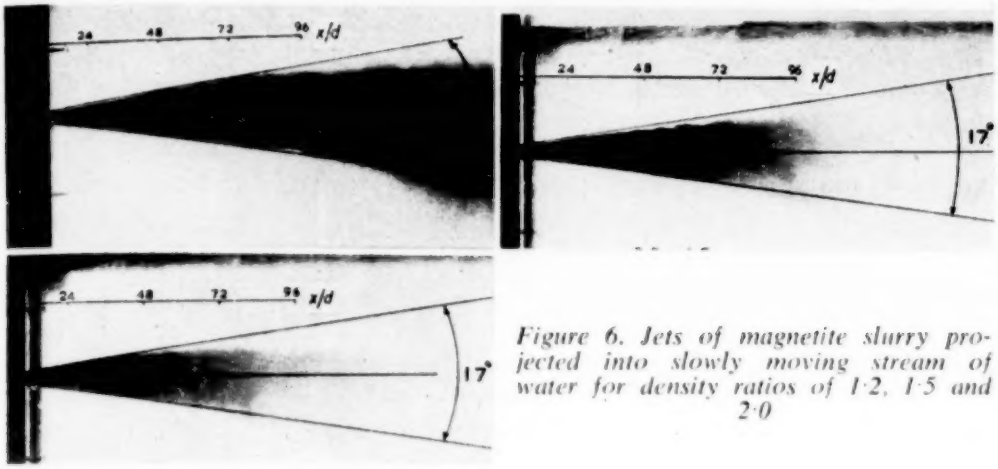

Figure 6. Jets of magnetite slurry projected into slowly moving stream of water for density ratios of 1·2, 1·5 and 2·0

supporting the generally held view that mass and temperature diffuse more rapidly than momentum. Sunavala's temperature results agree with those of H. B. SQUIRE[9], but are not altogether in accord with those of S. CORRSIN and M. S. UBEROI[16]. It is thought that the discrepancies may be associated with buoyancy effects since these workers used vertical jets. It is unfortunate too from the point of view of this comparison that W. R. KEAGY and A. E. WELLER[17], experimenting with carbon dioxide, nitrogen and

Table 4. Axial decay constants and half-jet angles in free jets

Investigator	*Velocity*		*Concentration*		*Temperature*	
	Constant	*Half-jet angle*	*Constant*	*Half-jet angle*	*Constant*	*Half-jet angle*
RUDEN[8]	0·155	5·15°			0·176(17° C)	6·65°
SQUIRE[9]	0·154	5·1°			0·21	6·7°
HINZE[4]	0·1565	5·1°	0·19	5·4°	0·19 (30° C)	5·4°
ALBERTSON et al.[10]	0·161					
FORSTALL *and* GAYLORD[11] *(water jet)*	0·161					
TAYLOR et al.[12]	0·1508					
WUEST[13] *(water jet)*	0·348					
CLEEVES *and* BOELTER[14]	0·143					
CORRSIN[15]					(10° C)	6·7°
CORRSIN *and* UBEROI[16]					(15° C)	5·7°
					(300° C)	6·9°
KEAGY *and* WELLER[17]						
Carbon dioxide		4·5°		5·2°		
Nitrogen		4·7°		6·0°		
Helium		—		9·0°		
SUNAVALA[18]			0·22	6·7°	0·22(320° C)	6·7°

helium, also used vertical jets, so that, here again, buoyancy may have affected the situation. It is noteworthy that W. R. KEAGY and H. H. ELLIS[19] using a schlieren technique found a total angle for a vertical helium jet of 21·5°, whereas Keagy and Weller[17] give a total angle of 38·6° on the basis of concentration measurements. The axial decay results of these workers are shown plotted on the basis of the density ratio correction factor in *Figure 7*. All the data, with the exception of those of V. CLEEVES and

L. K. M. BOELTER[14] (vertical jets which, in view of their low velocity an high temperature, must undoubtedly have been affected by buoyancy) fa on a band. An average line through the data has the equation

$$1/C_m = 0{\cdot}2\, x/d_0' \qquad \ldots.[5$$

and is accurate to about ± 20 per cent.

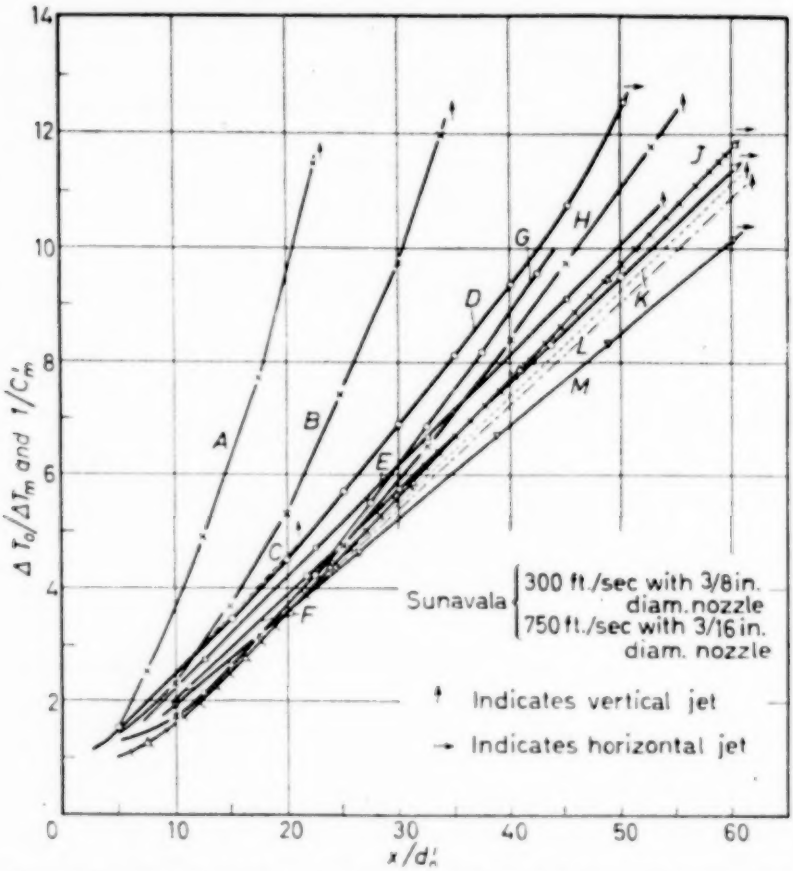

Figure 7. Data of various workers plotted on the basis of equivalent nozzle diameter, $d_0' = d_0\ [(T_a/T_0)\ (p_0/p_a)]^{\frac{1}{2}} P_c$ where P_c is the pressure correction factor, in this case equal to unity

It would seem that in spite of the somewhat conflicting evidence the general consensus is that the jet angle is approximately constant so that similarity may be applied on this assumption.

Free jet of burning town gas—Although not strictly applicable, results for turbulent diffusion flames of town gas emerging from $\frac{3}{16}$ in. and $\frac{5}{32}$ in. diameter nozzles have been treated on the basis of the density correction discussed under the heading 'Constancy of the jet angle'. As discussed in ref. 3 this correction applies on the assumption that temperature and density are nearly constant in the flame. With an open hearth furnace this assumption may not be far from the truth since the flame is in hot surroundings. With a relatively small gas flame in the open air, however, the departure in practice from this assumption might be expected to be more serious.

Nevertheless, it is apparent that the experimental points shown in *Figure 8* agree approximately with the isothermal free jet line; in fact they are, on average, about 30 per cent high. In view of the simplifying assumptions involved this must be regarded as satisfactory.

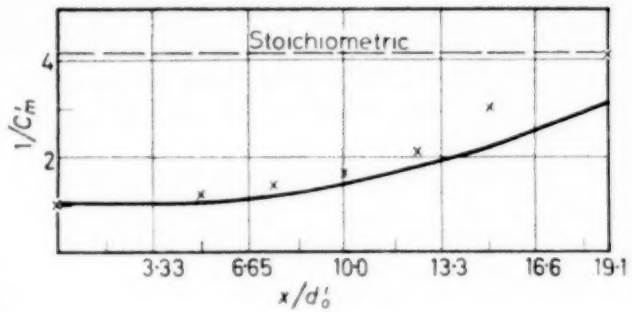

Figure 8. Axial concentration results for a town gas flame compared with isothermal model

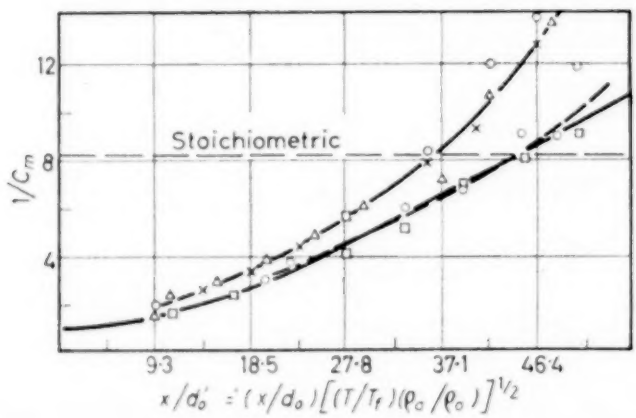

It should be noted that no account has been taken of unmixedness; $1/C_m$ values have been calculated on the basis of a hydrogen balance between the fuel and flame gases. A calculated flame length may be obtained by substituting the concentration corresponding to the stoichiometric mixture in the equation

$$1/C_m = 0{\cdot}22\,(x/d_o)\,[(T_o/T_f)\,(\rho_a/\rho_o)]^{\frac{1}{2}}$$

The stoichiometric concentration, calculated from the gas analysis, was 8·2. Corresponding calculated and observed flame lengths are as follows:

	in.	in.
Jet size	$\frac{3}{16}$	$\frac{5}{32}$
Calculated flame length	12·2	15·5
Observed flame length	10·2	14

Enclosed jets

Enclosed jets may differ from free jets for three reasons: (*i*) the quantity of entrainable fluid is limited. In practical combustion systems it is usually controlled at a value corresponding to the stoichiometric ratio; (*ii*) it is possible for the energy of the entrained air to contribute to mixing, and

(*iii*) the presence of the enclosing walls of the mixing chamber limits th expansion of the jet and may give rise to recirculation. W. FORSTALL an A. H. SHAPIRO[19] and H. B. SQUIRE and J. TROUNCER[20] have shown tha with coaxial gas streams the jet angle decreases as the flow of the surround ing fluid is increased, and at large values the jet boundary becomes curved Nevertheless, the behaviour of the type of enclosed jet considered here does conform roughly to that of an enclosed jet, subject to the three limitations mentioned above, since (*a*) in the type of practical application covered, open hearth furnaces and the like, the size of the jet nozzle is small compared with the size of the chamber, and (*b*) the surrounding fluid/nozzle fluid ratio is relatively small.

As discussed by Thring and Newby[3], it is necessary, for similarity between enclosed jets, to include a dimension characteristic of the chamber, say l the half-width. Recirculation depends on the relative values of x_{∞} and x_a, where x_{∞} is defined as the length at which a free jet boundary would hit the walls and x_a is the distance at which all the available surrounding air is entrained. If M_E is defined as the air entrainable by the jet before it strikes the walls, and the difference between the air supplied and the entrainable air, both per pound of jet fluid, is called the net air then

$$\text{net air} = M_a/M_o - M_E/M_o$$

Substitution of the axial decay equation, equation 1, with $K_{12}/K_{22}^{\frac{1}{2}}$ replaced by K gives

$$\text{net air} = M_a/M_o - Kx_{\infty}/d_o' + 1$$

$$\text{i.e.} \quad = (M_o + M_a)/M_o - (K/\tan\theta)(l/d_o') \qquad \ldots [5]$$

in which $(M_o + M_a)/M_o$ is equivalent to $1/C_{\searrow}$ and θ is the angle made by the jet boundary with its axis ($\tan\theta = \eta$).

If the net air is negative then recirculation will take place; when it is positive recirculation ceases. In the latter event it is possible for mixing to be more rapid than in the free jet. The reason for this may be visualized as follows. In a free jet a 'natural' flow pattern is set up in the surrounding fluid: air for entrainment arrives at the jet boundary at the appropriate place and time for entrainment. With an enclosed jet, however, the surrounding air would still flow even though the jet fluid were cut off. Thus, the surrounding air arriving at a given point on the jet boundary may be in excess of free jet requirements, and 'forced' mixing results.

Accordingly, to obtain similarity between enclosed jets, the concentration parameter is modified to $(1/C_m)(d_o'/l)$ and this is plotted as a function of x/l. Moreover, it is apparent that for similarity $(1/C_{\searrow})(d_o'/l)$ must also be the same, so that this factor is required as a third parameter.

Enclosed jet results are shown plotted in *Figures 9, 10* and *11*. *Figure 9* shows the relationship between $\Delta T_o/\Delta T_m$ and x/d_o' for three nozzle sizes. It is seen that as the nozzle size is increased the curve rises to higher values of $\Delta T_o/\Delta T_m$, and exceeds the values which would be obtained in a free jet. When experimental data are plotted as shown in *Figure 10*, however, the results for the different nozzle sizes are brought together. The results

for the $\frac{3}{8}$ in. nozzle appear to be slightly anomalous in this respect. This would be due to the fact that this nozzle differed from the others in that there was no insertion of smaller bore tube as shown in *Figure 2*. *Figure 10* gives results of both concentration and temperature measurements plotted on the same diagram. Up to a value of $(\Delta T_0/\Delta T_m)(d_0'/l)$ of 1·355 the curves are mutually compatible irrespective of whether based on temperature or concentration, but above this value they no longer agree. This has not as yet been satisfactorily explained.

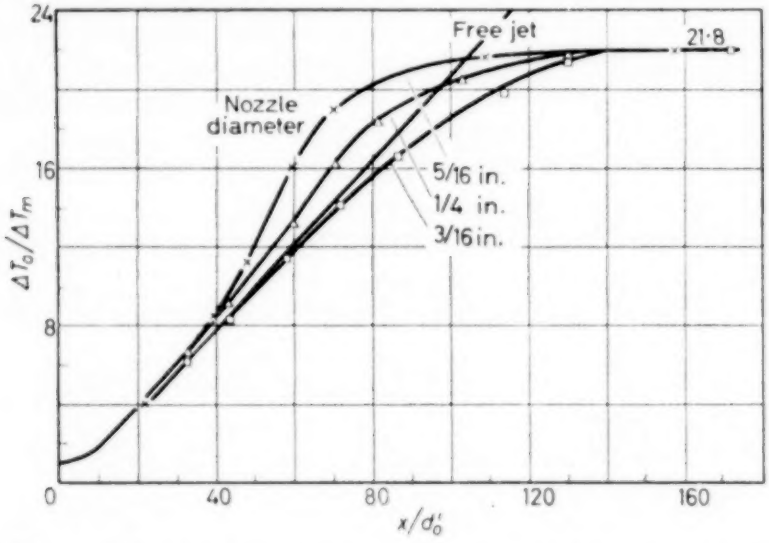

Figure 9. Enclosed jet temperature decay as a function of axial distance in equivalent nozzle diameter

Effect of high surrounding air/nozzle fluid ratios—As mentioned earlier various workers have shown that at high ratios of $\lambda = v_a/v_0$ the value of the axial decay constant and the jet angle are less than with free jets. It is possible to calculate the approximate magnitude of this effect in relation

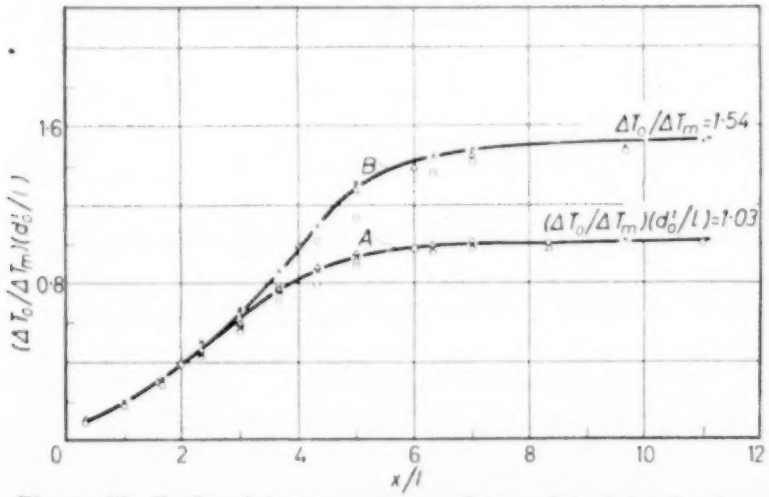

Figure 10. Enclosed jet temperature decay plotted in the form $(\Delta T_0/\Delta T_m)(d_0'/l)$ versus x/l

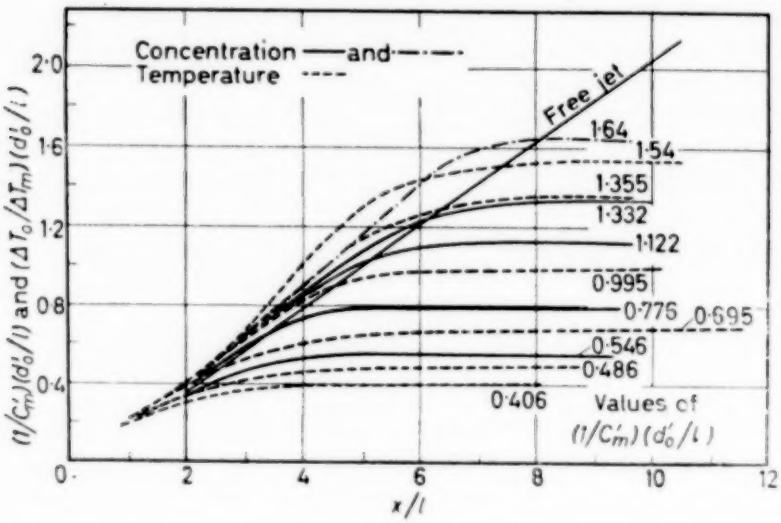

Figure 11. Concentration and temperature decay plotted as $(1/C'_m)(d_o'/l)$ *or* $(\Delta T_o/\Delta T_m)(d_o'/l)$ *versus* x/l *for a range of values of* $(1/C_\infty)(d_o'/l)$

to the present results. Calculated values of the ratio $K/\tan\theta$ based on values of K drawn from the work of Hottel[2] and values of $\tan\theta$ given by Squire and Trouncer[22] are as follows:

λ	0	0·25	0·50
$K/\tan\theta$	1·26	2·0	3·0

Inspection of equation 5 shows that as $K/\tan\theta$ increases the net air will decrease. For similarity, however, the net air must be constant. Similarity can be preserved, therefore, by replacing the criterion $(1/C_m)(d_o'/l)$ by $(1/C_m)(d_o'/l)\,f(\lambda)$.

In the range of experimental data covered by *Figure 10* the correction factor equal to $f(\lambda)$ is small, the maximum values being 1·06 and 1·04 for the concentration and temperature results respectively.

CONCLUSIONS

The experimental data given for an isothermal free jet are in substantial agreement with the results of other workers. When the nozzle fluid has a density and temperature different from that of the entrained air, evidence is given suggesting that the jet angle and axial concentration decay constants remain unaltered, provided that an equivalent nozzle diameter is used to replace the actual diameter in the axial decay equation. Accordingly, it is possible in model work to use a hot jet and make use of temperature measurements to investigate mixing effects.

Results obtained with an actual flame differ by about 30 per cent from the values predicted, the axial decay of concentration being greater.

Enclosed jets differ from free jets since the amount of mixing possible is determined by the quantity of surrounding fluid supplied. It has been

shown that, in general, over the experimental range covered, both isothermal and hot enclosed jets are similar on a plot of

$$(1/C_m)(d_o'/l) = f(x/d)[C_\lambda(l/d_o')]$$

Where the ratio of M_o/M_o is large, the expression on the left of the above relationship should theoretically include a correction term $f(\lambda)$: in the range of experimentation covered, however, the values of $f(\lambda)$ were too small to confirm empirically.

The hot jet work reported here was carried out in the research laboratories of the United Steel Companies through the kind offices of Mr F. H. Saniter and Dr J. H. Chesters. Their help and interest are gratefully acknowledged, and also that of Dr G. R. Mattocks.

REFERENCES

[1] COLLINS, R. D. and TYLER, J. D. *J. Iron St. Inst.* 162 (1949) 457
[2] HOTTEL, H. C. *Fourth International Symposium on Combustion* p. 90 Williams and Wilkins: Baltimore, 1953
[3] THRING, M. W. and NEWBY, M. P. *Fourth International Symposium on Combustion* p. 789 Williams and Wilkins: Baltimore, 1953
[4] HINZE, J. O. and VAN DER HEGGE ZIJNEN, B. G. *Appl. sci. Res., Hague* A1 (1949) 435
[5] HAWTHORNE, W. R., WEDDELL, D. S. and HOTTEL, H. C. *Third International Symposium on Combustion* p. 267 Williams and Wilkins: Baltimore, 1949
[6] HORN, G. *Ph.D. Thesis* University of Sheffield, 1955
[7] BINNIE, A. M. *Engineering, Lond.* 153 (1942) 503
[8] RUDEN, P. *Naturwissenschaften* 21 (1953) 375
[9] SQUIRE, H. B. *Airc. Engng* 22 (1950) 62
[10] ALBERTSON, M. L., DAI, Y. B., JENSEN, R. A. and ROUSE, H. *Proc. Amer. Soc. civ. Engrs.* 74 (1948) 1571
[11] FORSTALL, W. and GAYLORD, E. W. *J. appl. Mech.* 22 (1955) 161
[12] TAYLOR, J. F., GRIMMETT, H. L. and COMINGS, E. W. *Chem. Engng Progr.* 47 (1951) 175
[13] WUEST, W. *Z. Ver. dtsch. Ing.* 92 (1950) 1000
[14] CLEEVES, V. and BOELTER, L. K. M. *Chem. Engng Progr.* 43 (1947) 123
[15] CORRSIN, S. *Tech. Note Nat. Adv. Comm. Aero., Wash. No. 3L23*, 1943
[16] CORRSIN, S. and UBEROI, M. S. *Tech. Note Nat. Adv. Comm. Aero., Wash. No. 1865*, 1949
[17] KEAGY, W. R. and WELLER, A. E. *Heat Transfer and Fluid Mechanics Institute* p. 89 Berkeley, California, Feb. 1949
[18] SUNAVALA, P. D. *Ph.D. Thesis*, University of Sheffield, to be submitted
[19] KEAGY, W. R. and ELLIS, H. H. *Third International Symposium on Combustion* p. 667 Williams and Wilkins: Baltimore 1949
[20] FORSTALL, W. and SHAPIRO, A. H. *J. appl. Mech.* 17 (1950) 399
[21] SQUIRE, H. B. and TROUNCER, J. *Aero. Res. Comm. Min. Aircr. Prod. R. & M. No. 1974*, 1944

A Law of Similarity for Temperatures in Enclosed Turbulent Flames

C. CODEGONE

A series of measurements, carried out on enclosed turbulent flames of different lengths, has shown that by adoption of suitable dimensionless parameters the behaviour of the temperatures become similar following the same analytical laws with satisfactory approximation.

COMBUSTION tests have been carried out at a laboratory of the Fiat Co. in Turin, on a Ghost type burner. Study of the experimental results has shown that the behaviour of the temperatures, measured by means of an optical pyrometer, satisfies a similarity law.

DESCRIPTION OF MEASUREMENTS

The combustion chamber was of the aircraft jet engine Ghost type (*Figure 1*) and comprised a double envelope of stainless steel, the slightly tapered

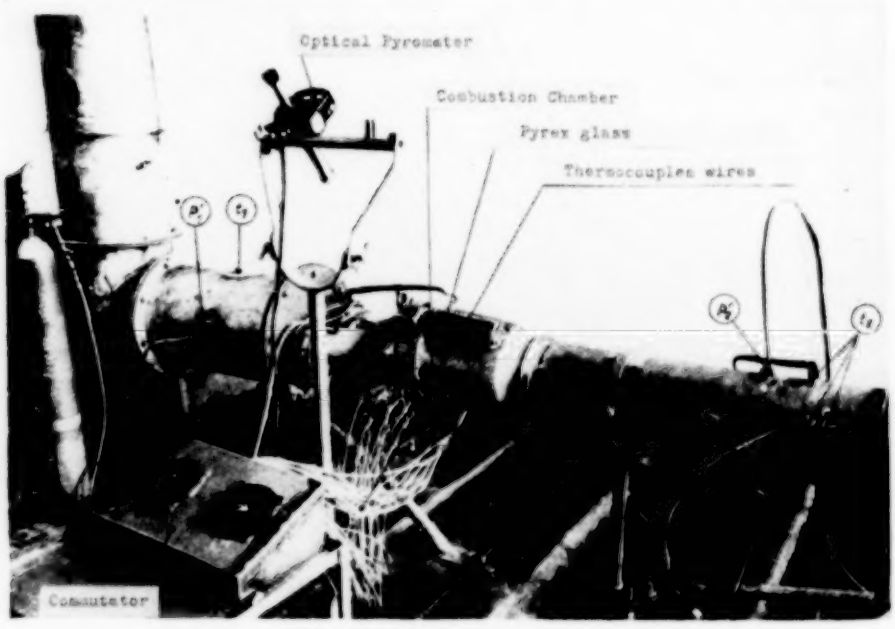

Figure 1

interior of which had an average diameter of about 23 cm. Secondary and dilution air passed through the space between the somewhat convergent external envelope and the inner envelope. Fuel consumption varied from 10 to 80 kg/h of kerosene. With regard to the latter, the amount of air (supplied by a blower) was made to vary between broad limits, the air being divided between a *primary* flow, embracing the burner itself, a *secondary* flow, filtering into a variety of small holes in the first portion of

the envelope, and a *dilution* flow pouring through the large holes of the end portion of the same envelope. Burnt gases were discharged freely to the atmosphere. Flame temperatures were measured by a Leeds and Northrup optical pyrometer of the 'disappearing filament' type, previously tested by the author at the Technical Physics Laboratory of the Turin Polytechnic School.

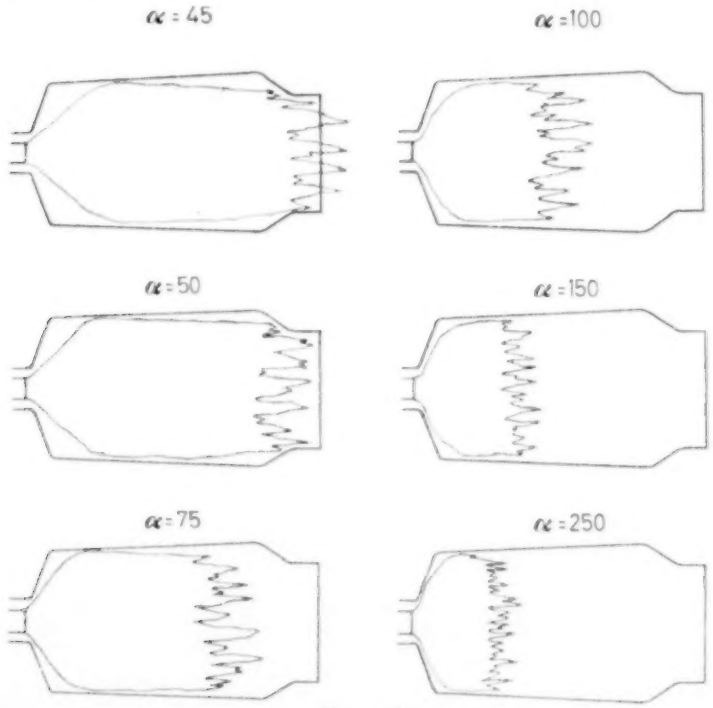

Figure 2

Small windows with Pyrex glass panes are provided to enable the operator to look through in a direction at right angles with the flame axis. These windows allowed the shape, colour and size of the flame to be observed. The absorption of the glass was taken into account in the tests. Measurements of envelope and air temperatures were taken at several points by chromel–alumel thermocouples (two rows, each of 20 couples, on the internal envelope; 6 couples on the external envelope; 6 shielded couples for the measurements in the air). Some inner reinforcing rings, which caused disturbed effects during the measurements made by thermocouples, had been removed. The overall air output G_t was measured by a Venturi meter placed within the feed pipe of the device, while some Pitôt tubes, arranged within the space between the envelopes, indicated the air flow distribution G in that space. Several experiments have been made for different combustion ratings, varying both the total air output (3000 to 4000 kg/h approximately) and the weight ratios z of air to fuel (from 45 to 300 approximately); this corresponds to a large dilution of the burnt gases.

With increasing air/fuel ratios, the flame which nearly filled the chamber became progressively shorter but terminated always in the typical turbulent notching (*Figure 2*).

EXPERIMENTAL DATA

The top section of *Figure 3* shows the results of the temperature measurements, the symbols having the following meaning:

$T_{max.}$ = maximum absolute temperature of flame (1620° K for G = 3000 kg/h; 1550° K for G = 4000 kg/h;

T = absolute temperature measured at a distance x from the burner;

l = length of flame (or, better, the length of the bright or visible portion of the flame).

Adoption of the following dimensionless parameters has enabled the results of all the experiments to be put on a single curve, which represents in effect a similarity law for the enclosed flames.

The curve following the average distribution of the points satisfies the equation

$$\frac{T-T_1}{T_{max.}} = \exp\left(-\frac{a}{x/l}\right) - \left[1-\exp\left(-\frac{bx}{l}\right)\right] \qquad \ldots\ldots[1]$$

where T_1 represents the starting absolute temperature of the supply air (comprised between 21° and 29° C), and the constants a and b have the values 0·04 and 0·3, respectively.

The lower section of *Figure 3* shows, for the absolute temperature T_p of

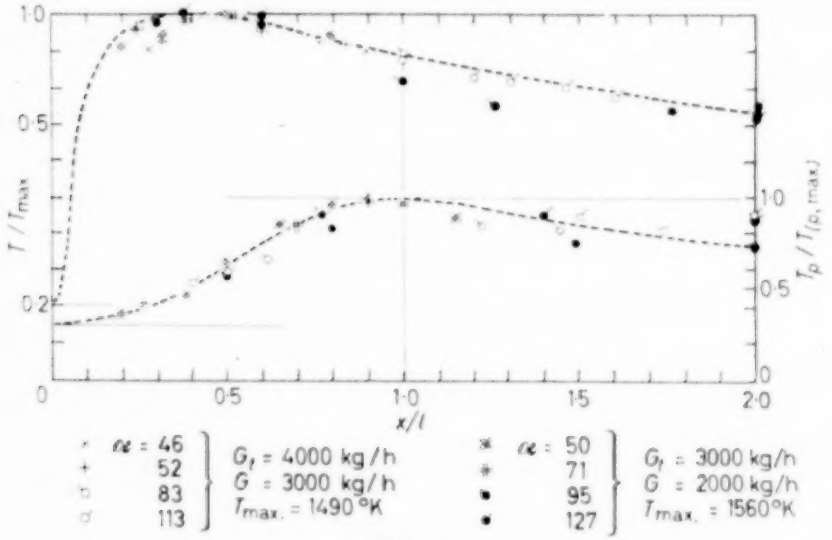

Figure 3

the walls, a behaviour similar to that of T, $T_{(p,\,max.)}$ being the maximum value (from 600° to 950° K) of T_p and the value being given as a function of the kerosene consumption per hour in *Figure 4*.

However, the maximum is displaced toward the end section of the device[1].

Another experiment

Another test of the above-mentioned similarity law has been carried out on a small scale at the Technical Physics Laboratory of the Polytechnic School of Turin, working on enclosed flames of different diameters.

For this test, a small oil burner of the mechanical injection type was employed, operating with an excess of air of about 20 per cent.

Figure 4

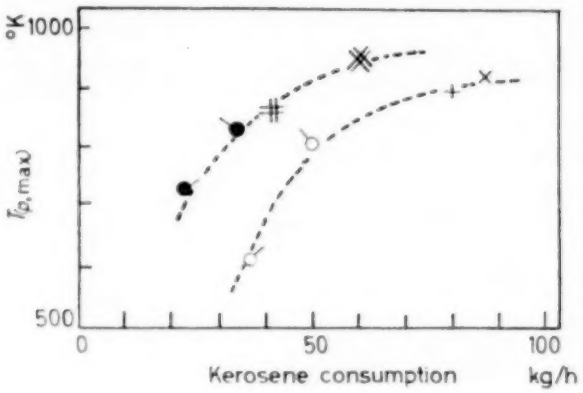

The flame, produced by a fuel rating of about 3 kg/h, was developed during the various tests within some stainless steel tubes provided with a tapered opening and having respectively the following diameters: 12·5, 18 and 24 cm.

Two sets of diametrically opposed holes, pierced in the walls of these tubes and closed by steel caps, allowed transverse temperature measurements to be made through the use of an integral radiation pyrometer, by which one can view two open, opposing holes.

The flames were controlled so as to reach a maximum temperature of 1620 K.

The readings E^* of the pyrometer, placed at a distance of 60 cm from the axis of the tube, provided values which are proportional to the small temperature rises of the thermocouple representing the radiation-sensitive member and, therefore, provided values which are also proportional to the radiated energy.

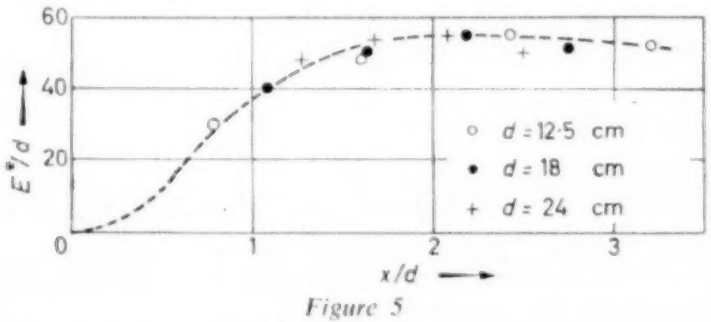

Figure 5

The flame, light yellow in colour, appeared to be turbulent and of a notched shape along the end sections of the tubes. The results of the tests are shown in *Figure 5*, where x represents the distance (from the burner) at which the E^* values have been measured, whereas d is the diameter of the tube.

The curve, characterized by the experimental points and representing the behaviour of the radiating power of the different flames, satisfies the following equation

$$E^*/d = A \exp(-d/x) - B(x/d) \qquad \ldots [2]$$

the constants A and B here having the values 150 and 18 respectively.

Istituto di Fisica Tecnica

Politecnico di Torino, Italy

(*Received July 1956*)

REFERENCE

[1] CODEGONE, C. Rayonnement des Flammes et Similitude. *Combustion Research and Review* p. 163 AGARD, London, 1955

On the Positive and Negative Ions in Diffusion Flames

TOSIRÔ KINBARA and HIDEO IKEGAMI

The mobilities of ions at various points in a diffusion flame were observed by the sheath method in an attempt to discover in what part of a flame the ions were produced and how they combined with other molecules or radicals.

WHEN an electric field is applied to a low pressure gas, the positive and negative ions flow in opposite directions and gather respectively about the negative and positive electrodes, producing regions of large potential gradient. By observing the potential in the regions, which J. J. THOMSON called layers or sheaths, one can derive the mobilities of the ions in them. Measurements have been carefully carried out by many investigators by the probe and potentiometer method, from the results of which some useful information about the nature of the ions has been obtained.

P. E. BOUCHER[1] successfully applied this method to premixed-gas flames which contain many ions produced by chemical reaction or thermal ionization. He observed the variation of potential near the cathode immersed in a flame and so measured the thickness of the sheath at the cathode. With a slight modification of J. J. Thomson's theory[2] of the potential in the sheath, he calculated the mobility of positive ions by means of the thickness of the sheath, the total potential drop in it and the current through it; and the result was 12·4 cm sec^{-1}/volt cm^{-1} for pure flames and 8·1 cm sec^{-1}/volt cm^{-1} for flames containing sodium chloride.

These estimates are pretty large compared with those ($1 \sim 2$ cm sec^{-1}/volt cm^{-1}) obtained by H. A. WILSON[3] or E. N. DA C. ANDRADE[4] by different methods. But H. E. BANTA[5] showed afterwards that the estimations are considerably dependent on the assumed rate of ionization and recombination in the sheath, and obtained with a different assumption the result: 1 cm sec^{-1}/volt cm^{-1}.

As to negative ions, however, Boucher considered the method no longer applicable, because the sheath was too thin and small to be observed, but the present authors found that by increasing the voltage between the two electrodes the sheath could grow thick enough to be measured. The mobility of negative ions measured in this way amounted to several thousand cm sec^{-1}/volt cm^{-1}, showing that the negative ion in the premixed-gas flames is a pure electron—a generally accepted belief amongst physicists.

Thus the sheath method has come to be considered as one of the useful means of inquiring into the mobilities of negative as well as positive ions in a flame. Moreover, the method has an advantage in that one can observe the mobility at any point where the electrode is inserted, and so is suitable for investigating whether the mobility differs from point to point in a flame.

T. KINBARA and J. NAKAMURA[8] have reported that in a diffusion flame most of the electrons and positive ions are both created in the lowest part of the flame, and ascend with the gas flow. If this is so, it may be reasonably supposed that these electrons will attach themselves to molecules and then these attached molecules will again be combined with others. Accordingly, it is quite possible that the negative ions grow larger and larger as they ascend, but it is still doubtful whether the same holds with positive ions, for their behaviour may be quite different.

All these problems would be settled by observing the mobilities of ions at several points in the diffusion flame, and in this paper the results obtained by the probe and potentiometer method are reported and discussed.

THEORY

It has been commonly assumed that an ion in an electric field drifts with a velocity v which is proportional to the field intensity X, that is $v=kX$, where k is the mobility of the ions. Objections have been raised to this by some authors who claim that the equation $v=k'\sqrt{X}$ is preferable for the electrons, but it will be assumed that $v=kX$, as commonly accepted, and the results for k will be compared with those obtained by many authors.

Let us now consider that in flames there are positive ions as well as negative ones, of various kinds, and that all of them have the same charge e. Let $n_+^{(1)}$, $n_+^{(2)}$, ... and $n_-^{(1)}$, $n_-^{(2)}$, ... be the number of each kind of positive and negative ion per unit volume at any point; $k_+^{(1)}$, $k_+^{(2)}$, ... and $k_-^{(1)}$, $k_-^{(2)}$, ... be the corresponding mobilities; and $v_+^{(1)}$, $v_+^{(2)}$, ... and $v_-^{(1)}$, $v_-^{(2)}$, ... be the drift velocities. For the sake of simplicity, it will be assumed that the drift velocities are not affected by the gas flow.

It would be appropriate to suppose that the production and recombination of ions would take place simultaneously at any point in the diffusion flame, so, let the number of ions created at any point in unit time per unit volume be z and the corresponding number of ions which disappear by recombination be β.

Mobilities of ions around a wire electrode—First, let us consider the case for a long cylindrical electrode of radius r_0 laid in a flame. It will be assumed that the potential distribution is concentric with the electrode and uniform along its axis. Let r be the distance at any point measured from the centre of the electrode. The fundamental equations are:

$$\frac{1}{r}\frac{\mathrm{d}}{\mathrm{d}r}(rX)=4\pi e\left(\sum_s n_+^{(s)}-\sum_s n_-^{(s)}\right) \qquad \ldots\ldots[1]$$

$$\frac{r}{r_0}\left(\sum_s n_+^{(s)}k_+^{(s)}+\sum_s n_-^{(s)}k_-^{(s)}\right)eX=j \qquad \ldots\ldots[2]$$

$$\frac{1}{r}\frac{\mathrm{d}}{\mathrm{d}r}\left(rX\sum_s n_+^{(s)}k_+^{(s)}\right)=z-\beta \qquad \ldots\ldots[3]$$

$$\frac{1}{r}\frac{\mathrm{d}}{\mathrm{d}r}\left(rX\sum_s n_-^{(s)}k_-^{(s)}\right)=-(z-\beta) \qquad \ldots\ldots[4]$$

where j is the current density at the electrode surface.

Then if

$$\sum_s n_+^{(s)} = n_+ \qquad \ldots\ldots [5]$$

$$\sum_s n_-^{(s)} = n_- \qquad \ldots\ldots [6]$$

$$\sum_s n_+^{(s)} k_+^{(s)} = n_+ k_+ \qquad \ldots\ldots [7]$$

$$\sum_s n_-^{(s)} k_-^{(s)} = n_- k_- \qquad \ldots\ldots [8]$$

and

$$r^2 = \xi \qquad \ldots\ldots [9]$$

the important equation can be deduced

$$\frac{d^2}{d\xi^2}(rX)^2 = 2\pi e(\alpha - \beta)\left(\frac{1}{k_+} + \frac{1}{k_-}\right) \qquad \ldots\ldots [10]$$

Now, if the observed potential V is plotted as a function of $\ln r$, a curve is obtained as in *Figure 1*. A characteristic of this curve is that $dV/d\ln r$,

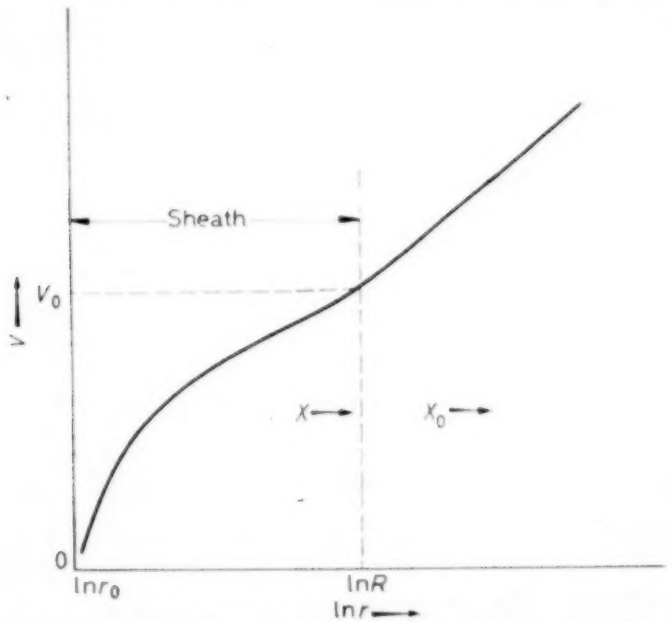

Figure 1. Potential distribution around wire electrode: V = potential referred to electrode; r = distance from centre of electrode; r_0 = radius of electrode; $R - r_0$ = thickness of sheath

i.e. rX, is constant when r is larger than a certain value R. For $r > R$, we have $n_+ = n_-$ as equation [1] shows, and we know that R is the distance from the wire axis to the sheath surface.

From equation [10] we can also conclude that $(\alpha - \beta) = 0$ outside the sheath surface, which means that either the recombination and the production are perfectly balanced, i.e. $\alpha = \beta$, or else both α and β are small enough to be justifiably neglected.

Next let us consider α and β inside the sheath. Unlike the electrical discharge in a Geisler tube, where the ions are produced by the electric force, the ions here are produced in the process of combustion, and the electric field serves only to collect the ions around the electrodes. So it can be properly assumed that α and β vary little in that small region of the sheath. Then as $(\alpha-\beta)$—which we shall denote Q hereafter—is constant, the equation [10] can be transformed into

$$\frac{\mathrm{d}}{\mathrm{d}\xi}(rX)^2 = 2\pi e\left(\frac{1}{k_+}+\frac{1}{k_-}\right)Q(\xi-R^2) \qquad \ldots\ldots[11]$$

The number of positive ions which are produced in the layer and carry the current at the sheath surface will be, according to the authors' assumption, equal to

$$l\int_{r_0}^{R} Q2\pi r\mathrm{d}r = 2\pi Rln(k_+X_0) \qquad \ldots\ldots[12]$$

where l stands for the length of the electrode and n is n_+ or n_- at the sheath surface. On the other hand, when equation [2] is applied to the sheath surface, then

$$2\pi Rl(nk_+ + nk_-)eX_0 = i \qquad \ldots\ldots[13]$$

where i is the total current through the flame. Thus, from equations [11], [12] and [13]

$$\frac{\mathrm{d}}{\mathrm{d}\xi}(rX)^2 = \frac{2i}{lk_-(R^2-r_0^2)}(\xi-R^2)$$

that is

$$(rX)^2-(RX_0)^2 = \frac{i}{lk_-(R^2-r_0^2)}(r^2-R^2)^2 \qquad \ldots\ldots[14]$$

If it were possible to observe the true gas potential V at any point of the sheath and plot V against r, $r\mathrm{d}V/\mathrm{d}r$ and $R(\mathrm{d}V/\mathrm{d}r)_0$ could be calculated from this curve and accordingly k_- could be obtained by equation [14]. But in reality, it cannot be expected that the potential observed by a probe is necessarily equal to the true flame potential especially in the sheath, for a reason which will be referred to later, so it is necessary to integrate equation [14] to eliminate V inside the sheath.

As will be seen in *Figures 6* and *7*, most of the $V/\ln r$ curves show that

$$RX_0 = -\left(\frac{\mathrm{d}V}{\mathrm{d}\ln r}\right)_{r=R} = \text{small.}$$

And accordingly, if it suffices only to meet the requirement of the order-of magnitude agreement of k_-, we can assume $X_0=0$ in all cases. Then

$$r\frac{\mathrm{d}V}{\mathrm{d}r} = -\sqrt{\left(\frac{i}{lk_-(R^2-r_0^2)}\right)(R^2-r^2)}$$

and

$$k_- = \frac{i[R^2\ln(R/r_0)-\frac{1}{2}(R^2-r_0^2)]^2}{lV_0^2(R^2-r_0^2)} \qquad \ldots\ldots[15]$$

This is the fundamental equation to calculate k_-, and also represents the mobility k_+ for positive ions around the negative electrode.

Mobilities of ions just above the burner port—For equation [15] to be applicable, the field around the electrode wire needs to be concentric. The requirement is hardly answered if the electrode wire is placed near the burner port—the other electrode. Moreover, combustion is just beginning in the region adjacent to the port, and a platinum wire inserted there might affect the chemical process catalytically. In view of this, insertion of a platinum wire in this region is not desirable. Thus, in order to observe the mobilities of the ions there, it is better to consider the sheath produced just above the port, the wire electrode being intentionally kept far away from it.

If a metal plate is put on the top of an ordinary burner and the fuel gas is made to blow out of a small hole drilled at the centre of the plate, one can then consider this metal plate to be a plane electrode inserted perpendicularly to the flame. For the plane electrode the equations must of course be modified. Let us now assume that the flame is homogeneous within a horizontal plane and let x be the distance measured from the plane electrode to any point. The fundamental equations corresponding to equations [1], [2], [3] and [4] are:

$$dX/dx = 4\pi e\,(\Sigma_s n_+^{(s)} - \Sigma_s n_-^{(s)}) \qquad \ldots\ldots [16]$$

$$eXS\,(\Sigma_s n_+^{(s)} k_+^{(s)} + \Sigma_s n_-^{(s)} k_-^{(s)}) = i \qquad \ldots\ldots [17]$$

$$(d/dx)\,(X \Sigma_s n_+^{(s)} k_+^{(s)}) = \alpha - \beta \qquad \ldots\ldots [18]$$

$$(d/dx)\,(X \Sigma_s n_-^{(s)} k_-^{(s)}) = -(\alpha - \beta) \qquad \ldots\ldots [19]$$

where S means the cross sectional area of the flame. Using equations [5], [6], [7] and [8] one can easily get the following equation corresponding to [10]

$$d^2X^2/dx^2 = 8\pi e\,(\alpha - \beta)\,(1/k_+ + 1/k_-) \qquad \ldots\ldots [20]$$

If the observed potential V is plotted as a function of x, a curve similar to that presented in *Figure 1* is obtained and one can easily find the sheath thickness d corresponding to $(R - r_0)$. Outside the sheath, the V/x relation becomes linear, i.e. $X = \text{constant} = X_0$, and accordingly $n_+ = n_- = n$, and $\alpha - \beta = Q = 0$. Unlike the case where a wire electrode is inserted into the upper part of the flame, it would be wrong to assume Q, from the beginning, to be a constant of small magnitude throughout the layer, because combustion begins to take place in this narrow layer a few millimetres thick. It is a question of the assumption of the way in which Q varies with x. But in view of the fact that Q must be zero when $x = d$ we shall assume for the present

$$Q = q\,(1 - x/d)^m \qquad \ldots\ldots [21]$$

where q and m are unknown constants. The assumption is the same as that proposed by Banta as tenable for the electrode inserted at any point of the premixed-gas flame, and the validity of the assumption will be discussed later on.

Integrating equation [20] and neglecting (dV/dx) at $x=d$, one can finally obtain

$$k=\frac{32\pi id^3}{(m+2)(m+4)^2SV_0^2} \quad \ldots\ldots [22]$$

where k denotes the mobility of negative ions on the positively charged burner port, as well as that of positive ions on the negatively charged port.

EXPERIMENTAL PROCEDURE

Burner—To make the former mathematical analysis applicable, the flame must be in a special form. With the diffusion flame of an ordinary bunsen burner, homogeneity of the ion distribution can hardly be expected even in a horizontal section of the flame because the combustion, and accordingly the production of ions, takes place mainly in the outer part of the flame. Strictly speaking, it is impossible to make the flame perfectly homogeneous, so far as the diffusion flame is concerned, but in practice one can meet the requirement by making the flame as thin as possible, because then the ions will soon diffuse to every part of the section. Thus a burner which gives a thin plane parallel flame has been devised.

Sixteen brass tubes (each about 1 mm inside diameter and 10 mm long) were mounted vertically in holes drilled close together in a row along the length of a rectangular brass plate about 10 cm long and 2 cm wide (*Figure 2*).

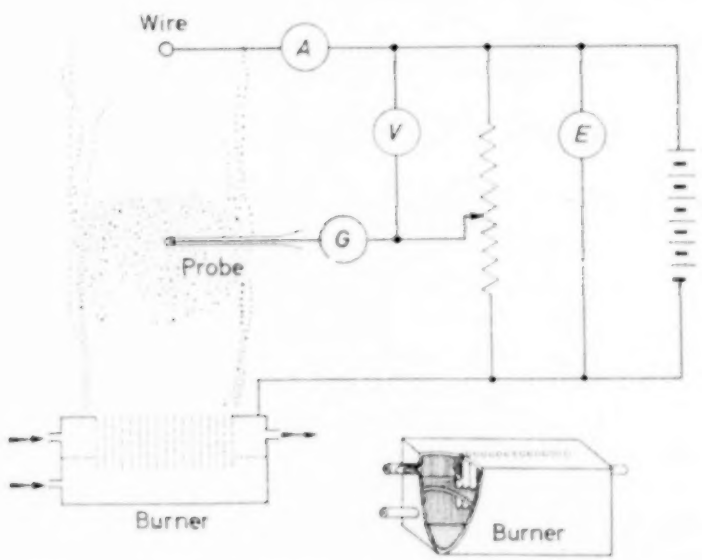

Figure 2. Flame, electrodes and probe; A = microammeter; G = galvanometer; (sens. = 10^{-10} amp); V, E = voltmeters

This plate separated the burner chest into two parts of which the upper carried circulating water to maintain the burner tubes at constant temperature while town gas was admitted to the lower portion.

This burner gives a nearly plane parallel flame about 5 cm long, 5 ~ 10 mm wide and of any desired height. The outer surface of the flame was located and determined by a very thin platinum-tipped wire which glowed red on approaching the flame from without.

Electrode—A platinum wire 2 mm in diameter and 10 cm long (sometimes 0·4 mm in diameter and 10 cm long) was used as the wire electrode. When ions around the wire electrode were investigated, the wire was inserted perpendicularly to the flame's surface (*Figure 2*) and, when ions on the port were studied, in the central plane of the flame. A potential difference was applied between the wire and the burner. A diagram of the circuit used is also shown in *Figure 2*.

It is important to earth the wire when the sheath around it is to be investigated, and to earth the burner when the burner sheath is to be observed, because otherwise the potential fluctuates and makes measurement difficult.

Probe—To observe the potential of a gas flame, a probe of platinum wire of 0·2 mm diameter was used, covered with a thin, fused silica tube (diam. = 0·4 mm) except for 5 mm at its end. It is desirable to use a probe of as small a radius as possible, but a finer wire would sag after a short time in a flame. The probe wire, together with its silica tube holder, was mounted on the movable carriage of a small cathetometer, the telescope being removed. The uncovered part of the probe (about 5 mm) was carefully adjusted so that it was just beneath and parallel to the electrode wire when the wire sheath was investigated, while it was kept parallel to the port plane when the port sheath was studied.

The sheath thickness is only of the order of 3 mm, hence it is most important to observe precisely the distance of the probe from the electrode. This distance was measured to within 0·1 mm.

RESULTS

Voltage applied—To make the sheath large enough, it is necessary to apply as large an electric voltage as possible between the electrodes, but it must be remembered that the ions produced by combustion might be accelerated so highly as to ionize other neutral molecules by collisions. If that occurs, new ions would be produced which have no relation to the process of combustion, and so care must be taken that these new ions are not produced by the applied electric field.

Whether the new ions are produced or not can easily be discovered by investigation into the relation between the applied voltage E and the current i through the flame. A description of this relation now follows, taking an ordinary bunsen burner diffusion flame 2 cm high as an example.

A horizontal wire electrode was held 1 cm above the yellow tip of the flame, the other electrode being the burner port. When the wire was charged positively and E was increased gradually, i increased rapidly at first ($E = 0 \sim 300$ V) but it soon seemed to reach a certain saturation value ($\simeq 2\mu$A) and, after remaining unaltered for a comparatively wide range of E (300 ~ 3000 V), it increased suddenly and markedly, showing that a lot

of ions were produced by collisions. When the wire was charged negatively, the i/E relation was not very different, except that the increasing rate of i in the first stage was far slower and the current at the saturated state was appreciably stronger.

Care was always taken in the experiment that the applied voltage should not be high enough to produce new ions by collisions.

Probe potential and true gas potential—To observe the potential, the potentiometer method was adopted (*Figure 2*). By adjusting the potential V of the probe with respect to the electrode under investigation, the probe current i_p could be reduced to zero, at which point the probe would be at the same potential as the adjacent gas, if the concentrations and the diffusion velocities of the positive and negative ions were equal.

We shall consider first the case where the probe is inserted outside the sheath—concentrations of both positive and negative ions here are equal, but since the diffusion velocities are quite different owing to the great difference between their masses, the voltage read when the galvanometer indicates zero probe current should be corrected to give the true gas potential. The voltage correction can be obtained by the usual method presented in any textbook[7], and it was found that it was only of the order of 1 V in the flame. As against this, the potential at the surface of the positive ion sheath amounted to as much as 100 V, so the correction could safely be neglected. But with a negative ion sheath, the potential at the sheath surface was often shown to be several volts, and the correction became important.

Inside the sheath the situation was more complicated. Not only the diffusion velocities but also the numbers of both ions differed markedly, and so it was possible for the probe potential for $i_p=0$ to be quite different from the true gas potential. *Figure 3* is an example which shows the probe potentials for $i_p=0$ at various points in the flame.

The drop of probe potential in the negative ion sheath was surprising, and the potential became, on several occasions, $200\sim300$ V lower than that of the points outside the sheath. In this case, however, the sheath around the probe seemed to be in an unstable state and i_p, once adjusted to zero, increased several times unexpectedly, and returned to its original state after a short time. The true gas potentials would be quite different from probe potentials thus obtained and the distribution of true potentials would be like that presented by the dotted curve in *Figure 3*.

Then it must be inferred that the observed probe potential is not necessarily equal to the true gas potential and that use can be made of the observed values only to determine the boundary point of the sheath, from which point the V/x (or $V/\ln r$) curve remains straight, on moving towards the other electrode.

Concentricity of field around the wire electrode—On application of this theory to the actual electrode in a diffusion flame, the question arises whether the electric field around the wire electrode is concentric as expected. So the potential distribution all around the platinum wire was observed.

Generally speaking, the distortion was not negligible except in a high temperature flame like that of a Méker burner. But as can be easily supposed, the part of the equipotential line confined within the narrow limits just below the electrode could be regarded as concentric. And so,

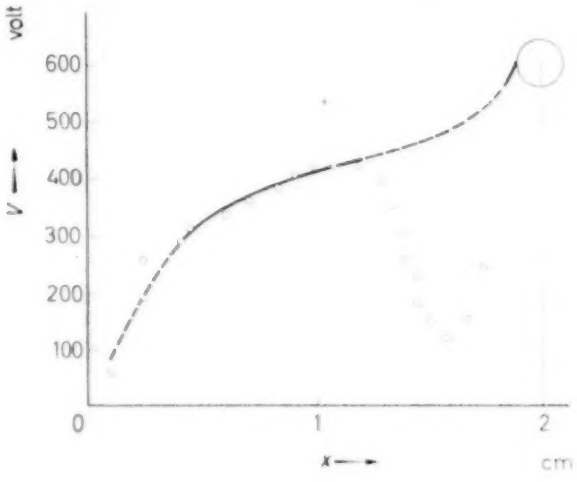

Figure 3. Probe potential (for $i_p=0$) at various points of the flame; V=probe potential; x=distance from port; flame (yellow tip) height=1 cm

if consideration is limited to this narrow region, it may be said that all the equations [1], [2], [3] and [4] hold unchanged, provided j is the current density at the bottom of the wire. This current density j_0 can be obtained in the following way.

The current density j at any point ought to be always proportional to the field intensity, that is, inversely proportional to the distance between two adjacent equipotential lines. Consequently, the approximate value of j/j_0 can be obtained graphically from the figure which shows equipotential lines around the wire. Then it will be easy to find the approximate relation between j_0 and i.

In practice it would be possible to use the expression $j_0=i/2\pi r_0 l$ when the electrode was inserted in a visible (blue, faint blue or yellow) part of the flame, and it would be possible to use the same expression even when the electrode was placed above the blue tip of the flame, in so far as the order of magnitude of k is considered.

Ions in middle and upper parts of the flame—First, the platinum wire electrode was earthed and the burner was charged positively. The probe potential for $i_p=0$ was observed carefully and the V/r relation was plotted semi-logarithmically. *Figure 4* shows an example. In some instances, the kink of the curve is not so distinct as this, and some ambiguities in deciding the position of the sheath surface are inevitable. But in so far as the approximate value of k_+ is concerned these ambiguities are not of importance.

The potential drop across the sheath amounts to several hundred volts and the voltage correction due to the difference of mobilities of both ions may be neglected.

The mean values of k_+ at several parts of the flame are shown in *Figure 8*.

Next, the burner was charged negatively, the wire being kept earthed as before. The results in one instance, when the wire was inserted above the yellow tip of a flame, are presented in *Figure 5*. When the wire was put in the part lower than the yellow tip, V became as low as a few volts,

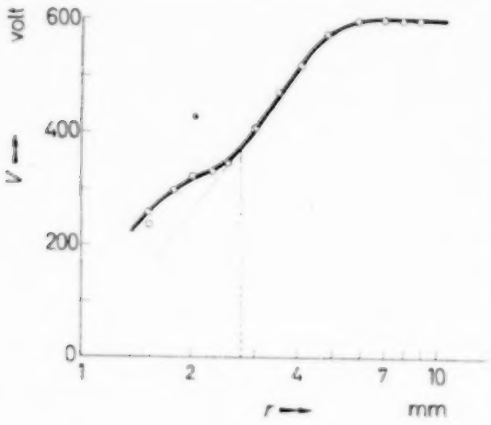

Figure 4. Potential under negatively charged wire: r = distance from wire centre; radius of wire = 1·0 mm; flame height = 1·2 cm; height of wire = 1·0 cm; length of wire within flame = 1·0 cm; potential of burner = E = 600 volt; i = 2·0 μA; R = 2·7 mm; V_a = 370 volt; k_+ = 0·3 cm sec^{-1}/volt cm^{-1}

and the voltage correction was now necessary. The potential difference between the electrodes could be increased to any extent, but the greater the difference, the greater the resulting cathode drop, the anode drop being only a few volts at most.

Well above the flame tip, both the potential drop and the sheath thickness are sufficiently large and the V/r curve resembles that of *Figure 4* in shape.

Figure 5. Potential under positively charged wire: radius of wire = 1·0 mm; flame height = 1·2 cm; height of wire = 1·9 cm; wire length within flame = 1·0 cm; potential of burner = E = −600 volt; i = 6·4 μA; R = 4·5 mm; V = 90 volt; k_- = 186 cm sec^{-1}/volt cm^{-1}

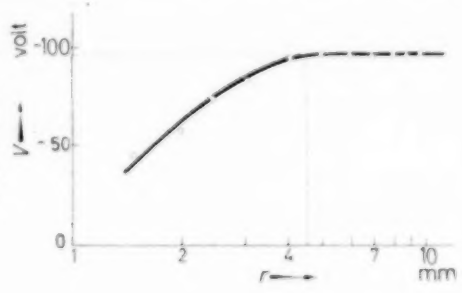

Thus the V/r relation presents very different characteristics at different parts of the flame, showing that the mobility varies largely with the height. The mobilities at several points are shown in *Figure 8*.

Ions just above burner port—The electrode wire was rearranged so as to be in the central plane of the flame and the burner was earthed. Typical results for negatively and positively charged burner ports are shown in *Figures 6* and *7* respectively.

To calculate k it is necessary to know the value of m in equation [21] but at present there is no means of obtaining information about it. So the values of k for $m = 0$ are shown in the captions of *Figures 6* and *7*.

Summary of results—Observation of k was repeated several times at a section of the flame, changing the current i or replacing the electrode wire by a thinner one. The results showed fluctuations to some extent, but an

order-of-magnitude agreement was always kept. The results are summarized and the average values of k at various points in a flame, assuming $m=0$ for the ions at the burner port, are shown in *Figure 8*. It has been the authors' supposition that there should be several kinds of positive as well

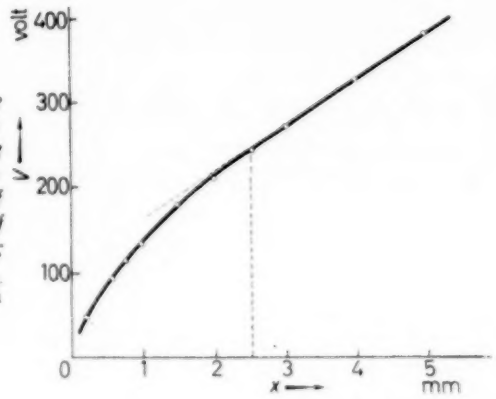

Figure 6. Potential above negatively charged port: x= distance from port; flame height =2·0 cm; height of wire= 3·0 cm; cross sectional area of flame=4·5 cm²; potential of wire=E=600 volt; i=7·3μA; d=2·4 mm; V_0=240 volt; k_+ (m=0)=1·1 cm sec⁻¹/volt cm⁻¹

as negative ions in a flame. Accordingly, k_+ and k_- denote respectively the weighted means of the mobilities of positive ions and of negative ions.

As shown in *Figure 8*, the mean mobility of the positive ion has a tendency to decrease only slightly with the height of the part in which the ion is found. On the other hand, the mobility of the negative ion decreases markedly with its distance from the port. It should follow from this that more than two kinds of negative ions coexist in a flame.

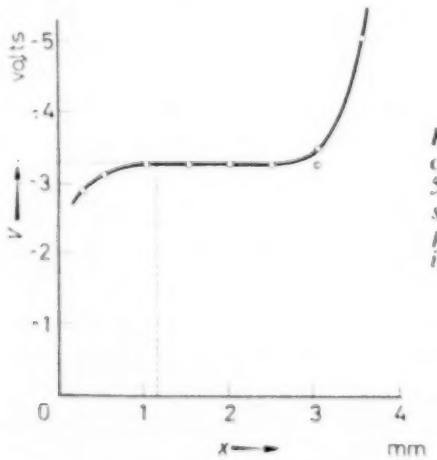

Figure 7. Potential above positively charged port: flame height=about 5 cm; height of wire=ca. 5 cm; cross sectional area of flame=4·5 cm²; potential of wire=E=−1200 volt; i=5·3μA; d=1·2 mm; V_0=−3·2 volt; Voltage correction=+1·0 volt; k_-(m=0)=982 cm sec⁻¹/volt cm⁻¹

DISCUSSIONS AND CONCLUSIONS

It was intended to discover in what part of a diffusion flame most of the ions were produced and how they combined with other molecules or radicals, and for this purpose an attempt was made to observe their mobilities at various points by means of the sheath method. This method of investigation, however, was attended with various difficulties, not only technical but also theoretical.

First, as to the velocity of ions, only the drift velocity ($=kX$) was taken into consideration and the diffusion velocity was neglected. This is the basis of the authors' theory but it demands close investigation in some cases. For instance, the potential distribution presented in *Figure 3* could hardly be explained unless the diffusion velocity of ions is taken into account. Secondly, X_0 has been neglected for the sake of simplicity, and so there are expected to be some cases where the correct values of k may not be obtained. Thirdly, the assumption for Q must be called in question. k was calculated under the assumption that Q is a small constant for the sheath around a wire and $m \simeq 0$ for ions above the port, and thus k was presented for various points of a flame in *Figure 8*. Setting aside the

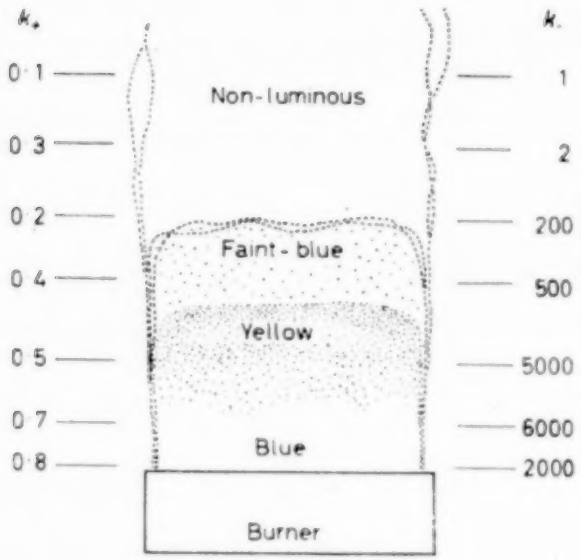

Figure 8. Mobilities at various parts of flame: k_+=mobility of positive ion in cm sec^{-1}/volt cm^{-1}; k_-=mobility of negative ion in cm sec^{-1}/volt cm^{-1}; m=0, for the ions at the port

question of Q around a wire-sheath, the mobility of ions above the port depends on the assumed magnitude of m, and if we suppose $m=2$ instead of $m=0$, k will be eight times as large.

In view of these difficulties, the authors found it necessary to apply their method to those flames of a Méker burner, in which the mobility of ions is well known, and to see if their method would give reasonable values of k.

The results were $k_+ \simeq 1$ cm sec^{-1}/volt cm^{-1} and $k_- = 3000 \sim 6000$ cm sec^{-1}/volt cm^{-1} for all parts of the flame, being in good agreement with the results given by many other authors. This fact seems to suggest that, on the one hand their method of investigation is applicable to all flames, on the other hand the results shown in *Figure 8* are quite reasonable, at least in their order of magnitude.

Thus it can be concluded with confidence that:

(*i*) The mobilities of positive ions in all parts of diffusion flames are nearly equal and are of the order of 1 cm sec^{-1}/volt cm^{-1}.

(*ii*) The average value of mobilities of negative ions decreases from the order of 10^3 to that of 1 cm sec^{-1}/volt cm^{-1} with their distance from the burner port.

From these conclusions it may be supposed that the ions in diffusion flames are mostly created in the lower part in the form of electrons and of positive ions, the latter having mobilities of nearly 1 cm sec^{-1}/volt cm^{-1}. The electrons thus produced become large negative ions as they ascend, being combined with molecules or radicals. The positive ions, on the contrary, seem to keep themselves uncombined with other neutral particles. Probably the slight systematic decrease of k_+ with the height is due not to the change of the ion in its nature, but to the variation in the temperature and the composition of flame gases. Anyway, the difference between the characteristics of both ions sets a very interesting problem which may be a key to the solution of the problem regarding the nature of positive as well as negative ions in diffusion flames.

Institute of Physics,
College of General Education,
University of Tokyo

(Received August 1956)

REFERENCES

[1] Boucher, P. E. *Phys. Rev.* 31 (1928) 833
[2] Thompson, J. J. *Conduction of Electricity through Gases* Chapters 3, 9. Cambridge University Press, London, 1903
[3] Wilson, H. A. *Phil. Trans.* A 216 (1916) 63
[4] Andrade, E. N. da C. *Phil. Mag.* 6th Series, 23 (1912) 865
[5] Banta, H. E. *Phys. Rev.* 33 (1929) 211
[6] Kinbara, T. and Nakamura, J. *Fifth International Symposium on Combustion* p. 285 Reinhold: New York, 1955; *Sci. Pap. Coll. Gen. Educ. Tokyo Univ.* 4 (1954) 9
[7] Loeb, L. B. *Fundamental Processes of Electrical Discharge in Gases* Wiley: New York, 1939

Influence of Diborane on Blow-off Limits of Hydrocarbon Flames

P. F. KURZ

Blow-off studies of hydrocarbon–diborane flames on a bunsen burner show that diborane influences the properties of hydrocarbon flames in an unusual manner. $Vc_xH_y/V^*c_xH_y$, the ratio of hydrocarbon in these binary mixtures at a given jet velocity, v_j, at blow-off to the hydrocarbon in a hydrocarbon flame at blow-off also at v_j decreases as v_j increases. In flames of binary hydrocarbon mixtures $Vc_xH_y/V^*c_xH_y$ increases as v_j increases. This unique behaviour of hydrocarbon–diborane mixtures is believed to result because diborane burns selectively. Consequently, the configuration of hydrocarbon–diborane flames would be different from those of hydrocarbon flames, and the two types are not directly comparable.

THIS paper describes the influence of diborane on the blow-off limits of propane and *iso*butane flames on a 1·11-cm i.d. bunsen burner.

It was shown earlier[1] in reporting the results of flame-speed work that the addition of small amounts of diborane to propane produced a fuel mixture in which propane appeared to inhibit appreciably the fast combustion reactions of diborane. In near-stoichiometric rich flames and in moderately rich flames, a progressive increase in the flame speed of propane–diborane flames was found only when the amount of diborane in the fuel was increased above about 15 volume per cent for the leaner mixture and about 7 volume per cent for the richer mixture. However, this is believed to have resulted from the selective burning of diborane to completeness in the rich binary fuel mixtures[2, 3]. Consequently, the propane could burn only to the extent that the deficient oxygen supply permitted. Hence, the increase in flame speed could not be ascribed to an accelerating influence of the diborane on the propane.

The blow-off experiments described in the present paper were carried out to find what effect the selective burning of diborane would exert on the stability limits of hydrocarbon flames.

EXPERIMENTAL PROCEDURE

Apparatus

The 1·11-cm i.d. bunsen burner and its auxiliaries used in the blow-off experiments have been described earlier[4]. Only unshielded flames burning in ambient air were studied in this work.

The diborane was diluted with argon just prior to use to minimize dissociation of diborane at room temperature and to facilitate flow measurements. Diborane–argon mixtures containing about 13·3 volume per cent diborane were used in these experiments.

Observation of blow-off limits

The following procedure was used to determine blow-off limits on the 1·11-cm i.d. bunsen burner. The flow of air (8·3 litres/min) and the flow of the secondary fuel (diborane–argon mixture, 133 to 511 cm^3/min in

various experiments) were set at predetermined rates and were held constant throughout a particular experiment. The flow of the primary fuel (a hydrocarbon) was adjusted to produce a stable flame. Argon was then introduced into the combustible mixture, stepwise, in equal increments of flow (100 cm^3/min) until blow-off occurred. Then the flow of argon was shut off. The flow rate of the primary fuel was increased by a convenient increment (10 to 20 cm^3/min), producing a richer mixture, and the mixture was re-ignited. Argon was again introduced stepwise in equal increments of flow (100 cm^3/min) until the flame blew off. This procedure was repeated until a range of fuel–air compositions had been covered.

Argon was used to cause blow-off in order that a much wider range of fuel–air compositions could be studied than would have been possible if air had been used to increase the jet velocity.

EXPERIMENTAL RESULTS

Blow-off limits of hydrocarbon–diborane flames

Figure 1 shows blow-off limit curves obtained by the procedure outlined above for two hydrocarbons and for three typical hydrocarbon–diborane

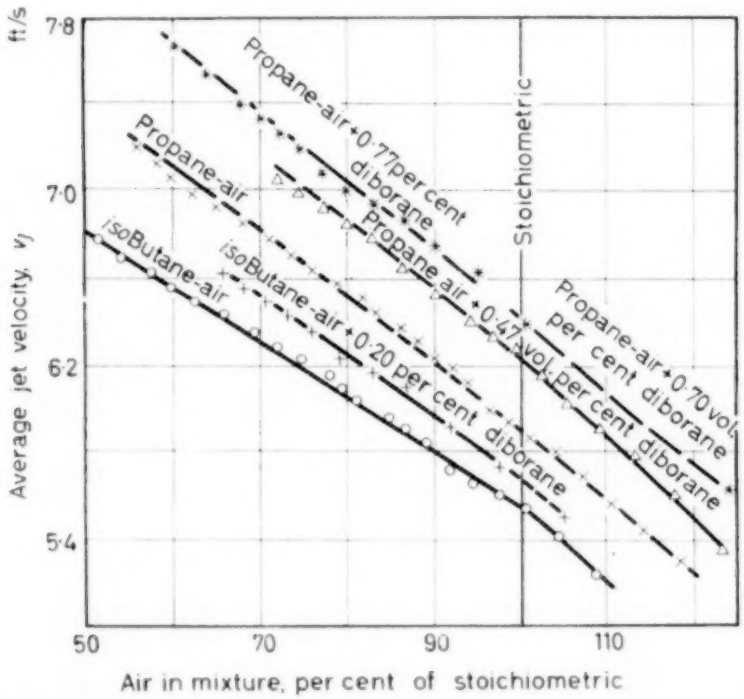

Figure 1. Stability limit curves for hydrocarbon and hydrocarbon–diborane flames on a 1·11-cm bunsen burner

mixtures. The coordinates are the average jet velocity at the burner port and the composition of the fuel–air mixture expressed as the percentage of stoichiometric air in the mixture. The data appear to show an approximately linear relationship between velocity at blow-off and mixture composition on either side of the stoichiometric point.

Figure 2 shows the influence of diborane on the propane required in the fuel–air mixture at the last stable composition before the blow-off limit, over a range of jet velocities. The divergence of the curves as the jet velocity increases suggests that diborane might be causing an accelerating action in the flame. This will be discussed later.

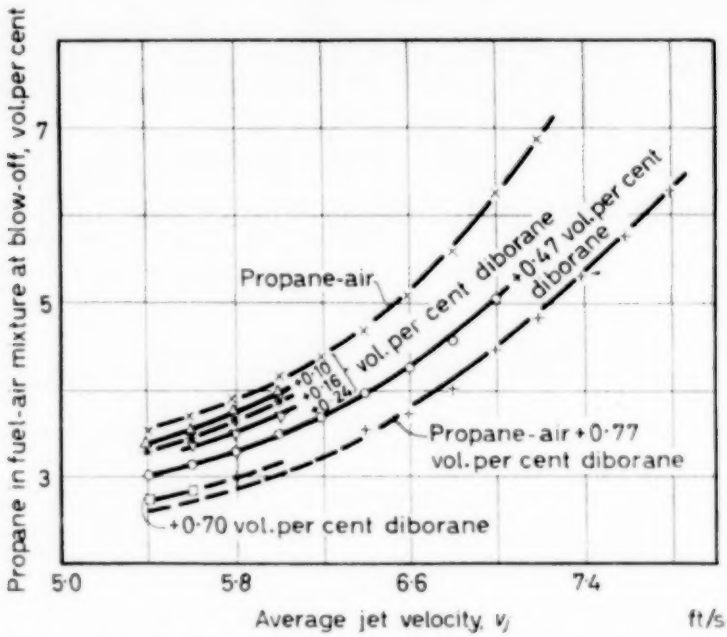

Figure 2. Influence of diborane on propane required in fuel–air mixture at blow-off

Figure 3 shows similar data for *iso*butane-diborane mixtures. These data suggest a tentative conclusion similar to that given above for propane–diborane mixtures.

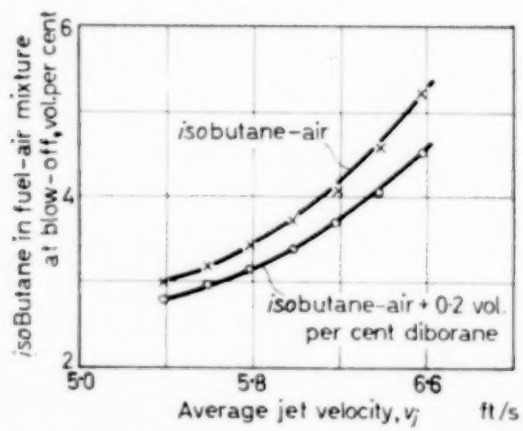

Figure 3. Influence of diborane on isobutane required in fuel–air mixture at blow-off

Further evidence supporting the suggestion that diborane might be exerting an accelerating influence in the flame is obtained when values of $V_{C_3H_8}/V^*_{C_3H_8}$ (the ratio of propane in the propane–diborane mixture at a given jet velocity, v_j, at blow-off to the propane in a propane flame at

blow-off also at v_j) are plotted against jet velocity. This is shown in *Figure 4* for propane–diborane mixtures and in *Figure 5* for *iso*butane–diborane mixtures. It is evident that in all mixtures containing diborane the values of $V_{C_3H_8}/V^*_{C_3H_8}$ or $V_{C_4H_{10}}/V^*_{C_4H_{10}}$ decrease as v_j increases. This is the opposite of the behaviour of hydrocarbon mixtures, such as propane–ethylene and *iso*butane–propane, where, as shown in *Figures 4* and *5*,

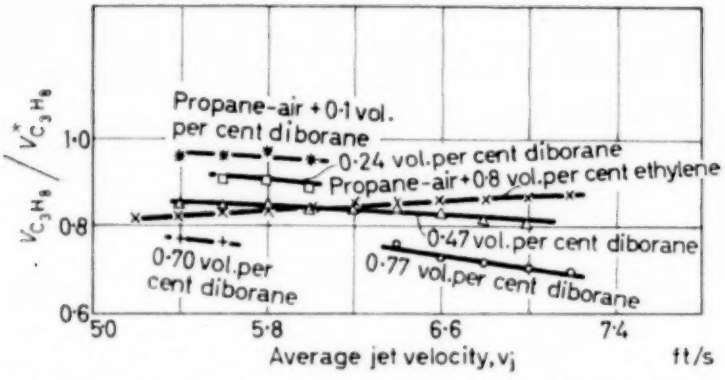

Figure 4. Changes in value of $V_{C_3H_8}/V^*_{C_3H_8}$ for propane–diborane and propane–ethylene mixtures at blow-off over a range of jet velocities

the respective ratios increase as v_j increases. It has been shown earlier[1] that two or more hydrocarbon fuels in a mixture affect each other in a predictable manner in accordance with the empirical equation

$$\frac{V_1}{V^*_1} + \frac{V_2}{V^*_2} + \ldots + \frac{V_n}{V^*_n} = \sum_{a=1}^{n} \frac{V_a}{V^*_a} = 1$$

For the ratios $V_{C_3H_8}/V^*_{C_3H_8}$ and $V_{C_4H_{10}}/V^*_{C_4H_{10}}$ to decrease as v_j increases and as $V_{B_2H_6}$ decreases (the flow rate of diborane was held constant during each experiment) the diborane must influence the flame properties of the hydrocarbon–diborane mixtures in an unusual manner.

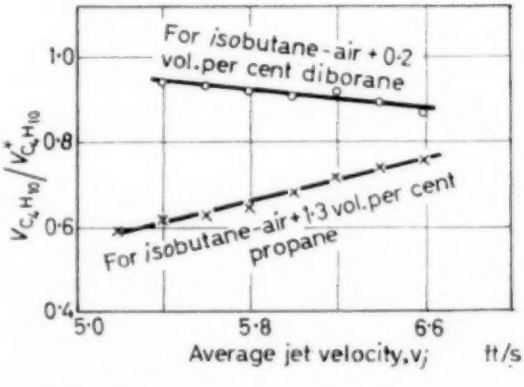

Figure 5. Changes in value of $V_{C_4H_{10}}/V^*_{C_4H_{10}}$ for iso-butane–diborane and iso-butane–propane mixtures at blow-off over a range of jet velocities

DISCUSSION

A plausible explanation for the unique behaviour of hydrocarbon–diborane flames in the blow-off experiments described above is that the diborane which has a very high flame speed may be burning selectively[2, 3], especially

in rich mixtures. Hence under conditions where 'twin flames'[2] may exist, the structure and configuration of rich hydrocarbon–diborane flames would be different from those of hydrocarbon flames. Most of the mixtures studied were rich. Accordingly, it is not too surprising that $V_{C_xH_y}/V^*_{C_xH_y}$ decreases when it should increase, because values of $V_{C_xH_y}$ and $V^*_{C_xH_y}$ are obtained from substantially different flames.

It is suggested that acceleration of the combustion reactions of one fuel by another without radically changing the flame is unlikely. It is believed that the most that can be expected normally of any fuel mixture is that each component should contribute its proportionate share to the stability or the flame speed of the mixture. Beyond this, the components cannot contribute without altering the flame to such an extent that it is no longer directly comparable to the flame of the slower-burning constituent at the same jet velocity.

This work was done under the sponsorship of the Chemistry Research Branch, Aeronautical Research Laboratory, Wright Air Development Center, Wright-Patterson Air Force Base, Ohio.

The author wishes to express his thanks to R. S. Litton who assisted ably and faithfully in the experimental work and to J. F. Byrne, Assistant Division Chief at Battelle, for his helpful interest.

Battelle Memorial Institute,
Columbus, Ohio, U.S.A.

(Received October 1956)

REFERENCES

[1] KURZ, P. F. *Industr. Engng Chem. (Industr.)* 48 (1956) 1863
[2] BERL, W. G. and DEMBROW, D. *Nature, Lond.* 170 (1952) 367
[3] KURZ, P. F. *Fuel, Lond.* 33 (1954) 250
[4] KURZ, P. F. *Industr. Engng Chem. (Industr.)* 45 (1953) 2361
[5] KURZ, P. F. *Fuel, Lond.* 34 (1955) 269

*Flame Zone Studies IV—Microstructure and Material Transport in a Laminar Propane–Air Flame Front**

R. M. FRISTROM and A. A. WESTENBERG

Experimental data for a stoichiometric, ¼ atm, propane–air flame are presented. The data include gas velocity normal to the flame front and stream tube area parallel to the flame front measured by the particle-track technique, and a derived temperature profile. Also included is a set of sampled composition profiles for all stable species present obtained with a quartz microprobe and mass spectrometric analysis. The total flux due to both convection and diffusion has been calculated for each species. The data are examined in terms of conservation of mass.

The experimental techniques involved in obtaining composition distribution data in laminar flames are discussed in detail elsewhere[1]. The data obtained on the flame described in that paper are presented here in their entirety, together with a discussion of material transport. All the primary data which are, in principle, necessary for a complete unidimensional analysis† of this particular flame are included, with the outstanding exception of any data on the distribution of atoms and free radicals for which no satisfactory experimental techniques are yet available. The data constitute the most nearly complete body of experimental information on a laminar flame obtained up to the present time. This paper, and a further one on energy considerations, deals with these data in detail. Chemical kinetic discussions are specifically postponed.

EXPERIMENTAL DATA

The flame used for this work was a premixed, conical, propane–air flame on a 1 in. burner at a pressure of ¼ atm. The initial mixture was stoichiometric with some water vapour present and had the following composition (in terms of mass fractions):

$$f_{C_3H_8}=0{\cdot}060;\quad f_{O_2}=0{\cdot}216;\quad f_{N_2}=0{\cdot}702;\quad f_{A}=0{\cdot}011;\quad f_{H_2O}=0{\cdot}010.$$

This is the same flame for which extensive particle-track studies have previously been reported[2]. The primary data obtained from these studies were the mass average gas velocity v normal to the flame front, and stream tube cross-sectional area a parallel to the flame front; the results are reproduced in *Figure 1* as dimensionless ratios relative to initial cold gas values. The coordinate Z represents distance normal to the centre of the luminous

*Work supported by the Bureau of Ordnance, U.S. Navy, under Contract NOrd 7386.

†The unidimensionality of this flame is discussed in references 1 and 2, especially the latter.

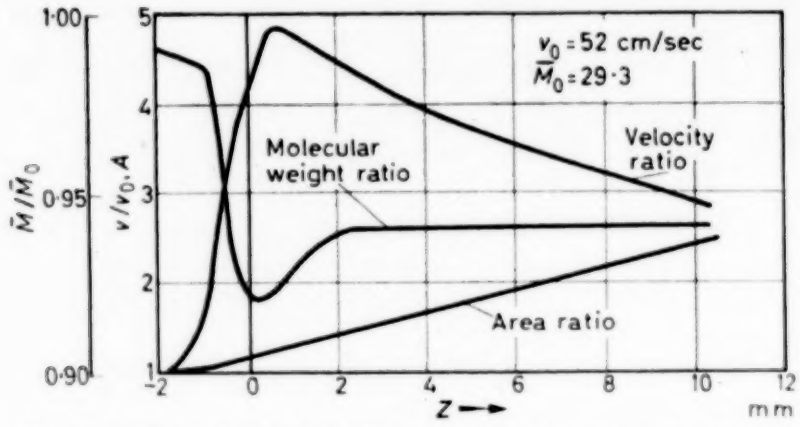

Figure 1. Dimensionless velocity normal to flame, stream tube area parallel to flame, and mean molecular weight of mixture as function of distance from centre of luminous zone

zone, negative on the cold gas side. The density at any point was derived from these quantities and the pseudo-unidimensional continuity relation

$$\rho_0 v_0 = \rho v A \qquad \ldots . [1]$$

where ρ is the density and A the stream tube area ratio a/a_0, the subscript $_0$ referring to cold gas. From the density, the temperature T was obtained using the equation of state

$$T = P\bar{M}/\rho R \qquad \ldots . [2]$$

where P is the pressure, $\bar{M}$ the mean molecular weight of the mixture, and R the universal gas constant. $\bar{M}$ at any point was obtained from the measured gas composition by means of the relation

$$\bar{M} = \Sigma_i x_i M_i \qquad \ldots . [3]$$

where x_i is the mole fraction of the i^{th} species and M_i its molecular weight. The $\bar{M}$ profile is given in *Figure 1* and the derived temperature profile in *Figure 2*. The adiabatic equilibrium flame temperature for this mixture

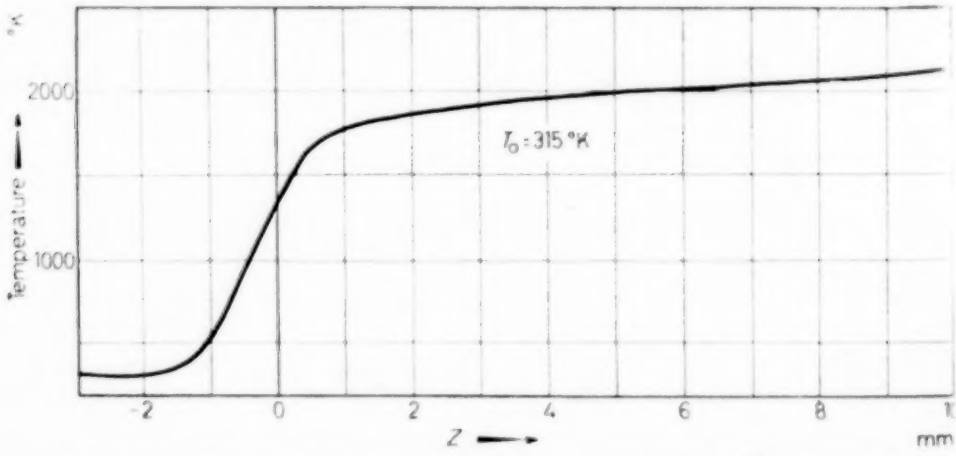

Figure 2. Temperature as function of distance from centre of luminous zone

was calculated* to be 2215°K, and the fairly close agreement between this value and the experimental asymptotic temperature (2130°K) promotes confidence in the results. The latter is lower probably because of diffusion of oxygen into the outer parts of the flame from the surrounding air.

The experimental composition data for the eleven molecular species found in the flame (besides nitrogen and argon) are presented as the solid curves in *Figures 3* to *13*. The primary mass spectrometer analyses are in terms of mole fractions, but these are readily converted to mass fractions f_i by means of the relation

$$f_i = x_i M_i / \overline{M} \quad \ldots . [4]$$

The actual points are included to give an idea of the amount of 'scatter'. As previously pointed out[1], the hydrogen results are by far the worst as

Table 1. Comparison of calculated and observed composition at hot boundary (Z=8·0 mm)

Species	*Mass fraction*	
	Calc.	*Obs.*
Oxygen	0·0077	0·0308
Carbon monoxide	0·0164	0·0157
Carbon dioxide	0·1544	0·159
Water	0·1041	—
Hydrogen	0·0004	0·0006

regards reproducibility, and the curve drawn through them should be taken only as an approximation. The carbon monoxide data also show more uncertainty than desirable for reasons discussed in the previous paper[1]; otherwise the distributions are quite smooth and generally reasonable.

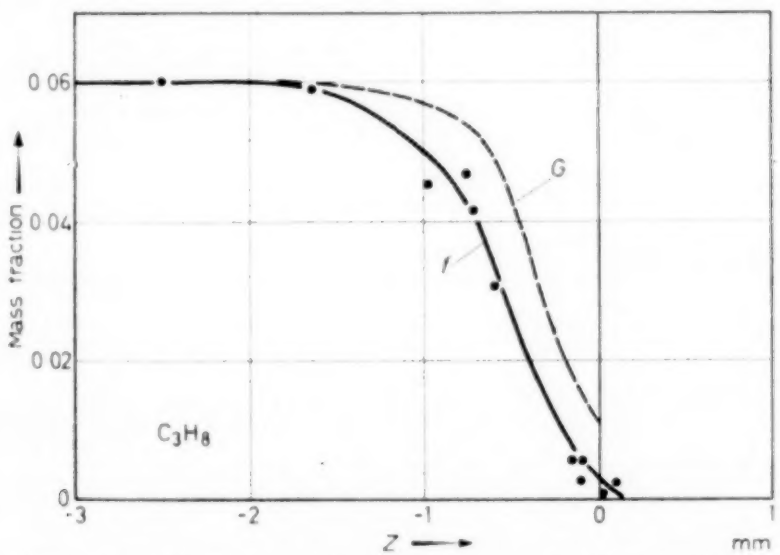

Figures 3 to 13. Concentrations (solid curves) and fractional mass rates of flow (broken curves) of stable species as function of distance from centre of luminous zone

*The authors are indebted to Mr W. A. Wright of the Ordnance Aerophysics Laboratory, Daingerfield, Texas, and Mr W. T. Renich of their own Laboratory, for this calculation.

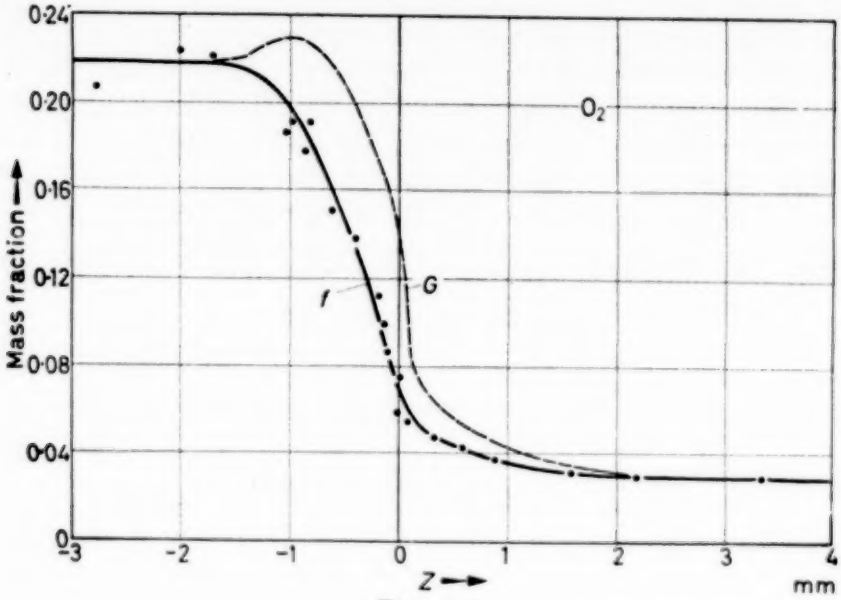

Figure 4

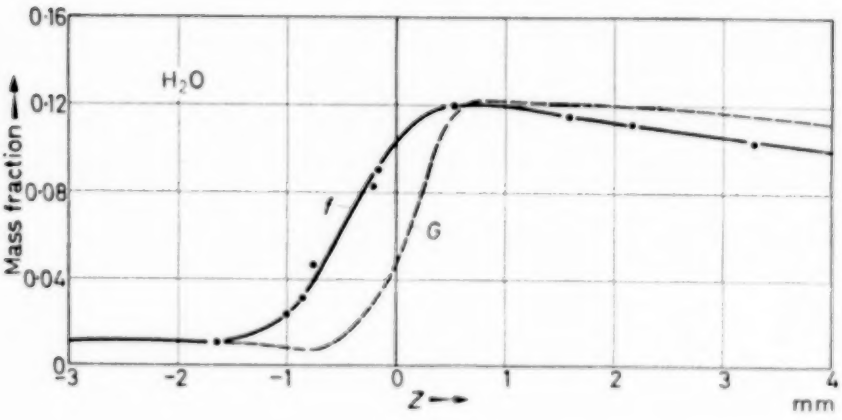

Figure 5

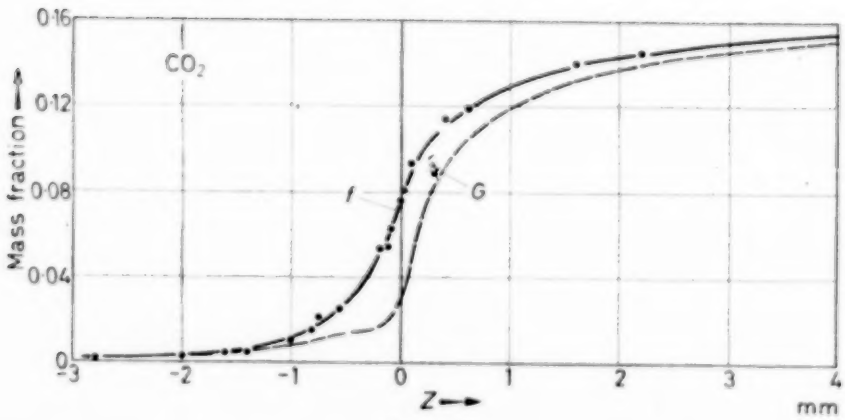

Figure 6

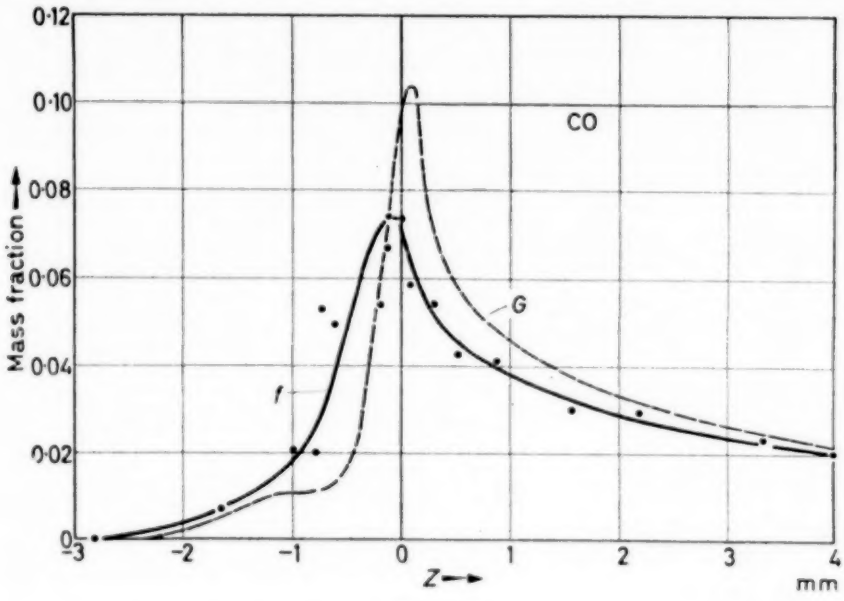

Figure 7

Figures 3 to *13* show data only as far as $Z = 4{\cdot}0$ mm; beyond this point the data approach asymptotically the values given in *Table 1*. The calculated equilibrium composition at the adiabatic flame temperature of 2215 °K is included for comparison. Agreement between the two compositions is generally quite good, except for oxygen which has a high concentration in

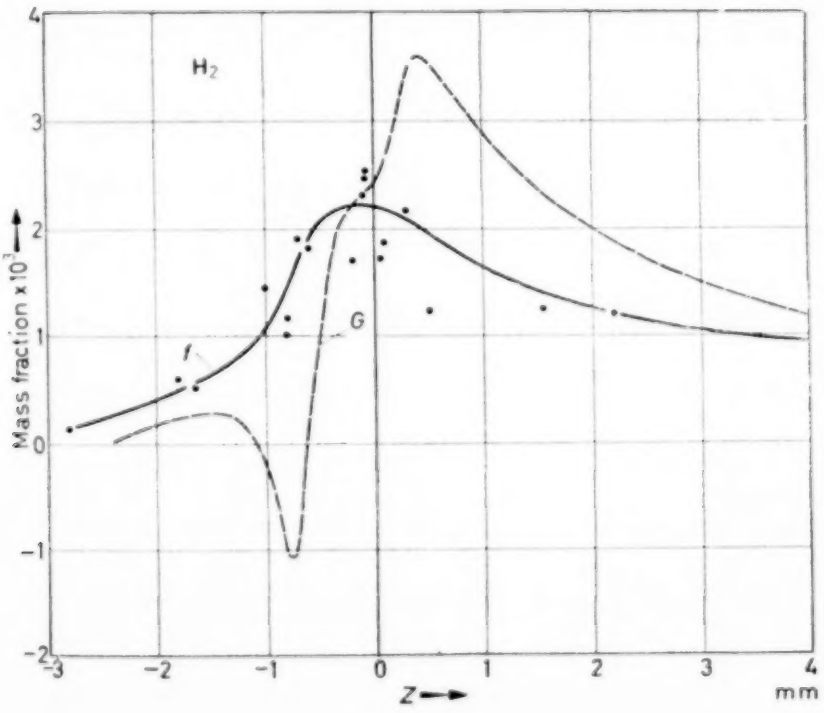

Figure 8

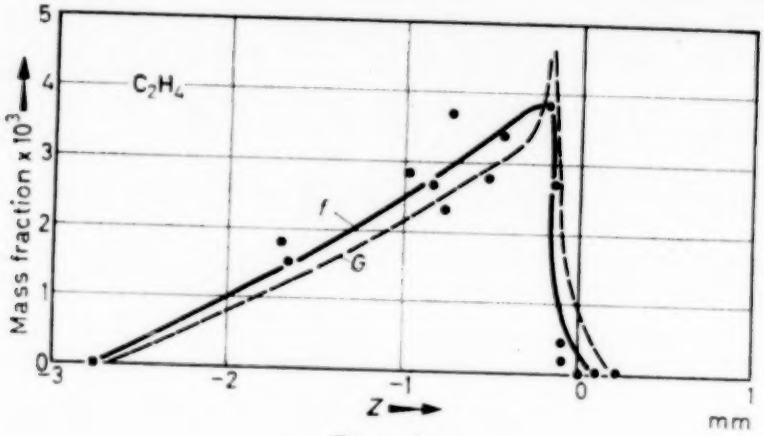

Figure 9

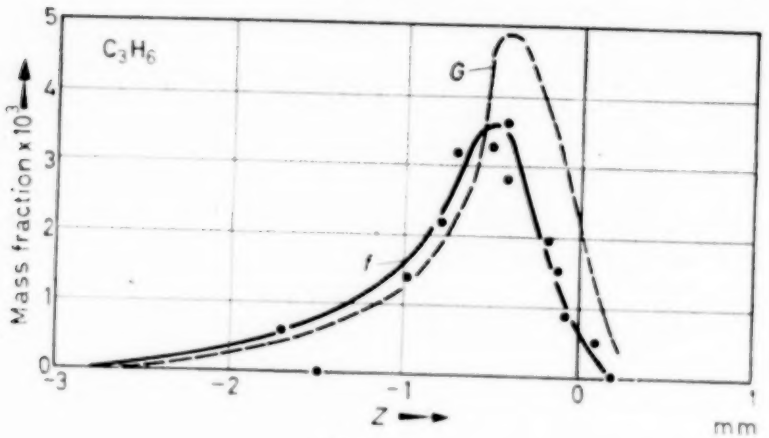

Figure 10

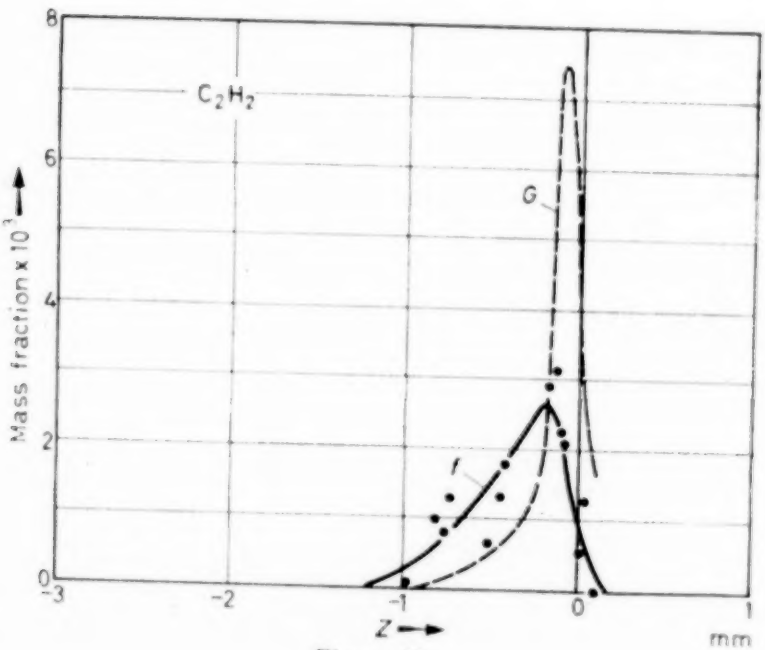

Figure 11

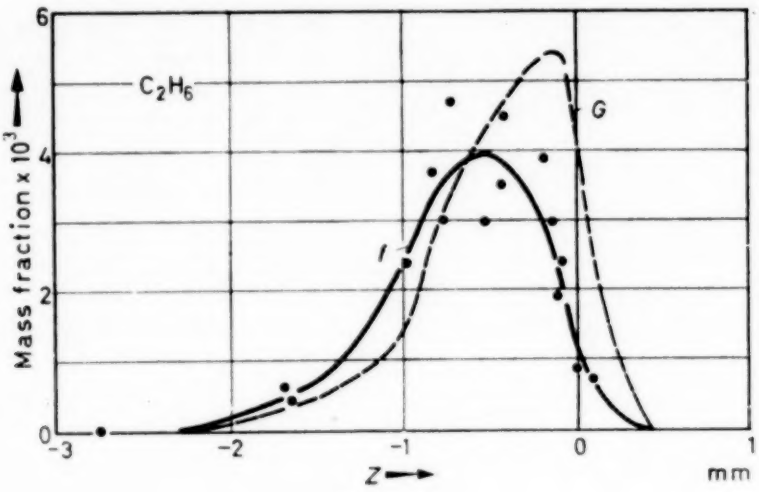

Figure 12

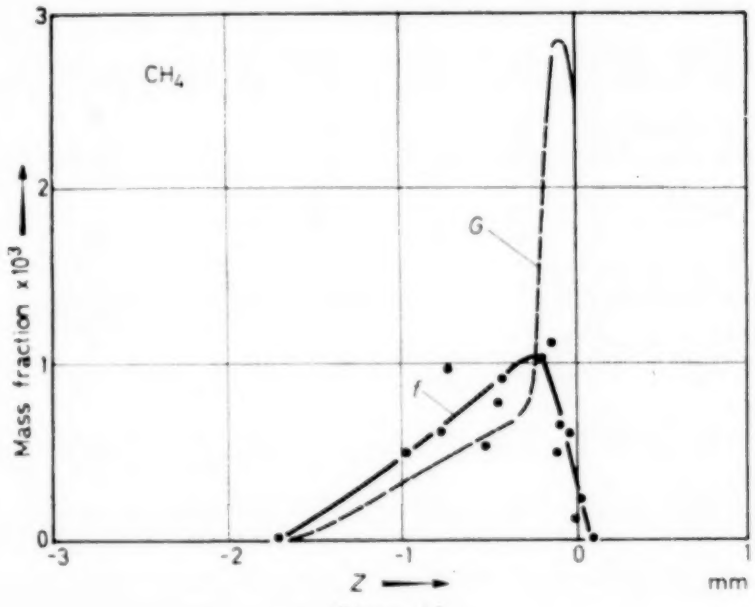

Figure 13

the sample—again probably owing to diffusion from the surrounding atmosphere. The observed value for water vapour is not included because this point was used to calibrate the mass spectrometer for water. It was necessary to use this procedure because the techniques available for making standard water vapour samples were unreliable. Instead, it was assumed that the sample taken at $Z = 8{\cdot}0$ mm had a water vapour content equal to the calculated adiabatic equilibrium value. This is obviously not an ideal procedure. The maximum in the water vapour curve is probably caused by loss to the outside by diffusion.

TREATMENT OF SAMPLING DATA

The problem of interpreting the probe samples from a laminar flame zone is complicated by the existence of concentration gradients—and hence

diffusion—of all species present. It is clear that the sample withdrawn from such a system by means of a small probe cannot—even in principle, i.e. assuming perfect chemical analysis and spatial resolution—represent *exactly* the composition of the gas mixture at the point of sampling. This is because the sampling process sets up an aerodynamic disturbance in what is initially a one-dimensional system, which causes diffusion in directions other than along the axis of flow. Thus the mixture entering the probe tip (sink) is different from that in the unperturbed zone. The higher the gas velocity at the probe entrance, the less important is the difference due to diffusion, however, and the authors have shown both experimentally and theoretically that, with the sampling rates employed in these studies (sonic flow at the probe throat), the error inherent in the sampling process attributable to this cause is negligible; details of this work will be published in a separate paper. For present purposes, the sampling data will therefore be taken to represent the true composition of the gas mixture which would exist at the sampling point if the probe were not present. A reservation is, of course, implicit in this statement, namely, that the sampled mixture is analysed only for stable species, so that radicals and atoms actually present in the flame are included in the measured stable components.

In order to make use of the experimental data for an analysis of the flame front structure, it is convenient to derive the quantities G_i defined by

$$G_i = N_i M_i (v + V_i)/\rho v = x_i M_i (v + V_i)/\overline{M} v \qquad \ldots [5]$$

where N_i is the number of moles of species i per unit volume, V_i is the diffusion velocity normal to the flame front and the other quantities are as already defined. G_i is thus the fraction of the total mass flow at any cross section contributed by species i, and contains terms due to both convection and diffusion. By definition, $\Sigma_i N_i M_i V_i = 0$.

The rigorous expression for the diffusion velocity* V_i in a multi-component mixture is a complex function of the composition and the binary diffusion coefficients of all the pairs of species present[3]. For our purpose such rigour would be hopeless and would not be warranted by the accuracy of the data. Since the mixture is nearly all nitrogen, it is a good approximation to regard each species as a trace component in a binary mixture with nitrogen. Then we can use the approximate relation

$$V_i = -(D_i/x_i)(\mathrm{d}x_i/\mathrm{d}Z) \qquad \ldots [6]$$

where D_i is the binary diffusion coefficient for species i and for nitrogen, and is a function of the space coordinate Z through its dependence on temperature. At the present time, the only way one can obtain the diffusion coefficients at flame temperatures is to use the kinetic theory calculations tabulated by J. O. HIRSCHFELDER, C. F. CURTISS and R. B. BIRD[3]. These are restricted to non-polar, or nearly non-polar, gases since the Lennard-Jones

*We neglect the effects of thermal diffusion in this paper. Calculations indicate that this is clearly justified for all the species present except hydrogen. For hydrogen in this flame, the contribution of thermal diffusion to the diffusion velocity is definitely not negligible, but is, at most, nearly comparable to that of the concentration diffusion. However, since this is true for only one species which is present in fairly small amounts, the effect of thermal diffusion on the overall characteristics of the mixture may safely be neglected.

12) potential used in the calculations is so restricted. All the species dealt h here are in this category with the exception of water vapour. Fortun- ly, experimental results[4] are available for water vapour–nitrogen, whose f fusion coefficient was found to be approximately proportional to T^2. F other species, it was convenient to make use of an empirical fit to the c lision integrals in Table 1-M of reference 3. A temperature dependence o $T^{1.67}$ fits the tabulated data to within 1 per cent over the range of interest h e, and this was used to compute the D_i values.

Calculations of all G_i were made at intervals of 0·2 mm through the flame, except in the region from $Z = -1{\cdot}2$ to $+0{\cdot}2$ where the interval was 0·1 mm. At each point and for each species, the appropriate diffusion coefficient was calculated as described above, the mole fraction gradient was obtained numerically from the smooth curve drawn through the experimental data, and V_i was calculated from equation 6. The diffusion velocities for several representative species are plotted in *Figure 14*, together with the mass average velocity v for comparison. It is apparent that the effect of diffusion is important in all cases and is quite pronounced for the lighter molecules. So far as the individual distribution is concerned, diffusion

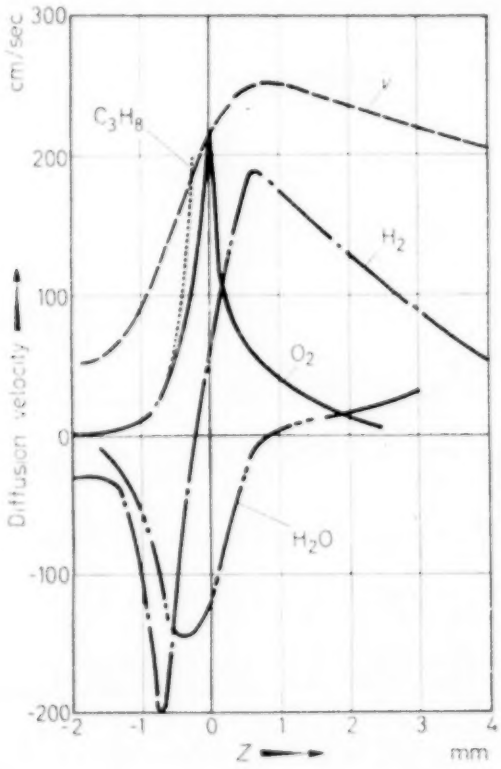

Figure 14. Comparison of diffusion velocities of various species with gas velocity v as function of distance from centre of luminous zone

could not be neglected for any species in a quantitative discussion of laminar flame structure. The fractional mass rate of flow G_i was then computed for each species at each point by means of equation 5; these values appear as the broken curves in *Figures 3* to *13*. For the species which show a maximum in the f_i curve, note that $f_i = G_i$ at the maxima, as then the diffusion velocities are zero. It is interesting to note also that the G_i curve for hydrogen actually

goes through a region of negative values. This means that, at these points, there is a net upstream flow of hydrogen molecules. In view of the uncertainty of the hydrogen data and the sensitivity of the G_i values to the derivative of these data, the negative region may or may not be real. The same reservation applies to the positive maximum in the G curve for oxygen —it may have arisen from the numerical treatment of the data.

ATOM BALANCE THROUGH THE FLAME

It is of great practical interest to be able to check in some way the experimental composition profiles and the treatment of diffusion described above. One way of doing this is by checking the conservation of atoms of a particular kind through the flame front. The pseudo-unidimensional continuity equation for species i, which includes area expansion of the stream tubes, is

$$\frac{\mathrm{d}}{\mathrm{d}Z}\left[N_i(v+V_i)A\right] = K_i A \qquad \ldots\ldots[7]$$

where K_i is the net molar rate of formation or disappearance of species i per unit volume caused by chemical reaction. Combining equation 7 with equation 5 yields $\frac{\mathrm{d}}{\mathrm{d}Z}\left(\rho v A \frac{G_i}{M_i}\right) = K_i A$ or, since $\rho v A$ and M_i are constants,

$$\left(\frac{\rho v}{M_i}\right)\left(\frac{\mathrm{d}G_i}{\mathrm{d}Z}\right) = K_i \qquad \ldots\ldots[8]$$

Multiplying this by n_i, the number of atoms of a particular kind in a molecule of species i, and summing over all species, gives

$$\rho v \sum_i \frac{n_i}{M_i}\frac{\mathrm{d}G_i}{\mathrm{d}Z} = \sum_i n_i K_i \qquad \ldots\ldots[9]$$

Since atoms are neither created nor destroyed, $\sum_i n_i K_i = 0$ and equation 9 becomes $\rho v \frac{\mathrm{d}}{\mathrm{d}Z}\sum_i \frac{n_i G_i}{M_i} = 0$

or

$$\sum_i \frac{n_i G_i}{M_i} = \text{constant} \qquad \ldots\ldots[10]$$

This relation was calculated for carbon, hydrogen and oxygen atoms at each point in the flame, with the results plotted in *Figure 15*. As might be expected, the carbon atom balance is the best of the three. For reasons previously mentioned, both the hydrogen and the water vapour analyses are subject to greater error than the others, and this would be reflected in the atom balances for hydrogen and oxygen. In spite of the water vapour uncertainty, the positive oxygen deviation is thought to be real; it can be ascribed to diffusion from the surrounding atmosphere. Considering the manipulations and unavoidable uncertainties which have entered into these calculations, it is felt that the atom balances are reasonably satisfactory and are really very good for carbon. The worst deviations occur in the rapid reaction region around the luminous zone where the gradients are subject to the greatest error.

REMARKS

ese data have provided a complete description of this flame, excluding ormation on free radicals. Energy fluxes and chemical kinetic infor- tion can also be derived, but the calculations are too extensive for lusion here. However, a few qualitative observations seem appropriate.

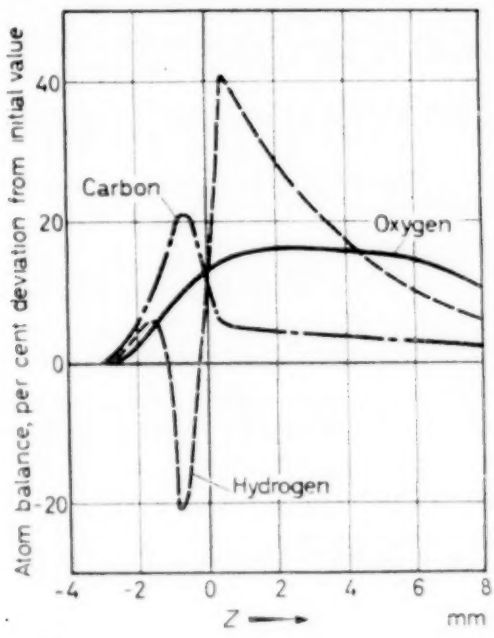

gure 15. Atom balance as function distance from centre of luminous zone

The first observation concerns the intermediates present in analytical ncentrations. These include carbon monoxide, hydrogen and all hydro- rbons lower than propane, with the exception of methyl-acetylene. Higher drocarbons and oxygen-containing intermediates such as alcohols, alde- des (in particular formaldehyde), ketones, and acids are not present. To tablish that this absence was not due to faulty sampling or abnormally gh disappearance rates, both methyl alcohol and formaldehyde were troduced into the incoming gas and were successfully detected. Spot tests r formaldehyde were also made on large samples, and it was felt that the pper limit of concentration for these materials was 0·1 per cent. The bsence of oxygen-containing intermediates appears to be typical of hot mes—as opposed to cool flames and low temperature oxidations—since milar results have been reported in the methane diffusion flame[3]. These sults would appear to exclude formaldehyde as an intermediate in flame actions, and the absence of higher hydrocarbons would appear to exclude drocarbon radical recombination as an important process in flames.

The temporal order of positive formation rates of the intermediates can derived from the G curves. The concentration curves are shifted by the ects of diffusion and can be very misleading if diffusion is not considered. hylene and propylene are the first hydrocarbon intermediates which pear, and carbon monoxide and hydrogen also make their first appearance

at the same point. Ethane formation begins at a somewhat later point, followed by methane and acetylene, which appear to be secondary products. As might be expected, the peak in carbon monoxide and hydrogen formation is reached at the point of most rapid hydrocarbon disappearance. Hydrocarbons have completely disappeared by $Z=0{\cdot}1$ mm, although carbon monoxide and hydrogen continue reaction over an extended region, finally reaching equilibrium conditions nearly 1 cm beyond the luminous zone. This confirms previous observations that hydrocarbon–air flames can be considered as two regions: one of rapid reaction of hydrocarbon disappearance, and one of slow reaction associated with carbon monoxide and hydrogen. Water vapour formation is 90 per cent complete at the outer edge of the luminous zone.

The atomic mass balance curves for oxygen indicate that there is definite transport of oxygen into the slow reaction zone, but this complication does not interfere with the analysis of the data as the measurements form a complete set, but it does severely restrict the application of any one-dimensional theory to this region of the flame. The maximum in the water vapour curve probably indicates a loss of water vapour by diffusion. The hydrogen mass balance data are too unreliable to allow evaluation of hydrogen loss, but it certainly should be appreciable. The importance of diffusion in this post-luminous reaction region is demonstrated qualitatively by experiments in which breathing helium (20 per cent oxygen–80 per cent helium) was used in the shroud surrounding the flame. Just outside the luminous zone at the tip of the flame, the helium concentration was 2 per cent. This became a trace less than 0·2 per cent at the inner edge of the luminous region.

Many members of the Applied Physics Laboratory, The Johns Hopkins University, have contributed to this work. The authors are especially grateful to Miss Geraldine Ashour and Mrs J. S. Kimrey for performing parts of the numerical calculations, and to Drs W. H. Avery and W. G. Berl for helpful discussions.

Applied Physics Laboratory,
The Johns Hopkins University,
Silver Spring, Maryland, U.S.A.

(Received October 1956)

REFERENCES

[1] FRISTROM, R. M., PRESCOTT, R. and GRUNFELDER, C. *Combustion & Flame* 1 (1957) 102
[2] FRISTROM, R. M. *J. chem. Phys.* 24 (1956) 888
[3] HIRSCHFELDER, J. O., CURTISS, C. F. and BIRD, R. B. *Molecular Theory of Gases and Liquids* Wiley: New York, 1954
[4] SCHWERTZ, F. A. and BROW, J. E. *J. chem. Phys.* 19 (1951) 640
[5] SMITH, S. R. and GORDON, A. S. *J. phys. Chem.* 60 (1956) 759

On Generalized Scaling Procedures for Liquid-fuel Rocket Engines*

S. S. Penner and A. E. Fuhs

The scaling procedures of Penner and Tsien, of Crocco and of Barrère have been generalized by using the assumption that the mean drop size is proportional to the product of powers of the Weber number and the Reynolds number, together with the hypothesis that the total conversion time varies as a power (usually the second) of the drop diameter. The results obtained for the steady aerothermochemistry and for unstable motor operation (low-frequency and high-frequency oscillations) are shown to reduce to previously published rules when suitable simplifying assumptions are made.

In recent publications on similarity analysis for the scaling of liquid-fuel rocket engines[1–4], procedures have been developed both for scaling the steady aerothermochemistry and for maintaining similar conditions with respect to low-frequency and high-frequency motor oscillations. An important practical problem concerned with rocket motor development is the result of occurrence of uncontrolled high-frequency motor oscillations. The value of similarity analysis must ultimately be assessed in terms of our ability to design large engines with predictable performance on the basis of small-engine test experience. In this connection, the most urgent experimental problem is that of determining minimum conditions required for effective practical scaling.

We may consider qualitatively three separate components which are changed on scaling, any combination of which may be of dominant importance in producing uncontrolled motor oscillations. Thus high-frequency oscillatory combustion involves, in general, the following separate phenomena: (*a*) a driving mechanism for producing the oscillations; (*b*) a coupling process which allows sustained oscillations; (*c*) damping mechanisms for preventing or minimizing motor oscillations.

A study of published scaling procedures shows clearly that it is impossible, except under very special conditions and for particular (and generally invalid) assumptions relating to the factors determining the chemical conversion time, to maintain exact similarity with respect to all phases of motor operation. For this reason, a preliminary experimental programme in the development of rational scaling procedures should be designed to show which physicochemical processes are of dominant importance for a particular motor design.

If a strong driving mechanism is generally sufficient to induce unstable motor operation, we may be reduced to a study of microscopic phenomena involving the details of injector performance and combustion reactions. On

* The work described in this paper was supported by the U.S. Air Force Office for Advanced Study, under contract AF 18(603)-107 with the American Machine and Foundry Co. and Jet Propulsion Research, Inc.

the other hand, if we can prevent disastrous motor oscillation merely by preventing strong coupling between the driving and sustaining mechanisms, then motor oscillations can presumably be avoided by retaining an invariant ratio of chemical conversion time to wave propagation time. Finally, it is conceivable that motor oscillation can be prevented by maintaining adequate damping, irrespective of the nature of the driving and sustaining processes. In this case a detailed analysis of the steady aerothermochemistry, of frictional losses, and of damping associated with oscillating gas flow through the nozzle may be required.

It is the purpose of theoretical studies on similitude in engine scaling to provide useful guides for experimental work. Meaningful answers to the questions raised in the preceding paragraphs can only be obtained empirically. To facilitate this programme, a concise and more general approach to the scaling problem than has yet been used is presented in the following section. The results contain the rules of S. S. PENNER and H. S. TSIEN, of L. CROCCO, and of M. BARRÈRE as special cases.

GENERALIZED SCALING RULES

For a given propellant system with fixed injector temperature the important similarity groups for stable motor operation are the Reynolds (R_e) and first Damköhler (D_I) similarity parameters; the Mach number (M) may become important for high-velocity processes involving oscillations.

Here

$$R_e = \rho v L/\eta \qquad \ldots.[1]$$

$$D_I = (L/v)/\tau \qquad \ldots.[2]$$

and

$$M = (\rho v^2/\gamma p)^{\frac{1}{2}} \qquad \ldots.[3]$$

where ρ denotes density, v linear flow velocity, L a characteristic chamber dimension, η viscosity coefficient, τ chemical conversion time, γ ratio of specific heats, and p chamber pressure. Except for the orifice diameter, we shall impose the conditions of geometric similarity with respect to all chamber dimensions in order to make all Reynolds numbers constant. For fixed propellants and injection temperature, the coefficients η and γ are fixed whereas ρ becomes effectively equivalent to p. Surface reactions are neglected throughout the following discussion although they may be important in selected motor applications.

We denote by n_i the ratio i_H/i_{Mo} where H and Mo denote, respectively, the large motor (H for *Hauptausführung*) and prototype (Mo for *Modell* = model). Here i may represent any of the independent variables. We expect, in general, that the ratio of mean droplet diameter D to orifice diameter h is a function of the Weber (W_e) and Reynolds numbers based on the orifice diameter*. In particular, we assume that

$$\overline{D}/h \sim (W_e)^{-\alpha}(R_e)^{-\beta}$$

$$\sim (h\Delta p/\sigma)^{-\alpha}(\rho v h)^{-\beta} \qquad \ldots.[4]$$

*For a detailed discussion of this problem, as well as for some experimental correlations, see M. E. SHAFER and H. L. BOWEN, *J. Res. nat. Bur. Stand.* 52 (1954) 141.

where Δp is injector pressure drop, σ interfacial tension, and α and β represent parameters which must be determined empirically. Finally, we introduce the hypothesis that the conversion time τ is determined through $\bar{D}$ and p, viz.

$$\tau \sim \bar{D}^{\delta} p^{-m'} \qquad \ldots . [5]$$

with δ and m' denoting parameters which must also be obtained experimentally. Equation 5 is known to hold when $m' = 0{\cdot}2$, $\delta = 2$, for the burning of stationary fuel droplets in an oxidizing medium[5]. A value $\delta = 2$ has been observed also in the burning of monopropellants and premixed bipropellant droplets in an inert atmosphere[6]. Finally, the observed dependence of τ on chamber pressure and injection pressure drop for a nitric acid–furfuryl alcohol rocket engine, which follows from equations 4 and 5 with fixed values of h and $\beta = 0$, is in accord with the values[7] $\delta = 2$, $m' = 0{\cdot}3$, and $\alpha = 0{\cdot}8$*.

In the following discussion we shall neglect the Mach number as a similarity parameter, thereby restricting our analysis to the development of scaling procedures for stably operating rocket engines. This is of practical importance in engine development programmes†.

Similarity of steady aerothermochemistry

The conditions for maintaining constant Reynolds and first Damköhler numbers are

$$p_H v_H L_H = p_{M_0} v_{M_0} L_{M_0} \quad \text{and} \quad L_H / v_H \tau_H = L_{M_0} / v_{M_0} \tau_{M_0}$$

whence it follows that

$$n_t = 1 / n_p n_v \qquad \ldots . [6]$$

and

$$n_t / n_v = n_\tau \qquad \ldots . [7]$$

Combining equations 6 and 7 we find the universal relation

$$n_\tau = 1 / n_p n_v^2 \qquad \ldots . [8]$$

which has been discussed for chemical reactors, particularly[8, 9] for the case $n_p = 1$.

From equations 4 and 5 we find the following alternate relation for n_τ:

$$\begin{aligned} n_\tau &= n_s^{\delta\alpha} n_h^{\delta(1-\alpha-\beta)} n_p^{-(\delta\beta+m')} n_{\Delta p}^{-\delta(\alpha+\frac{1}{2}\beta)} \\ &= n_s^{\delta\alpha} n_h^{\delta(1-\alpha-\beta)} n_p^{-(\delta\beta+m')} n_v^{-2\delta(\alpha+\frac{1}{2}\beta)} \qquad \ldots . [9] \end{aligned}$$

where we have assumed that

$$\Delta p \sim v^2, \; n_{\Delta p} = n_v^2 \qquad \ldots . [10]$$

Eliminating n_v between equations 8 and 9 we find

$$n_p^{1-(\delta\beta+m')} n_v^{2-2\delta(\alpha+\frac{1}{2}\beta)} = n_s^{-\delta\alpha} n_h^{\delta(\alpha+\beta-1)}$$

*It might be more logical to represent τ as the sum of times associated with evaporation, diffusion, chemical reaction, etc. In the absence of adequate data, however, we shall use the functional form of equation 5.

†In laboratory tests which are designed to test scaling rules rather than to develop engines, it may be important to scale also an unstably operating combustion chamber. In this case the Mach number should not be neglected as an important similarity group.

and after using equation 6 to eliminate n_p

$$n_c^{1-2\delta z+m'} = n_z^{-\delta z} n_h^{\delta(z+\beta-1)} n_L^{1-(\delta\beta+m')} \quad \ldots . [11]$$

By the use of equations 6 and 11 we find also that

$$n_p^{-1+2\delta z-m'} = n_z^{-\delta z} n_h^{\delta(z+\beta-1)} n_L^{2-\delta(2z+\beta)} \quad \ldots . [12]$$

(1) *Relation between geometric scale factor n_L and thrust scale factor n*—The continuity equation for the rocket chamber is

$$(pvd^2)_H/(pvd^2)_{Mo} = n \quad \ldots . [13]$$

where d identifies the chamber diameter and n is the thrust scale factor.

Hence $$n_p n_c n_L^2 = n$$

and, using equation 6,

$$n = n_L \quad \ldots . [14]$$

i.e. the geometric and thrust scale factors are identical. The relatively small effect of n_p on thrust, for pressures exceeding the normal operating pressure, is neglected.

(2) *Scale factor for the orifice hole diameter*—The continuity equation for flow through the orifice holes is

$$(vh^2)_H/(vh^2)_{Mo} = n = n_L \quad \ldots . [15]$$

since the number of orifice holes remains unchanged if geometric similitude is enforced. Hence

$$n_c n_h^2 = n_L \quad \ldots . [16]$$

We may combine equations 11 and 16 in order to obtain the appropriate scaling rule for the orifice diameter. The result is

$$n_h = n_z^{\frac{\delta z}{2(1+m')-\delta(1+3z-\beta)}} n_L^{\frac{2m'-\delta(2z-\beta)}{2(1+m')-\delta(1+3z-\beta)}} \quad \ldots . [17]$$

(3) *Scale factor for the linear flow velocity*—The scale factor for the linear flow velocity may be obtained from equations 16 and 17. The result is

$$n_v = n_z^{\frac{-2\delta z}{2(1+m')-\delta(1+3z-\beta)}} n_L^{\frac{2(1-m')-\delta(1-z+\beta)}{2(1+m')-\delta(1+3z-\beta)}} \quad \ldots . [18]$$

(4) *Scale factor for the chamber pressure*—From equations 6 and 16 it is apparent that

$$n_p = n_h^2/n_L^2$$

Hence, using equation 17, we find

$$n_p = n_z^{\frac{2\delta z}{2(1+m')-\delta(1+3z-\beta)}} n_L^{\frac{2\delta(z+1)-4}{2(1+m')-\delta(1+3z-\beta)}} \quad \ldots . [19]$$

(5) *Scale factor for the nozzle throat diameter*—From the continuity equation for flow through the nozzle throat of diameter r we obtain

$$\frac{(pr^2)_H}{(pr^2)_{Mo}} = n = n_L \quad \ldots . [20]$$

since the linear flow velocity at the nozzle throat is sonic irrespective of the motor size. Hence

$$n_p n_r^2 = n_L \qquad \ldots . [21]$$

and, using equation 19,

$$n_r = n_\alpha^{\frac{-\delta\alpha}{2(1+m')-\delta(1+3\alpha-\beta)}} n_L^{\frac{(3+m')+\frac{1}{2}\delta(\beta-5\alpha-3)}{2(1+m')-\delta(1+3\alpha-\beta)}} \qquad \ldots . [22]$$

(6) *Scale factor for the feed system*—From the continuity equation for the feed system in which the linear flow velocity is v_f and the cross sectional area A_f we obtain

$$(v_f A_f)_H / (v_f A_f)_{Mo} = n = n_L$$

whence

$$n_{v_f} = n_L / n_{A_f} \qquad \ldots . [23]$$

Similarity of regenerative cooling system[2]

Since the Reynolds and Prandtl numbers are fixed, the Nusselt heat transfer number also remains the same in the model and in the large engine. Hence the total heat Q which must be transferred to the interior motor walls, for chambers operating under similar conditions of temperature, pressure and internal aerothermochemistry, must be directly proportional to the propellant consumption rate; this, in turn, varies linearly with the geometric scale factor, as has been shown in equation 15. Thus

$$n_Q = Q_H / Q_{Mo} = n_L \qquad \ldots . [24]$$

Correspondingly, the heat transfer per unit area q must obey the scaling requirement

$$n_q \equiv q_H / q_{Mo} = 1 / n_L \qquad \ldots . [25]$$

For motors operating with maintenance of complete similarity, the interior and exterior wall temperatures are fixed. Therefore, since the heat transfer per unit area varies as $1/n_L$, the temperature gradient must be changed by the same factor, i.e. the wall thickness W must be scaled in geometric proportions:

$$n_W \equiv W_H / W_{Mo} = n_L \qquad \ldots . [26]$$

The heat transfer problem has now been reduced to a determination of the requirements in the cooling passages for transferring heat per unit area in accordance with the scaling condition expressed by equation 25. The Reynolds number in the cooling coils remains fixed if the cooling coils of diameter C are also scaled in geometric proportions, viz.

$$n_C \equiv C_H / C_{Mo} = n_L \qquad \ldots . [27]$$

In the special case of a regeneratively cooled motor, the cooling passages correspond to the feeding system. For fixed propellants, constant Prandtl, Reynolds, and Nusselt numbers are maintained if

$$[v_f A_f^{\frac{1}{2}}]_H / [v_f A_f^{\frac{1}{2}}]_{Mo} = n_{v_f} n_{A_f}^{\frac{1}{2}} = 1$$

or

$$n_{v_f} = 1 / n_L \qquad \ldots . [28]$$

a relation which is evidently consistent with equation 23 if geometric similarity is maintained for the cooling coils.

In practice, the scaling requirements for the wall thickness and cooling coil dimensions may be undesirable because of excessive weight, or they may be inconsistent with design restrictions such as those imposed by similarity analysis for maintenance of low-frequency stability.

The thickness of the outer wall of the cooling coils may be changed at will without affecting any of the other design restrictions obtained from similitude considerations.

Similarity of sweat cooling

If a fraction ε' of the total propellant flow is used for sweat cooling, this fraction must be maintained at a fixed value as the engine is scaled. Details concerning the scaling of pore size in motor walls are easily worked out but will not be considered in the present discussion.

Low-frequency stability

L. Crocco[2] has discussed scaling procedures for a rigid and rigidly supported feeding system neglecting the compressibility of the propellants. Low-frequency stability depends on several parameters including the ratio of the chemical conversion time τ to the residence time τ_r, the relative pressure drop $\Delta p/p$ (Δp = pressure drop across injection orifices, p = steady operating pressure in the combustion chamber) and an inertia parameter which equals the ratio of the kinetic energy of the propellants in the feeding system to the work done on the propellants by the pressure drops during the residence time.

The ratio of the chemical conversion time τ to the residence time τ_r is maintained invariant by enforcing the condition that the first Damköhler similarity group must remain fixed. This requirement has been introduced in the discussion relating to the steady aerothermochemistry and is given explicitly in equation 7. In view of equation 18, the result may be stated in the form

$$\pi_7 \equiv \pi_{\tau_r} = \pi_2^{\frac{2\delta_2}{2(1+m)-\delta(1+3\alpha-\beta)}} \pi_{L_c}^{\frac{2(2m-2\delta_2+\delta\beta)}{2(1+m)-\delta(1+3\alpha-\beta)}} \qquad \ldots [29]$$

Next we consider the implications of the low-frequency stability requirement that

$$\frac{(\Delta p/p)_{II}}{(\Delta p/p)_{M_\infty}} = \frac{(\Delta p)_{II}}{(\Delta p)_{M_\infty}} \frac{p_{M_\infty}}{p_{II}} = 1 \qquad \ldots [30]$$

Since $\Delta p \sim v^2$, equation 30 is equivalent to the relation

$$(v^2/p)_{II}/(v^2/p)_{M_\infty} = \pi_v^2/\pi_p = 1$$

By using equations 18 and 19 it may then be shown that equation 30 reduces to the condition

$$\pi_2^{\frac{-6\delta_2}{2(1+m)-\delta(1+3\alpha-\beta)}} \pi_{L_c}^{\frac{4(1+m)-2\delta(\beta+2)}{2(1+m)-\delta(1+3\alpha-\beta)}} = 1 \qquad \ldots [31]$$

For $n_\tau = 1$, $n_l \neq 1$, equation 31 corresponds to either of the relations

$$\left.\begin{aligned} 2(2-m') &= \delta(\beta+2) \\ \text{or} \qquad 2(1+m') - \delta(1+3\alpha-\beta) &= \infty \end{aligned}\right\} \qquad \ldots\ldots [31a]$$

The inertia parameter

$$J = K \frac{l_f}{A_f} \frac{F}{p\tau} \frac{p}{\Delta p} \qquad \ldots\ldots [32]$$

must also remain invariant to maintain low-frequency stability[2]. Here K is a constant, l_f represents the equivalent length of the feeding system with cross sectional area A_f, F is the total propellant injection rate, and the other symbols have their usual meaning. The condition

$$J_H / J_{M_0} = 1 \qquad \ldots\ldots [33]$$

then becomes

$$\frac{(l_f/A_f)_H}{(l_f/A_f)_{M_0}} = n_p n_\tau / n_L \qquad \ldots\ldots [34]$$

in view of equation 30 and of equations 13 and 14. Using equations 19 and 29 we find the result

$$\frac{(l_f/A_f)_H}{(l_f/A_f)_{M_0}} = n_\tau^{\frac{4(2-m')}{2(1-m')-\delta(1+3\alpha-\beta)}} n_L^{\frac{\delta(3+\alpha+\beta)-2(m'-3)}{2(1-m')-\delta(1+3\alpha-\beta)}} \qquad \ldots\ldots [35]$$

For scaling of the feeding system and cooling coils with maintenance of geometric similarity, the left-hand side of equation 35 evidently reduces to

$$(l_f/A_f)_H / (l_f/A_f)_{M_0} = 1/n_L$$

Crocco[2] has indicated the need for extending the analysis presented in this section in order to make allowance for compressibility of the propellants, non-rigid feeding systems and/or non-rigid mountings, systems involving pumps for pressurization, etc. Details concerning studies of this type are best worked out in connection with motor development programmes.

High-frequency stability

High-frequency instabilities can presumably be controlled, for operating conditions otherwise similar, if the ratio of the chemical time τ is fixed with respect to the wave propagation times τ_W. But the latter are linear functions of the chamber dimensions for sound waves as well as for shock waves provided the sound velocity remains invariant. Hence, for fixed temperature and γ, the similarity requirement for high-frequency instability may be written in the form

$$n_\tau = n_{\tau_W} = n_L \qquad \ldots\ldots [36]$$

It is apparent that the condition expressed by equation 36 is not usually consistent with the similarity requirement for the steady aerothermochemistry or for low-frequency stability, both of which lead to the result given in equation 29.

Equation 36 expresses only the condition for similitude of the driving and coupling forces for oscillations. The forces producing oscillations must be balanced against the damping forces, of which the principal sources must be frictional losses. These, in turn, should be similar as long as the Reynolds number is constant. Damping associated with the oscillating gas flow through the nozzle is not similar unless the nozzles are scaled with maintenance of complete geometric similarity. However, for a well designed prototype it appears unlikely that damping through nozzle oscillations plays a dominant role.

SUMMARY OF RESULTS AND DISCUSSION

In *Table 1* the similitude requirements for different aspects of the scaling problem have been summarized.

The Penner–Tsien (P.–T.) relations correspond to the special case in which $m' = \alpha = \beta = 0$, $n_s = n_p = 1$, and $\delta = 2$; they can be derived from the generalized results formally by letting m' approach infinity. The scaling procedure for the P.–T. rule is summarized in *Table 2*.

Crocco's second rule corresponds to the special condition $\delta = 0$; the results thus obtained are listed in *Table 3*.

Barrère's scaling rule is based on an empirical expression for τ (derived from motor tests with red fuming nitric acid and furfuryl alcohol) which is inconsistent with the assumptions expressed by equations 4 and 5. Thus Barrère starts from the relation

$$\tau \sim \Delta p^{-r'} p^{-m'} \qquad \ldots\ldots [37]$$

which is in agreement with equations 4 and 5 if $\delta\alpha = r'$, $\beta = 0$, $n_s = 1$, and $n_b = 1$ in the relation for $\overline{D}$ only. This last requirement is probably to be attributed to the fact that motor tests were carried out without variations in orifice diameter. The statement $n_b = 1$ in the expression for $\overline{D}$ is inconsistent with Barrère's scaling rule for n_b derived from other considerations. It will be interesting to see if motor tests with variable injection orifices are really correlated better by equations 4 and 5 than by equation 37. The scaling procedure of Barrère can be obtained by repeating the analysis described in detail in the text with equation 37 substituted for equations 4 and 5. The results derived from this study are summarized in *Table 4*.

Reference to *Tables 1* to *4* shows that the scaling requirements for the steady aerothermochemistry are not generally consistent either with those for low-frequency stability or with those for high-frequency stability*. Thus it is impossible to scale with maintenance of complete similarity with respect to all the important variables. From the practical point of view, the most important discrepancy is that between the usually contradictory requirements for n_b in the analysis for the steady aerothermochemistry and for high-frequency stability. As was stated in an earlier paper[3] and mentioned again in the introduction to the present survey, we are as yet

*The only exception is provided by Crocco's second rule in the unlikely case that $m' = 1$; see *Table 3*.

nable to assess the significance of this discrepancy. For this reason a reliminary test programme on engine scaling should involve an investiation of high-frequency stability of properly performing engines in which nly the scaling rule $n_\tau = n_L$ is accounted for.

The steady aerothermochemistry and high-frequency stability requirements are satisfied simultaneously if

$$n_\tau^{\frac{2\delta z}{2(1+m')-\delta(1+3z-\beta)}} n_L^{\frac{2(2m'-2\delta z+\delta\beta)}{2(1+m')-\delta(1+3z-\beta)}} = n_L$$

or

$$n_\tau^{\frac{2\delta z}{2(1+m')-\delta(1+3z-\beta)}} n_L^{\frac{2(m'-1)+\delta(1+\beta-z)}{2(1+m')-\delta(1+3z-\beta)}} = 1 \qquad \ldots.[38]$$

According to equation 38, variation of n_τ can, in principle, be used to maintain similarity for the steady aerothermochemistry and high-frequency stability. Whether or not this programme is practically feasible remains to be seen and cannot, in any event, be decided until reliable empirical information is available, not only on the validity of the functional relations given in equations 4 and 5, but also on the absolute values of the parameters δ, z, β and m'.

It is interesting to note that equation 38 is satisfied exactly when $n_\tau = 1$ if either

$$\left.\begin{aligned} 2(1-m') &= \delta(1+\beta-z) \\ 2(1+m') &\neq \delta(1+3z-\beta) \end{aligned}\right\} \qquad \ldots.[39]$$

or

$$\left.\begin{aligned} 2(1+m')-\delta(1+3z-\beta) &= \infty \\ 2(1-m')-\delta(1+\beta-z) &\neq \infty \end{aligned}\right\} \qquad \ldots.[40]$$

The latter relation would never be expected to apply*. For $m' = 0$, $\delta = 2$, $z = \beta = 0$, the first expression given in equation 39 is satisfied; however, in this case all the exponents for n_L appearing in the scaling rules for n_h, n_c, n_p, n_r and n_τ become indeterminate and, furthermore, the second condition given in equation 39 is not satisfied. In fact, the rule $m' = 0$, $\delta = 2$, $z = \beta = 0$ for $n_\tau = 1$ corresponds simply to the P.–T. procedure.

According to Barrère's findings for a bipropellant motor utilizing red fuming nitric acid and furfuryl alcohol, $m' = 0{\cdot}3$, $\delta = 2$, $\delta z = 1{\cdot}6$, $\beta = 0$. Then

$$2(1-m') = 1{\cdot}4$$

and

$$\delta(1+\beta-z) = 0{\cdot}4$$

Therefore the conditions given in equation 39 are far from satisfied.

Rather than pursue the interpretation of the generalized results for other speculative cases, we conclude the present discussion with the observation that extensive tests yielding a correct functional form for τ are the first

*The statement given in equation 40 should not be confused with the *formal procedure* used to derive the P.–T. results from the generalized expressions by setting $m' = \infty$.

Table 1. Generalized scaling rules for liquid-fuel rocket engines deduced from similitude considerations

	A *Steady aerothermochemistry*	B *Regenerative cooling*	C *Low-frequency stability*	D *High-frequency stability*
(1)	$n=n_L$			
(2)	$n_h=n_g\left(\frac{\delta\alpha}{2(1+m')-\delta(1+3\alpha-\beta)}\right)_{n_L}\left(\frac{2\alpha-\delta(2\alpha-\beta)}{2(1+m')-\delta(1+3\alpha-\beta)}\right)$	(8) $n_{c_f}=1/n_L$	(12) $n_g\left(\frac{-6\delta\alpha}{2(1+m')-\delta(1+3\alpha-\beta)}\right)_{n_L}\left(\frac{4(2-m')-2\delta(\beta+2)}{2(1+m')-\delta(1+3\alpha-\beta)}\right)=1$	
(3)	$n_v=n_g\left(\frac{-2\delta\alpha}{2(1+m')-\delta(1+3\alpha-\beta)}\right)_{n_L}\left(\frac{2-\delta(1-m')-\delta(1-\alpha-\beta)}{2(1+m')-\delta(1+3\alpha-\beta)}\right)$	(9) $n_a=1/n_L$		
(4)	$n_p=n_g\left(\frac{2\delta\alpha}{2(1+m')-\delta(1+3\alpha-\beta)}\right)_{n_L}\left(\frac{2\delta(\alpha+1)-4}{2(1+m')-\delta(1+3\alpha-\beta)}\right)$		(13) $\frac{(I_t/A_t)_H}{(I_t/A_t)_{M_0}}\left(=\frac{1}{n_L}\right)_{G.S.}=n_g\left(\frac{4\delta\alpha}{2(1+m')-\delta(1+3\alpha-\beta)}\right)_{n_L}\left(\frac{\delta(3+\alpha+\beta)+2(m'-3)}{2(1+m')-\delta(1+3\alpha-\beta)}\right)$	
(5)	$n_r=n_g\left(\frac{-\delta\alpha}{2(1+m')-\delta(1+3\alpha-\beta)}\right)_{n_L}\left(\frac{(3+m')+\frac{1}{2}\delta(\beta-5\alpha-3)}{2(1+m')-\delta(1+3\alpha-\beta)}\right)$	(10) $n_H=n_L$		
(6)*	$n_{v_f}=\frac{n_L}{n_{A_f}}\left(=\frac{1}{n_L}\right)_{G.S.}$	(11) $n_t=n_L$		(14) $n_T=n_L$
(7)	$n_T=n_g\left(\frac{2\delta\alpha}{2(1+m')-\delta(1+3\alpha-\beta)}\right)_{n_L}\left(\frac{2(2m'-2\delta\alpha+\delta\beta)}{2(1+m')-\delta(1+3\alpha-\beta)}\right)$		(7) *Repeat* — — —

Table 3. Crocco's second scaling rule for liquid-fuel rocket engines ($\delta=0$, $n_2=1$)

A Steady aerothermochemistry	*B* Regenerative cooling	*C* Low-frequency stability	*D* High-frequency stability
(1) $n=n_L$			
(2) $n_h=n_L^{m'/(1+m')}$			
(3) $n_v=n_L^{(1-m')/(1+m')}$	(8) $n_{v_f}=1/n_L$	(12) $n_L^{-(2-m')/(1+m')}=1$	
(4) $n_p=n_L^{-2/(1+m')}$	(9) $n_{q_f}=1/n_L$		
(5) $n_r=n_L^{1/2+1/(1+m')}$	(10) $n_H=n_L$	(13) $\dfrac{(l_f/A_f)_H}{(l_f/A_f)_{H_0}}\left(=\dfrac{1}{n_L}\right)_{G.S.}=n_L^{(3-m')/(1+m')}$	
(6) $n_{A_f}=\dfrac{n_L}{n_{A_f}}\left(=\dfrac{1}{n_L}\right)_{G.S.}$	(11) $n_C=n_L$		
(7) $n_\tau=n_L^{2m'/(1+m')}$		(7) $n_\tau=n_L^{2m'/(1+m')}$	(14) $n_\tau=n_L$

Table 4. Barrère's scaling rule for liquid-fuel rocket engines ($\delta=2$, $\delta_2=r'$, $\beta=0$, $n_2=1$, $n_h=1$ in the expression for D/h); the effect of setting $n_h=1$ in the expression for D/h can be accounted for by repeating the entire analysis

A Steady aerothermochemistry	*B* Regenerative cooling	*C* Low-frequency stability	*D* High-frequency stability
(1) $n=n_L$			
(2) $n_h=n_L^{\left(\frac{m'-r'}{1-2r'+m'}\right)}$			
(3) $n_v=n_L^{\left(\frac{1-m'}{1-2r'+m'}\right)}$	(8) $n_{v_f}=1/n_L$	(12) $n_L^{2\left(\frac{-(m'+r')}{1+m'-2r'}\right)}=1$	
(4) $n_p=n_L^{\left(\frac{-2(1-r')}{1-2r'+m'}\right)}$	(9) $n_{q_f}=1/n_L$		
(5) $n_r=n_L^{\frac{1}{2}\left(\frac{3+m'-4r'}{1+m'-2r'}\right)}$	(10) $n_H=n_L$	(13) $\dfrac{(l_f/A_f)_H}{(l_f/A_f)_{H_0}}\left(=\dfrac{1}{n_L}\right)_{G.S.}=n_L^{\left(\frac{3-m'-2r'}{1+m'-2r'}\right)}$	
(6) $n_{A_f}=\dfrac{n_L}{n_{A_f}}\left(=\dfrac{1}{n_L}\right)_{G.S.}$	(11) $n_t=n_L$		
(7) $n_\tau=n_L\left(\frac{2(m'-r')}{1-2r'+m'}\right)$		(7) $n_L=\left(\frac{2(m'-r')}{1-2r'+m'}\right)$	(14) $n_\tau=n_L$

requirement of an intelligent scaling programme. Important steps in this direction have already been made by Crocco and Barrère but additional quantitative experimental work, for a variety of propellant systems, is urgently needed.

Daniel and Florence Guggenheim Jet Propulsion Center,
California Institute of Technology,
Pasadena, California

(*Received October 1956*)

REFERENCES

[1] PENNER, S. S. Models in Aerothermochemistry in *I Modelli nella Tecnica* Vol. I pp. 652-669, Accademia Nazionale dei Lincei, Rome, 1956; See also *Tech. Rep. No. 13* Contract DA 04-495-Ord-446, California Institute of Technology, Pasadena, 1955
[2] CROCCO, L. Considerations on the Problem of Scaling Rocket Motors, *Selected Combustion Problems II* p. 457, AGARD, Butterworths Scientific Publications: London, 1956
[3] PENNER, S. S. *Jet Propulsion* 27 (1957) 156
[4] BARRÈRE, M. *Similarity of Liquid-fuel Rocket Combustion Chambers* Office Nationale d'Etudes et de Recherches Aéronautiques: Paris, 1956
[5] See, for example, PENNER, S. S. *Chemical Reactions in Flow Systems* Chapter 4 Butterworths Scientific Publications: London, 1955
[6] BARRÈRE M. and MOUTET, H. *Rech. aéro.* 50 (1955) 31
[7] BARRÈRE, M. Preliminary experimental results obtained at the Office Nationale d'Etudes et de Recherches Aéronautiques, Paris; personal communication
[8] DAMKÖHLER, G. *Z. Elektrochem.* 42 (1936) 846
[9] PENNER, S. S. *Combustion Researches and Reviews 1955* Chapter 12 AGARD, Butterworths Scientific Publications: London, 1956

Experimental Techniques for the Study of Flat Flames by Infra-red Spectroscopy

D. J. COLE* and G. J. MINKOFF

In order to make full use of the possibilities presented by flat flame burners, it is necessary to use a narrow beam of light. The factors affecting the spatial resolution and the radiation intensity are discussed, and the construction of a double-beam i.r. spectrometer incorporating this principle is described. The instrument has been used for the study of flat diffusion flames, and the different possible modes of operation are considered in relation to methane–oxygen and ethylene–oxygen flames. For absorption work, the pre-chopped, single-beam technique has been found to be the most useful. The potentialities and the difficulties of the study of flames by i.r. absorption spectroscopy with such an instrument are discussed.

THE development of flat flame burners (J. POWLING[1]; A. C. EGERTON and S. K. THABET[2]; H. G. WOLFHARD and W. G. PARKER[3]) has led to the possibility of determining spatially the variation in concentration of reactants, and possibly of intermediates, as the gases approach the flame zone. With visible and u.v. spectroscopy, parallel light is passed through the whole flame, and a photograph of the spectrum is taken. The latter shows continuously the variation of the spectrum across the zone under investigation. When photoelectric methods are used, however, it is necessary to record a number of spectra, each corresponding to a different position across the flame. Ideally, a narrow slit in front of a lens or mirror producing a parallel beam would give a beam of light narrow enough to examine each region of the flame without being affected by the conditions in the adjoining regions. With i.r. spectroscopy, however, the loss of intensity caused by eliminating the greater part of the light would make it impossible to operate with a satisfactory combination of noise and of slit width and it is, therefore, not possible to discard any of the light available. Instead, it is essential to collect all the light into a narrow beam which is as nearly parallel as is practicable. The present instrument has been built according to this principle.

Since several communications have been published on the *i.r.* spectroscopy of flames carried out with conventional optics[4, 5], it is necessary to show that a very narrow beam of light can be used with no loss of intensity.

Let us consider an element of area dS_1 of an object of brightness B_1 of which an image of area dS_2 is formed by a concave mirror. Let the distances involved be as shown in *Figure 1*.

The amount of light from dS_1 falling on the mirror in unit time is $B_1 dS_1 \sin^2 \theta_1$. If the mirror reflects a fraction k of the light falling on it, then the amount of light falling in unit time on the image is $k\pi B_1 dS_1 \sin^2 \theta_1$.

*Present address: Northampton Polytechnic Institute, London.

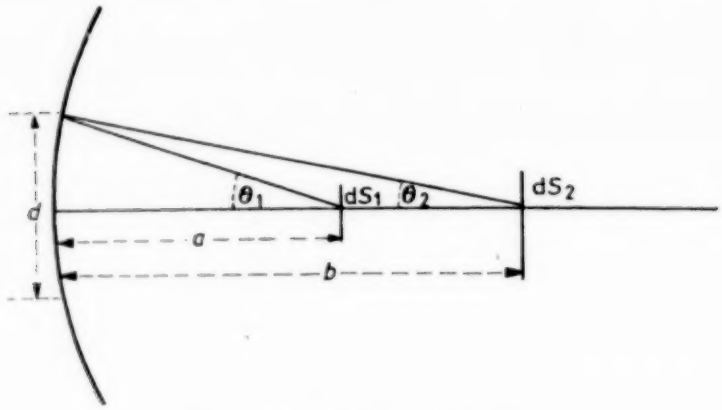

Figure 1. Brightness of image

Now if B_2 is the brightness of the image, the amount of light emitted by it in unit time is $\pi B_2 dS_2 \sin^2\theta_2$, so that

$$k\pi B_1 dS_1 \sin^2\theta_1 = \pi B_2 dS_2 \sin^2\theta_2$$

$$B_2 = kB_1 (dS_1 \sin^2\theta_1)/(dS_2 \sin^2\theta_2)$$

$$= kB_1 a^2 \sin^2\theta_1 / b^2 \sin^2\theta_2$$

For small angles

$$a^2 \sin^2\theta_1 = \tfrac{1}{4}d^2 = b^2 \sin^2\theta_2$$

$$B_2 = kB_1$$

That is, for small angles, the angular brightness of the image is dependent only upon the reflectance of the mirrors and is independent of the beam width. Thus, provided the aperture of the monochromator is filled, no radiation is lost by using a narrow beam system.

It is clear that if wider aperture optics are used, then light emitted by the flame and focused on the slit may have travelled through several different stages of the flame. Similarly with absorption, radiation at any point of the image on the slit will have come from a wider angle than is at first apparent. Thus in order to obtain good spatial resolution, it is not sufficient for the slit of an ordinary i.r. spectrometer, utilizing a wide beam of radiation, merely to select an area of the image focused on it.

SPECTROMETER

External optics

The external optical system is indicated in *Figure 2*. The narrow ang at the flame was obtained by placing the source and the flame at the san distance (100 cm) from collecting mirror *A*, the focal length of *A* (50 cn being such as to form the image in the middle of the flame. The imag was then 1½ mm wide at the centre of the flame and rather less than 2 m at the edges. For double beam operation, mirror *B* sent another beam light through a comparison system and the two beams were eventuall

collected into a common path by the chopper mirror; half of the latter was transparent, and the other half was front aluminized on both faces. A final mirror then produced an image on the entrance slit of the monochromator one third the size of the original Nernst filament. The dimensions were such that the beam entering the monochromator filled the aperture of the latter. The chopper was rotated at 15 c/s.

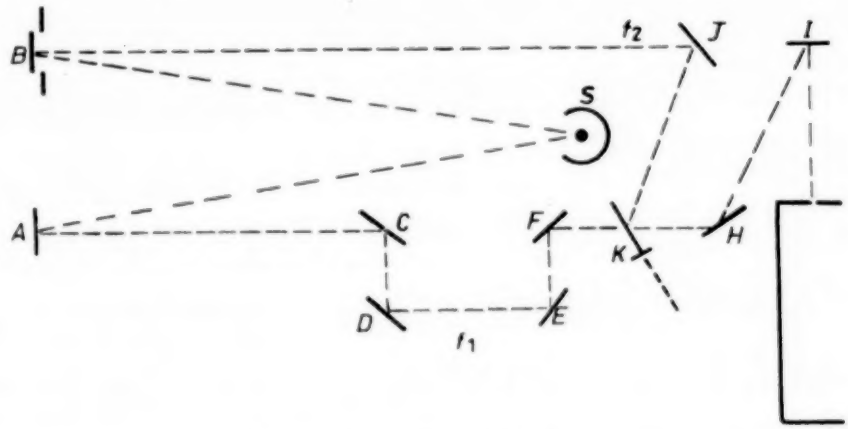

Figure 2. External optical system

The shutter driven by the servo mechanism moved across mirror *B*, and it was cut in such a shape that smaller absorptions caused relatively large movement of the shutter, so that a non-linear absorption scale was obtained on the recorder paper. Another 15 c/s chopper could be placed in front of the source for single beam operation so that the light was periodically interrupted before it entered the flame.

Monochromator

The monochromator was constructed in a duralumin box and was of the standard Littrow design with the exception of the slits. These were built according to a design provided by Professor Price. The entrance and exit slits were in the same plane and therefore the two slits were mounted on the same metal base. The left hand limbs of both slits were mounted on one piece of duralumin and the right hand sides were fixed on another piece of duralumin in the same plane, attached to the structure of the monochromator. The relative movement of these slit components was effected by a lever system operated by a micrometer. Conventional drive units, etc., were built to link up wavelength drives and slit drives. The resolution obtained was comparable to that obtained by Price, Tetlow, etc., and is illustrated by *Figures 3* and *4*, the former showing a single beam spectrum of water absorption, and the latter a double-beam, servo, absorption spectrum of ammonia vapour.

Electronics

The amplifiers (H. W. THOMPSON, C. H. MILLER and R. RICHARDS[6]) and servo mechanisms were of conventional design and were built by the Infra red Development Company.

Applications

So far the instrument has been used for the study of carbon formation in flat diffusion flames (D. J. COLE and G. J. MINKOFF[7]). Four modes of operation were possible which will be briefly reviewed with regard mainly to methane flames.

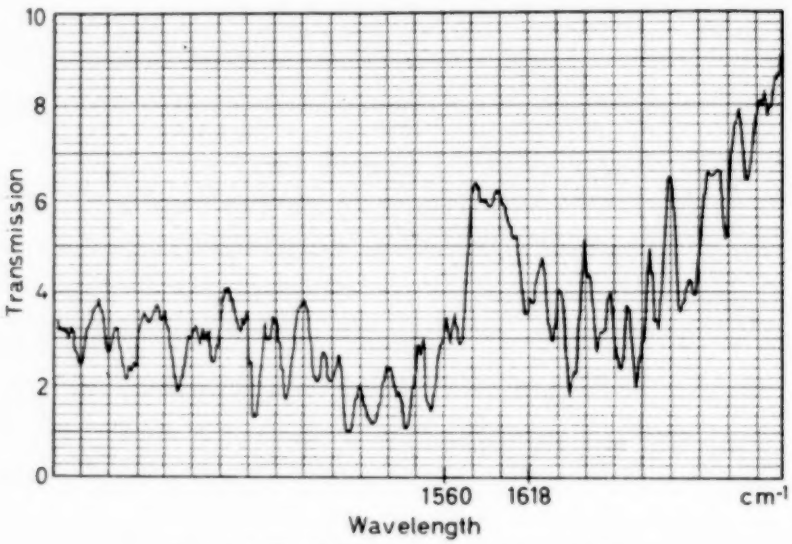

Figure 3. Single beam water vapour spectrum

Spectra were obtained with the burner mounted, as previously described, at focus f_1 of the spectrometer. It was lined up so that the radiation from the Nernst filament passed straight along the division between the fuel and oxygen channels and subsequently it was moved normally to this radiation by means of the micrometer. Thus the flame could be scanned by moving

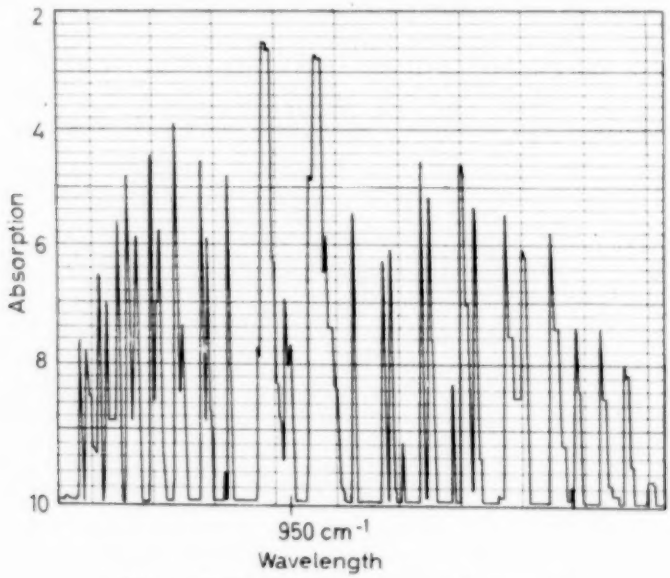

Figure 4. Double beam ammonia spectrum

the burner bodily across the optical path of the spectrometer. The position of the burner relative to the slit of the monochromator was determined by observing, through a cathetometer, when the image of the luminous carbon zone was brought on to this slit.

Attempts were made to obtain spectra by running the spectrometer in each of a number of different ways:

(*a*) Conventional double-beam working for absorption (Post-chopped double-beam absorption)

(*b*) Single-beam working, with conventional chopping of radiation after the sample, for absorption (Post-chopped single-beam absorption)

(*c*) Single-beam working for emission spectra (Emission)

(*d*) Single-beam working, with chopping of the radiation before the sample for absorption (Pre-chopped single-beam absorption).

The results are presented under these various headings.

(*a*) *Post-chopped double-beam absorption*—Attempts were made to examine a methane–oxygen flame, using this technique with the servo unit and shutter. On the fuel side of the flame, at the short wavelength end of the spectrum, the bands at 4264, 3030, and 1430 to 1250 cm^{-1}, due to methane, were clearly obtained. However, the zero line drifted continuously upwards with increasing wavelength, and it soon became impossible to balance the servo system. As parts of the flame nearer the reaction zones were brought on to the optical axis of the spectrometer, it became progressively more difficult to obtain balance at any part of the spectrum, due to emission from the flame. This system of working had to be abandoned, since balance in the long wavelength region, where interesting information might be expected, was quite impossible.

In the restricted range for which it was possible to obtain spectra, the only notable feature was that the 1430 to 1250 cm^{-1} band system became sharper, and the resolution appeared to be better than that found in spectra of the cold gas. It was not ascertained whether this was due to a temperature effect on the actual spectrum or to an effective lowering of pressure of the methane by the approximately tenfold increase of temperature.

When using ethylene as the fuel, there was a tendency for a solid sheet of carbon to grow nearly vertically from the top of the metal division between the fuel and oxygen channels. In experiments during which this happened, the solid carbon could almost completely obscure the radiation from the Nernst filament at one particular position, and so render it impossible to obtain the corresponding spectrum. This carbon sheet was hard and brittle and could be removed intact from the burner. *Figure 5* is a photograph of such a sheet. Ultimate analysis of a sample of this sheet gave a composition of C 99·41, H 0·31, and O 0·28 per cent, corresponding to an empirical formula of approximately $C_{300}H_{11}O$. X-Ray diffraction examination (by Dr Wilman) showed it to be graphitic, with twisted planes, and much more crystalline than soot. The crystal size was approximately 400 Å. Thus, this material had a structure approaching more closely to that of pure graphite than any previously isolated from such flames.

However, the relatively low hydrogen and oxygen contents may have be[en] due to a baking-out effect after the sheet had been formed. It was fou[nd] that the build-up of a carbon sheet did not occur if the tops of the fuel a[nd] oxygen channels of the burner were carefully freed of all traces of carb[on] before the gas was ignited.

(*b*) *Post-chopped single-beam absorption*—Towards the long wavelen[gth] end of the spectrum, absorption was found to give way to emission, whi[ch] caused the spectrum trace to rise above the 100 per cent transmission lin[e].

Figure 5. Sheet of carbon fro[m] ethylene fuel

This emission commenced at about 1110 cm^{-1} and continued to beyond 690 cm^{-1}. Nearer the flame front the emission became correspondingly stronger.

It was decided that this system could be studied more easily in emission.

(*c*) *Emission*—Emission spectra of flames of methane–oxygen and ethylene–oxygen were examined over the whole spectral range from 5000 cm^{-1} to 690 cm^{-1}. The following band systems were studied.

(*i*) A complicated system extending from 1110 cm^{-1} to longer wavelengths was identified with the OH and H_2O rotational system previously studied with a hydrogen–oxygen flame by E. K. PEYLER and C. J. HUMPHREYS[5]. The intensity of emission reached a maximum between the luminous carbon zone and the blue zone of the flame, probably at the position of maximum temperature.

In the absence of data concerning the dependence of emissivity on concentration and temperature for these bands it was not possible to convert the intensities to concentrations.

(*ii*) Systems at 2380 to 2175 cm^{-1}, 5000 to 3300 cm^{-1}, and 1800 to 1670 cm^{-1}, due to carbon dioxide and water, were found to have maxima at the same position in the flame as the OH and H_2O rotational system.

(*iii*) At one position only, in each flame, about 2·5 mm to the fuel side of the luminous carbon zone, a weak emission band at 729 cm^{-1} was detected. The band was much weaker in the methane flame than in the ethylene flame. This band has been shown to be due to acetylene and its role in carbon formation in these flames has been discussed elsewhere[7].

It was not possible to detect bands due to the fuel with either flame.

(*d*) *Pre-chopped single-beam absorption*—This method of working eliminated interference due to emission, and the spatial distributions of the fuel and acetylene bands were, therefore, examined in some detail[7].

DISCUSSION

The flames which have been studied in this work have maximum temperatures approaching 3000°K, and the spectra of the species present may therefore be expected to have undergone some modification. This modification may take either or both of two forms. Characteristic wavelengths of bands may have effectively changed, either due to broadening as has been demonstrated for carbon dioxide, or to bands appearing or disappearing; or alternatively the intensity of a particular band may have altered.

The theoretical prediction of the effect of temperature on i.r. spectra is an extremely difficult problem, as the populations of various rotational levels are governed by complex exponential functions which vary with the degree of symmetry of the molecule and, even if these populations could be calculated, the transition probabilities corresponding to the various bands would still be unknown. The few experimental studies that have been performed on this subject have only covered a temperature range of up to about 500°C, and are restricted to such molecules as carbon dioxide.

J. C. PIMENTEL *et al.*[4] have assumed that because the ammonia absorption bands at 950 cm^{-1} and 3360 cm^{-1} obey Beer's law at room temperature they will also do so at the flame temperature.

With the results reported here it was not considered justified to attempt any deductions regarding concentrations. The small amount of information obtained about temperature effects suggested that the intensity of absorption of bands may vary with temperature in different ways. For example, the 3030 cm^{-1} C—H absorption of methane appeared to have the same intensity on the outer edge of the flame as in the cold gas flowing at the same rate. This would suggest a greater intensity of absorption by the hot gas, since the latter should be at a lower effective pressure than the cold gas. With acetylene added to methane and ethylene flames, however, the absorption at 729 cm^{-1} near the edge of the flame was very much weaker than that given by an equal flow of the cold gas. With all gases, it is difficult to know how far the intensity effects are due to temperature and how far to chemical reaction, but at least with the added acetylene it would seem more likely that the effect is due either to the effectively reduced pressure or to an effect on the spectrum, rather than to chemical reaction.

The skeletal vibration bands of the spectra of the hydrocarbons used in this work did not seem to alter detectably in the flame, as regards appearance or position, except that there appeared to be a general sharpening or improvement of resolution, which may well have been due to the lower effective pressure of the gases. This was noticed particularly with the methane bands at 3030 cm^{-1} and at 1430 to 1250 cm^{-1}.

The possible variation of intensity of absorption bands with temperature provides a possible alternative explanation of the non-detection of intermediates in the flame, but if the effect is operative it is probably only a contributory one, which is coupled with the low stationary concentrations of such intermediates. If the assumption is made that the absorption of any particular compound is as strong at the flame temperature as at room temperature, a stationary concentration of the order of 0·1 per cent of the

fuel gas is probably the lowest that could be detected by i.r. spectroscopy, using a burner of the type used for this work, even for the strongest absorbers in the infra-red.

The extensive emission from 1100 cm^{-1} down, due to water and OH, and the broadening of the carbon dioxide emission at 2200 cm^{-1} renders fruitless the study of emission spectra from hot flames at wavelengths longer than about 2500 cm^{-1}. Both in emission and absorption, useful information might be obtained if an instrument with sufficient resolving power to split the 3300 cm^{-1} C—H vibration bands were used.

The work of R. E. DONOVAN and W. G. AGNEW[5], and of D. P. NEEDHAM and J. POWLING[9], suggests that with lower temperature flames it is possible to detect other intermediates, but Pimentel *et al.*, using the same type of flame as was used for the work in this paper, were unable to detect intermediates. This may be explained by assuming that the reactions in the higher temperature flames are far more rapid, possibly radical chain reactions which do not allow the build-up of any appreciable concentration of intermediates. The experimental evidence available indicates that lower temperature, premixed, flat flames of the type used by Powling, are more amenable to investigation by i.r. spectroscopy than are higher temperature diffusion flames. Lower temperature diffusion flames burning with air might also be suitable, but these are narrower, more difficult to stabilize than oxygen-supported flames, and are more unsteady.

Before any exhaustive investigation of any of these flames can be undertaken by this technique, however, more information on high temperature emissivity and absorptivity of molecules in the infra-red is needed.

Practical difficulties of a narrow beam system

The necessity for the use of a narrow beam spectrometer if a flat flame is to be spatially resolved has already been considered. Certain practical difficulties attend the use of such an instrument, which are not present in ordinary broad-beam spectrometry. These difficulties all arise from the fact that the image which is formed on the entrance slit of the monochromator is very small. This, coupled with the long light paths used in the instrument, makes adjustment far more critical than in an ordinary instrument. This effect is especially pronounced where the first two concave mirrors, *A* and *B*, are concerned. A very small movement of the angle of either of these mirrors may throw the corresponding image right off the slit. The adjustment of mirrors farther along the optical path is also very sensitive. Due to the critical nature of the external optical alignment vibration is a major problem in a narrow beam instrument, for the slightest oscillation of a mirror may superimpose a large noise level on the output. All motors used in the spectrometer have to be specially mounted to reduce vibration to the lowest possible value.

The second difficulty which arises is that any imperfections in the shape of the Nernst filament source make it impossible to have the image on the slit along the whole of its length. This necessitates the careful selection of Nernst filaments, and the effect can be lessened to some extent by rotating

the filament so that it has least curvature in the direction presented to the concave mirrors.

The third, and perhaps most serious, difficulty is that the narrowness of the image imposes an artificial limit on how far the slits of the monochromator can be opened. At short wavelengths this is of little consequence, but at wavelengths towards 750 cm^{-1} the signal decreases severely unless the slits can be opened considerably; dispersion of rock-salt in this region is sufficiently good to allow this to be done without loss of resolution. This means that it is necessary to reach a compromise between the narrowness of the beam used, and the width to which the slits may be opened. With the spectrometer described here the final image was found to be too small, since it was not possible to prevent the signal level from decreasing to some extent in the long wavelength regions of the spectrum.

In conclusion, it may be said that i.r. spectroscopy may provide useful information about the structure of flames, when it is applied to comparatively low temperature flat flames. With suitable prior calibration, it will be possible both to detect and to plot the concentration of a number of molecules. For higher temperature flames it may be more difficult to obtain the necessary calibration data, and the indications are that fewer species are present in the flame in sufficient concentration to allow their detection with the system in use at present. Narrow-beam i.r. spectroscopy, however, offers a potential field of study which is limited only by the experimental difficulties.

The authors gratefully acknowledge the invaluable assistance of Mr G. Barrett in the construction of the spectrometer, and also helpful discussion with Professor W. C. Price.

Chemical Engineering Department,
Imperial College of Science and Technology,
London, S.W.7.

(Received February 1957)

REFERENCES

[1] POWLING, J. *Fuel, Lond.* 28 (1949) 25
[2] EGERTON, A. C. and THABET, S. K. *Proc. Roy. Soc.* A 211 (1952) 445
[3] WOLFHARD, H. G. and PARKER, W. G. *Proc. phys. Soc., Lond.* A 62 (1949) 722
[4] DOWS, D. A., WHITTLE, E. and PIMENTEL, J. C. *J. chem. Phys.* 23 (1955) 499
[5] DONOVAN, R. E. and AGNEW, W. G. *J. chem. Phys.* 23 (1955) 1592
[6] THOMPSON, H. W., MILLER, C. H. and RICHARDS, R. *Rep. Inst. Petrol. Hydr. Gp. No. 23*, 1947
[7] COLE, D. J. and MINKOFF, G. J. *Proc. Roy. Soc.* A 239 (1957) 280
[8] PLYLER, E. K. and HUMPHREYS, C. J. *Res. Pap. U.S. Bur. Stand No. 1890* (1948) 449
[9] NEEDHAM, D. P. and POWLING, J. *Proc. Roy. Soc.* A 232 (1955) 337

Recent Developments and Notes

PREDICTION OF COMBUSTION CHARACTERISTICS OF TOWN GAS

A paper by M. G. GILBERT and J. A. PRIGG, of the London Research Station, Gas Council, has recently been published, dealing with the prediction of the combustion characteristics of town gas from its analysis (*The Gas Council, Res. Commun. GC 35;* 1956). In this paper a method of predicting has been presented which is based on the work of E. R. WEAVER in America [*J. Res. nat. Bur. Stand.* 46 (1951) 213], and of P. DELBOURG in France (*Ass. Tech. de l'Ind. Gaz en France Congrès*, 1951; see also *I.G.U. Comm. 4–52*, 1952). Both of these methods are largely concerned with the performance of an appliance on a gas relative to an adjustment gas, that is, the problem of interchangeability. But it is also important to know the characteristics of a gas in order that burners and appliances may be designed for it.

The methods used by Weaver and Delbourg are essentially similar. They have been examined in detail in a previous publication (*The Gas Council, Res. Commun. GC 21*; 1954). Weaver calculates a series of six indexes for a gas relative to a gas normally available which has been used for the design and adjustment of appliances so as to give satisfactory performance. He suggests limits to these indexes. In the calculation of the indexes, the two factors $A/d^{\frac{1}{2}}$, where A is ft^3 of air required for the combustion of 1 ft^3 of gas and d is the sp. gr. of the gas, and S, the calculated maximum flame speed of the gas relative to hydrogen, are important. Delbourg uses a diagrammatic method in which Wobbe number is plotted against *combustion potential*, and an area of satisfactory performance is drawn on the diagram. Both these methods appear to provide a good indication of the performance of a gas, but the limits have been developed in terms of American and French appliances.

In order to adapt the methods to British conditions the authors of the present communication have constructed a diagram with axes which are primarily Weaver's flame speed factor, S, and Wobbe number, with hydrogen content and $A/d^{\frac{1}{2}}$ as possible alternatives. Lines of equal aeration number are also shown on the diagram. This number is an important criterion of combustion characteristics and is used in defining two of the limits of satisfactory performance, lighting back and incomplete combustion. The calculation of aeration numbers is by a formula depending on readings of the air shutter opening on a particular type of aeration test burner.

This method of predicting the combustion characteristics of a gas involves the use of a calculated flame speed and, therefore, cannot be considered entirely satisfactory, check testing of existing appliances remaining necessary.

RADIATION FROM OIL FLAMES

An investigation has been made by D. K. HOLLIDAY and M. W. THRING, Department of Fuel Technology and Chemical Engineering, University of Sheffield, of the relation existing between the radiation from oil flames and

the carbon-to-hydrogen weight ratio of the fuels [*J. Inst. Fuel* 30 (1957) 127]. The investigation arose out of the work of the International Committee for Flame Radiation Research at the Experimental Station at IJmuiden, Holland. The experimental furnace used was designed so as to enable the laboratory scale results to be related to larger scale work and to industrial furnaces.

The burner was designed so that a flame 4 ft long was produced, using a fuel flow rate of less than 2 gallons per hour; a twin-angle total radiation pyrometer developed in the B.I.S.R.A. laboratories was used for measurement of the flame radiation; and water-cooled probes were developed for measurements of temperature, soot concentration and velocity. Fourteen different oil fuels covering a wide range of chemical composition were used and the flame emissivity and temperature were measured along the length of a turbulent jet diffusion flame.

A relationship was found between flame emissivity and fuel property, whereby the average total flame emissivity ($\varepsilon_{T.AV.}$) is predictable for different fuels under identical combustion conditions, solely from the carbon-to-hydrogen weight ratio (R) and the mean average boiling point (T) of the fuels. This relationship, for the particular furnace conditions used, is

$$\varepsilon_{T.AV.} = 0{\cdot}282 \ln (R - 5)/4 + 0{\cdot}002 (T - 200) + 0{\cdot}484$$

A relation exists between carbon particle concentration on the flame axis (C g/l. at n.t.p.) and flame total emissivity (ε_T), for five of the fuels used, which is applicable to turbulent jet diffusion flames of different widths (l cm) from any liquid fuel and is of the form

$$\varepsilon_T = 1 - n^{-0{\cdot}0025\, Cl}.$$

Using this relationship emissivity distribution in the flame from any fuel in the IJmuiden furnace can be predicted from the emissivity distribution for that fuel in the experimental furnace used in this research. The axial soot concentration is, however, higher in the small furnace for a given fuel at the equivalent distance along the flame than in the IJmuiden furnace. This is attributed to the shorter mixing and combustion time allowing the soot to survive relatively longer in the small furnace.

RADIATION OF HIGH-PRESSURE FLAMES

Spectroscopic studies of flames at high pressure have covered up to the present time only a very limited range of pressures and flame conditions. Recent work, however, by J. DIEDERICHSEN and H. G. WOLFHARD, of the Royal Aircraft Establishment, Rocket Propulsion Department, has provided an important contribution to remedy this defect [*Proc. Roy. Soc.* A236 (1956) 89]. Their investigation has been concerned with the spectrographic examination of flames of methane, ethylene, hydrogen and carbon monoxide, burning at pressures up to 40 atm. Both premixed and diffusion flames were used.

At higher pressures the equipartitioning of energy released by chemical reaction is faster. This is shown to lead to the suppression of unstable

radicals which are observed in low-pressure flames. The total light intensity of flames burning with air is little pressure-dependent; but the continuous gas radiation and emission from carbon particles become predominant at higher pressures. The radiation of oxygen flames is mainly determined by the increase in temperature of flames burning at high pressure. There is consequently a strong increase in the emission from those products which are present in equilibrium such as OH and O_2.

Continuous gas radiation increases very strongly with pressure and two types of continua can be distinguished, one in the carbon monoxide flame and one in the hydrogen flame. The first of these has been attributed by A. G. GAYDON (*Spectroscopy and Combustion Theory*. Chapman and Hall, London, 1948) to the process

$$CO + O \longrightarrow CO_2 + h\nu$$

and the present investigations support this view. The so-called 'after-burning', observed in closed-vessel explosions, is almost certainly connected with the increase in temperature and pressure which occurs in part of the burnt gases due to adiabatic compression. It should not be regarded as an indication of delayed chemical reaction. Light emission due to

$$CO + O \longrightarrow CO_2 + h\nu$$

is very dependent on pressure and temperature and is consequently able to account for this phenomenon alone. The present authors propose that the association

$$OH + OH \longrightarrow H_2O_2 + h\nu$$

accounts for the hydrogen flame continuum, which would be in accord with the pressure-dependence of the continuum in oxygen and air flames. Continua occurring in hydrocarbon flames are a superposition of the two referred to above.

FREE RADICALS RESEARCH

A three-year programme of research on free radicals has been undertaken by the National Bureau of Standards, Washington. A special section of the Bureau has recently been established under H. P. BROIDA, for the overall direction and coordination of the experimental and theoretical investigations. These will be carried out to a considerable extent by scientists on loan from industrial laboratories and others from universities and various government agencies. The work is receiving support from the Department of Defense through the Office of Ordnance Research, U.S. Army [*Tech. News Bull. U.S. Bur. Stand.* 41 (1957) 1].

Ordinary free radicals exist for only very short periods in systems such as flames and gases. Recently, however, by freezing the products of an electric discharge at a few degrees above absolute zero, it has been found possible at the Bureau to store some types of free radicals in highly excited states, making it possible to study and analyse them by spectroscopic methods [*Tech. News Bull. U.S. Bur. Stand.* 40 (1956) 112].

A symposium on the *Formation and Stabilization of Free Radicals* will be held at the Bureau on 18–20 September 1957. The meeting will be

sponsored jointly by the Applied Physics Laboratory of the Johns Hopkins University, the Catholic University of America, and the National Bureau of Standards.

TURBULENT FLAME STRUCTURE

An investigation, which had for its objective the elucidation of the structure of turbulent flames, has yielded important results for testing the theories of this type of burning. The work has been carried out by J. GRUMER, J. M. SINGER, J. K. RICHMOND and J. R. OXENDINE, of the Division of Explosives Technology, U.S. Bureau of Mines [*Industr. Engng Chem. (Industr.)* 49 (1957) 305]. Schlieren and smoke photographs were obtained of the turbulent flame brush and these were compared with direct photographs with a view to resolving uncertainties in previous interpretations of similar photographic studies. Turbulent natural gas–air flames with Reynolds numbers from 10 000 to 160 000 were used.

It is concluded that schlieren and shadow photography are not reliable techniques for analysing the structure of the turbulent flame brush and that the view derived from such studies, of the turbulent flame being composed of a single fluctuating, laminar wave, is not upheld by the results of direct photography. It was found in these experiments that observed density gradients in the schlieren photographs have apparent velocities greater than those of the turbulence intensity, the laminar burning velocity and the cold approach flow. Moreover, there are changes in the observed density gradients with turning of the schlieren knife-edge, and there are differences in the schlieren records for turbulent flames piloted by a laminar hydrogen–air flame and those piloted by heating the burner port rim electrically.

In the opinion of these investigators schlieren, and probably shadow and smoke, photography do not provide evidence for the concepts of either a wrinkled, fluctuating laminar wave or continuous reaction zone as being valid for explaining turbulent burning. In their view the turbulent flame brush is a zone of non-homogeneous and partly discontinuous burning. The discontinuous flamelets within the brush, according to their results, are extinguished by turbulent mixing of burnt and unburnt gas, ignited by turbulent transport of enthalpy into transient zones of ignitable gas. Ignition appears to depend significantly on chemical considerations affecting ignition lag and ignition temperature. They suggest that a significant function of turbulence in burning processes as compared to laminar burning can be better visualized in terms of 'early ignition' or 'turbulence-induced early ignition', rather than by models of 'flame-generated turbulence'.

OPEN-HEARTH FURNACE INVESTIGATIONS

The results of investigations on combustion and heat transfer in producer gas-fired open-hearth furnaces, carried out at the Templeborough works of the United Steel Companies Ltd were described some few years ago [*Spec. Rep. Iron St. Inst., Lond. No. 37* (1946)]. These trials were followed in 1954 by a study of a 100-ton oil-fired furnace in the same shop and an account of these has recently been published by (the late) S. W. PEARSON, M. W. THRING and J. H. CHESTERS [*Spec. Rep. Iron St. Inst., Lond.*

No. 59 (1956)]. This detailed and extensive report has been summarized by J. H. CHESTERS, Assistant Director of Research, United Steel Companies Ltd [*Iron Coal Tr. Rev.* 174 (1957) 553]. The trials were a cooperative effort between the Research and Development Department and the Steel Peech and Tozer branch of United Steels, the University of Sheffield, and the British Iron and Steel Research Association. The test furnace had not only single uptakes but also single slag pockets and single checkers chambers in order to simplify interpretation of the results. The actual trial only lasted about nine hours, but a considerable amount of time was taken in preparation and in the subsequent studies of flow pattern and mathematical calculations. In addition to the standard instruments, suction pyrometers were used for measurement of preheat and waste gas temperatures. The Schmidt method, as used at IJmuiden, was used for measurements of flame temperatures and emissivity [L. F. DAWS and M. W. THRING, *J. Inst. Fuel* 25 (1952) 28].

Amongst the interesting results of this investigation, it was noted that whilst the roof temperature was reduced by as much as 200°C in half-an-hour whenever scrap or pig-iron was charged, the waste gas temperature undergoing a similar change, the preheat temperature of the incoming air remained surprisingly constant throughout the heat.

A qualitative study was made of flow pattern in the furnace as a check on the mixing patterns that have been found in water models which are now generally agreed as of value for predicting the patterns in full-size furnaces. The most important observation made was that the flow pattern in the furnace was far from being symmetrical although this furnace was of an unusually symmetrical character. The explanation is stated to be found in the downstairs region, the air sweeping out of the checker chamber, over the bridge-wall, into the slag pocket, hitting the pit-side wall and rushing up it at a velocity far greater than that near the charge-side wall.

A comparison was made between the calculated and the observed heat transfer, and although there are appreciable uncertainties in these values, it is concluded that the actual heat transfer in this particular case can be largely explained in terms of existing radiation theory and that it is unlikely that convection played a major part in the charge-plus-melt period. It is pointed out, however, that if the contribution by convection is only 10 per cent of the whole heat transfer, it may still be very important, so that, for example, increasing the steam/oil ratio might result in doubling this factor and consequently an increased driving rate.

W. A. KIRKBY

ERRATUM

In line 18 on page 59 of the March 1957 issue of *Combustion and Flame*, read 'methyl nitrate' for 'methyl nitrite'.

OVERSEAS CORRESPONDENTS' NOTES

Professor Laffitte has sent the following summary of a paper entitled 'Research on Oxidation and Auto-ignition of Paraffinic Hydrocarbons in the Gas Phase' by E. Fréling [Thesis, Paris (1955) published in the *Revue de l'Institut Français du Pétrole*, 10 (1955) 1224 and 1543; 11 (1956) 134].

The introduction surveys oxidation and auto-ignition phenomena in gaseous fuel mixtures.

In the first part methods and set-ups for determining the ignition temperatures and measuring the oxidation rates are described and a report is given on the preparation of normal hexane starting from hexanol.

The second part contains curves of critical pressure limits of ignition of hexane–air mixtures (cool flame, hot flame) and a discussion of the experimental data with the help of ignition theories. The effect of the characteristic parameters of the vessels on the ignition temperatures are studied. It is shown that the hydrocarbon ignition peninsula corresponds with inhibited ignition of mixtures of hydrogen and carbon monoxide; a general reaction scheme is put forward. Methane ignition at high temperature (auto-inhibition) is studied and reaction schemes and computation of the oxidation rate are discussed. Then follows a report on a comparative study of the combustion of methane and hexane in the presence of a platinum wire.

The ignition curves of the higher hydrocarbons have been used to construct an ignition 'solid' diagram for the most general case, using the parameters of temperature, pressure and concentration. In the course of a comprehensive examination of the critical lags of hydrocarbons and their compounds, it was shown that the variation of the lag can be correlated with the build-up of intermediate products, and especially that there is a critical lag maximum for hot flames for those compounds which have a cool ignition region. A general classification of fuels into three groups is given, based on the curves of ignition.

In the third part, the results are reported of a kinetic study of combustion by recording the changes of pressure of the hexane–air mixtures in the range of temperatures 250° to 750°C (pressure < 1 atm). In particular, the lags of single and multiple cool flames are studied and two theories are given (kinetic and thermal-kinetic) which permit a forecast of the existence of periodic cool flames, of two-stage flames and of a negative temperature coefficient. The oxidation rates outside and inside the cool and hot flame domains have been measured; it is shown that the slow oxidation between the cool and the hot flame regions is a two-stage process (<540°C), while for higher temperatures the process is in one stage and corresponds with a degenerate branching chain reaction. The oxidation rate of this reaction was computed, making it possible to determine the maximum rate in terms of the initial pressure and temperature of the gaseous mixture. The experimental study of the maximum rates gives the apparent order and the apparent activation energy of the reaction. Hot flame lags were studied in terms of pressure, temperature and concentration, making possible the determination of the apparent order and the apparent activation energy. These values were compared with those arrived at with the help of the

maximum rates and it was established that the isothermal chain reaction theory cannot alone account for the observed happenings.

Studies of the effect of inert gases (helium, argon, nitrogen and carbon dioxide) on the ignition temperatures of hexane–oxygen and butane–oxygen mixtures show that the experimental facts are accounted for logically provided the isothermal chain reaction theory and the thermal theory are used conjointly. In particular, the study of the isochronal curves showed that the isothermal chain reaction theory is unable to predict the existence of a critical lag maximum of hot flames. This theory can only be applied within a restricted area of the domain of hot ignition of hydrocarbons.

In the last part the oxidation mechanisms of hydrocarbons between 250° and 750°C are considered and it was shown that, in the mechanism at low temperature, the structure of the molecule plays a major part. An account is given of the mechanism of the build-up of primary products, with the help of the peroxide theory and the aldehyde–peroxide theory; reaction mechanisms for hydrocarbon breakdown are also given. In studying oxidation mechanisms at high temperature (> 450°C), that of methane was first examined; two reaction mechanisms are given and it is shown that, above 600°C, a new mechanism must be introduced in order to account for the inhibitory effect of methane on its own combustion. For the higher hydrocarbons, oxidation in the range 400° to 520°C is a two-stage process in which both the low and high temperature mechanisms take part. The one-stage oxidation possesses the same characteristics as that of methane. Two reaction mechanisms are given to describe the breakdown of hydrocarbons and it is shown that, at very high temperatures (>600°C), the breaking of the C–C bonds becomes frequent, the mechanism bringing in only single radicals.

FUEL

Attention is drawn to the following *Notes* which were published in the April 1957 issue of *Fuel* and which may be of interest to readers of *Combustion and Flame*:

Carbon–oxygen reactions
Additives in fuels
Fire fighting foams